DYNAMICS OF RIGIDLY ROTATING SPIRAL WAVES UNDER LOCAL AND NON-LOCAL FEEDBACK CONTROL IN THE LIGHT-SENSITIVE BELOUSOV-ZHABOTINSKY REACTION

CHANANATE UTHAISAR

A THESIS SUBMITTED IN PARTIAL FULFILLMENT
OF THE REQUIREMENTS FOR
THE DEGREE OF MASTER OF SCIENCE
(CHEMICAL PHYSICS)
FACULTY OF GRADUATE STUDIES
MAHIDOL UNIVERSITY
2005

ISBN 974-04-5697-9

Thesis

entitled

DYNAMICS OF RIGIDLY ROTATING SPIRAL WAVES UNDER LOCAL AND NON-LOCAL FEEDBACK CONTROL IN THE LIGHT-SENSITIVE BELOUSOV-ZHABOTINSKY REACTION

.....
Miss Chananate Uthaisar
Candidate

.....
Asst. Prof. On-Uma Kheowan,
Ph.D.
Major advisor

.....
Prof. Stefan C. Müller,
Dr.rer.nat.habil.
Co advisor

.....
Assoc. Prof. Prapin Wilairat,
Ph.D.
Co advisor

.....
Assoc. Prof. Rassmidara Hoonsawat,
Ph.D.
Dean
Faculty of Graduate Studies

.....
Assoc. Prof. Pongtip Winotai,
Ph.D.
Chair
Master of Science Programme
in Chemical Physics
Faculty of Science

Thesis

entitled

DYNAMICS OF RIGIDLY ROTATING SPIRAL WAVES UNDER LOCAL AND NON-LOCAL FEEDBACK CONTROL IN THE LIGHT-SENSITIVE BELOUSOV-ZHABOTINSKY REACTION

was submitted to the Faculty of Graduate Studies, Mahidol University
for the degree of Master of Science (Chemical Physics)
on
25^{th} February 2005

.....
Miss Chananate Uthaisar
Candidate

.....
Asst. Prof. On-Uma Kheowan,
Ph.D.
Chair

.....
Assoc. Prof. Prapin Wilairat,
Ph.D.
Member

.....
Asst. Prof. Michael A.Allen,
Ph.D.
Member

.....
Assoc. Prof. Rassmidara Hoonsawat,
Ph.D.
Dean
Faculty of Graduate Studies
Mahidol University

.....
Prof. Amaret Bhumiratana,
Ph.D.,
Dean
Faculty of Science
Mahidol University

ACKNOWLEDGEMENTS

I would like to express my sincere gratitude to my advisor, Dr. On-Uma Kheowan, for her excellent supervision, valuable guidance and encouragement throughout this research. I am grateful to Prof. Stefan C. Müller for his kind of providing many suggestions and fruitful discussions of this thesis. I am also thankful to Assoc. Prof. Prapin Wilairat and Asst. Prof. Michael A.Allen for his helpful suggestions and comments for completion of the thesis.

I gratefully acknowledge the scholarship granted by Postgraduate Education and Research Program in Chemistry (PERCH) and I also wish to thank the Teacher Assistant (TA) scholarship for partial financial support.

I would like to thank Mr. Supichai Kantrasiri for his kind suggestion for helping preparation of computer program for the experiments. The appreciation is also expressed to the physical chemistry, chemical physics and polymer students for their kindness, readiness to help and being great friends.

Finally, I am grateful to all people in my family, for their love, understanding and encouragement throughout my study.

Chananate Uthaisar

DYNAMICS OF RIGIDLY ROTATING SPIRAL WAVES UNDER LOCAL AND NON-LOCAL FEEDBACK CONTROL IN THE LIGHT-SENSITIVE BELOUSOV-ZHABOTINSKY REACTION

CHANANATE UTHAISAR 4437290 SCCP/M

M.Sc. (CHEMICAL PHYSICS)

THESIS ADVISORS : ON-UMA KHEOWAN, Ph.D. , STEFAN C. MÜLLER, Dr.rer.nat.habil. , PRAPIN WILAIRAT, Ph.D.

ABSTRACT

The light-sensitive $Ru(bpy)_3^{2+}$-catalyzed Belousov-Zhabotinsky (BZ) reaction is used to observe the dynamics of a rigidly rotating spiral wave. This version of the BZ reaction can be effectively manipulated by applying external illumination with local or non-local feedback algorithms. For the dynamics of the spiral wave under local feedback control, each light pulse is applied at the moment that corresponds to the passage of the wave front through a particular measuring point. The light pulses induce a drift of the spiral wave core away from the measuring point and finally along circular orbits centred at this point. The trajectory of the spiral wave describes a resonance attractor. For a small distance (less than 0.15 of the spiral wavelength) between the measuring point and the initial location of the unperturbed spiral wave, a resonance attractor with hypocycloidal shape is observed, whereas for a larger distance an epicycloidal resonance attractor occurs. The size of the attractors can be changed by introducing a time delay into the feedback loop. When the time delay in the feedback loop becomes relatively long, the shape of the hypocycloidal resonance attractors deviates strongly from circular orbits. Experimental results are compared with an earlier developed theory on the resonance attractor.

Non-local feedback that computes the feedback signal proportional to the average wave activity, taken over a sensory domain that covers only part of the reaction layer, is introduced. In this work, the illumination intensity is proportional to the average wave activity within a square-shaped sensory domain of the reaction layer. The investigations show a broad spectrum of dynamical responses which result in square-shaped trajectories of the spiral tip, including reflections at the virtual walls. Experimental results show that the geometry of the sensory domain is crucial in determining the size and shape of the tip trajectories that are asymptotically reached.

KEY WORDS : SPIRAL WAVE DYNAMICS / BZ REACTION / FEEDBACK CONTROL / LOCAL / NON-LOCAL / HYPO- AND EPICYCLOIDAL RESONANCE ATTRACTORS / SQUARE-SHAPED SENSORY DOMAIN

86 pp. ISBN 974-04-5697-9

พลศาสตร์ขดคลื่นที่หมุนเกร็งภายใต้การควบคุมแบบป้อนกลับชนิดเฉพาะที่และชนิดไม่เฉพาะที่ในปฏิกิริยาเบลูซอฟจาโบทินสกีที่ไวแสง (DYNAMICS OF RIGIDLY ROTATING SPIRAL WAVES UNDER LOCAL AND NON-LOCAL FEEDBACK CONTROL IN THE LIGHT-SENSITIVE BELOUSOV-ZHABOTINSKY REACTION)

ชนเนษฎ์ อุทัยสาร 4437290 SCCP/M

วท.ม. (ฟิสิกส์เชิงเคมี)

คณะกรรมการควบคุมวิทยานิพนธ์: อรอุมา เขียวหวาน, Ph.D., Stefan C. Müller, Dr.rer.nat.habil., ประพิณ วิไลรัตน์, Ph.D.

บทคัดย่อ

คุณสมบัติทางพลศาสตร์ของขดคลื่นที่หมุนเกร็ง (rigidly rotating spiral wave) ถูกศึกษาในปฏิกิริยาเบลูซอฟจาโบทินสกี (Belousov-Zhabotinsky reaction) ที่ไวแสง ซึ่งปฏิกิริยานี้สามารถถูกควบคุมโดยการเปลี่ยนความเข้มแสงจากภายนอกภายใต้หลักการการควบคุมแบบป้อนกลับ (feedback control) ชนิดเฉพาะที่ (local) และชนิดไม่เฉพาะที่ (non-local) การควบคุมขดคลื่นแบบเฉพาะที่ (local feedback) ทำได้โดยการฉายแสงเป็นช่วงสั้น ๆ ในขณะที่หน้าคลื่นเคลื่อนที่ผ่านจุดวัด (measuring point) ที่เลือกไว้ในระบบ การฉายแสงภายใต้วงจรการควบคุมแบบป้อนกลับ (feedback loop) ทำให้การเลื่อน (drift) ของแกนของขดคลื่น (spiral wave core) เป็นวงโคจรที่เคลื่อนที่เป็นวงกลม (circular orbit) มีจุดศูนย์กลางอยู่ที่จุดวัด เส้นโคจร (trajectory) ของการเลื่อนบริเวณหัวของขดคลื่น (spiral tip) มีลักษณะเป็นเรโซแนนซ์แอตแทรกเตอร์ (resonance attractor) ถ้าระยะห่างระหว่างจุดวัดและตำแหน่งเริ่มต้น (initial location) ของขดคลื่นมีค่าน้อยกว่า 0.15 เท่าของความยาวคลื่น การเลื่อนของแกนของขดคลื่นเป็นเรโซแนนซ์แอตแทรกเตอร์แบบไฮโพไซคลอยด์ (hypocycloid) และเมื่อระยะห่างมีค่ามากกว่า 0.15 เท่าของความยาวคลื่น เรโซแนนซ์แอตแทรกเตอร์ที่พบเป็นแบบเอพิไซคลอยด์ (epicycloid) โดยที่ขนาดของเรโซแนนซ์แอตแทรกเตอร์ทั้งสองแบบสามารถถูกเปลี่ยนแปลงได้ด้วยการหน่วงเวลา (time delay) ในวงจรการควบคุมแบบป้อนกลับ และเมื่อค่าหน่วงเวลามีค่าสูงมาก ๆ รูปร่างของไฮโพไซคลอยด์เรโซแนนซ์แอตแทรกเตอร์เกิดการบิดเบี้ยว (deviation) อย่างชัดเจนไปจากวงโคจรที่เป็นรูปวงกลม หลังจากนั้นผลการทดลองถูกนำไปเปรียบเทียบกับทฤษฎีที่เกี่ยวกับเรโซแนนซ์แอตแทรกเตอร์ที่มีการพัฒนามาก่อนหน้า

กลไกการควบคุมป้อนกลับชนิดแบบไม่เฉพาะที่ (non-local feedback) สามารถคำนวณได้โดยสัญญาณของการควบคุมป้อนกลับซึ่งคือความเข้มแสงเป็นสัดส่วนกับค่าเฉลี่ยของกิจกรรมคลื่น (wave activity) ภายในพื้นที่รูปสี่เหลี่ยมที่ตอบสนองต่อการกระตุ้นของระบบ (square-shaped sensory domain) ที่ครอบคลุมเฉพาะบางส่วนของปฏิกิริยา (reaction layer) การศึกษาการควบคุมป้อนกลับแบบไม่เฉพาะที่แสดงให้เห็นถึงการเลื่อนของแกนขดคลื่นที่ตอบสนองสัญญาณของการป้อนกลับ ซึ่งส่งผลให้เกิดการเคลื่อนที่ของเส้นโคจรที่เป็นรูปสี่เหลี่ยม และมีการสะท้อนบริเวณที่ด้าน (virtual wall) ของพื้นที่รูปสี่เหลี่ยม นอกจากนั้นขนาดของโดเมนรูปสี่เหลี่ยมมีอิทธิพลต่อขนาดและรูปทรงของเส้นโคจรขดคลื่น

86 หน้า ISBN 974-04-5697-9

CONTENTS

LIST OF TABLES

LIST OF FIGURES

CHAPTER 1

INTRODUCTION

The spontaneous formation of self-organized structures is one of the most fascinating phenomena observed in many physical, chemical, and biological systems. The complexity and diversity of self-organized systems may occur in nonlinear dynamics under conditions far from thermodynamics equilibrium, governed by the laws of nonlinear dynamics [1]. A typical phenomenon is the formation of patterns showing complex temporal or spatio-temporal dynamics [1, 2]. These observations of patterns of chemical origin are important for biology, since every living system consists of many chemical compounds in a mixture. At the beginning of the 1950s, A.M. Turing [3] discovered that a condition for pattern formation is the interaction of two substances with different diffusion constants. He described a mechanism associated with a reaction-diffusion model for the chemical basis of morphogenesis, which is, for instance, the formation of chemical patterns in the skins of animals during their embryonic development [3]. Many phenomena in nonlinear systems, such as propagation of active electrical pulses along a nerve axon [4], a wave on the skin of the marine angelfish *Pomacanthus* [5], and chemical waves in an oscillating chemical reaction [6] can be explained by a reaction-diffusion model.

During the 1950s, an oscillating chemical reaction was discovered experimentally by B.P. Belousov [7]. Later, in 1961, A.M. Zhabotinsky [8] carried out extensive studies on the same system and developed a modified version of the reaction known as the Belousov-Zhabotinsky (BZ) reaction [6]. This reaction exhibits chemical oscillatory behaviours that can generate travelling chemical waves, such as target patterns and spiral waves [6, 9]. The travelling waves in the BZ reaction are observed in a class of reaction-diffusion systems called excitable media [9, 10, 11]. These media are characterized by

the existence of at least one steady state that is stable to small perturbations. However, if the perturbations exceed a critical threshold then the system responds with an excitation. The medium goes through a refractory period once it has been excited. The refractory period enables steady, periodic oscillations to be set up, giving rise to spatio-temporal patterns [10, 11, 12, 13]. The property of excitable media in the BZ reaction exhibits an interesting behaviour that is the variety of possible wave patterns.

Breaking of a wave front leads to a spiral wave, which occurs as a rotating wave of chemical activity in the BZ reaction [6, 9]. The spiral-shaped pattern is a well known structure seen in organisms. Spiral wave dynamics has been found extensively in excitable media, for instance action potentials in neural tissues [14, 15], travelling waves in the BZ reaction [9, 16], excitation waves in heart muscle fibres [17, 18], aggregating patterns of slime mold colonies [19, 20], CO-oxidation on platinum surfaces [21, 22], and NADH and proton waves during oscillatory glycolysis [23] (see Fig. 1.1). Among the systems, the BZ reaction is the most suitable laboratory system to study the dynamics of spiral waves and to find suitable means of control.

One important feature of a spiral wave is the motion of the spiral tip, which has been studied both experimentally [24, 25, 26, 27] and numerically [28, 29, 30, 31] in the BZ reaction. The dynamics of spiral wave can be described by tip trajectories with different rotation frequencies including flowerlike and circular orbits, which are referred to as meandering and rigid rotations, respectively [24, 29]. The dynamics of tip motion depends on the excitability of the system. If the light-sensitive $Ru(bpy)_3^{2+}$ catalyst is used, an externally applied illumination can completely suppress the excitability of the medium. Thus the dynamics of a spiral wave in the light-sensitive $Ru(bpy)_3^{2+}$-catalyzed BZ reaction can be effectively controlled by external illumination [32, 33, 34, 35, 36, 37, 38, 39].

Control of the dynamics of a spiral wave can be done by external forcing [33, 34, 37] or more complex feedback algorithms [34, 35, 36, 38, 39]. One of the feedback schemes

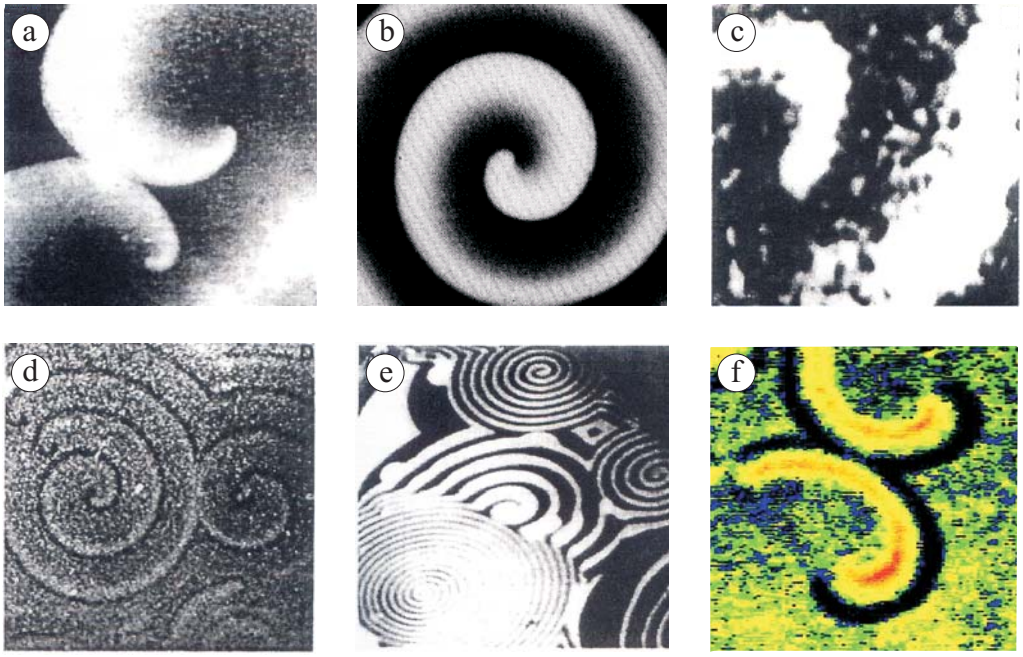

Figure 1.1: Example of spiral waves in excitable media: (a) colliding spiral-shaped front in neural tissue with spreading depression waves on chicken retina (from [15]), (b) spiral wave in the Belousov-Zhabotinsky reaction, revealing the front of oxidized ferroin catalyst (from [16]), (c) clock-wise rotating wave of isolated canine cardiac muscle (from [18]), (d) aggregation of social amoebae in the cellular slime mold *Dictyostelium discoideum* (from [20]), (e) population of spiral waves with different rotation periods and wavelengths in the catalytic CO-oxidation on a platinum surface (from [22]) and (f) spiral waves of NADH during the glycolysis in cytoplasm extracted from yeast cells (from [23]).

known as a local feedback control is based on the activity level of the system. The activity level can be measured at a particular measuring point, and then a light pulse is applied at the moment corresponding to the passage of the wave front through the point. The local feedback mechanism was investigated originally for a spiral wave with a meandering tip [34]. Under this type of feedback control two dynamical regimes, called the entrainment attractor and resonance attractor, have been observed depending on the initial distance between the centres of the initial location of the spiral core and the measuring point [34]. More recently, the resonance attractor was observed in the dynamics of a rigidly rotating spiral wave under this type of feedback [35, 40, 41]. Hence

in this work we will be interested in the features of the resonance attractor starting with a rigidly rotating spiral wave. In an extension of the local feedback control, the feedback signal is taken to be proportional to the average of the wave activity within sensory domain that covers only a part of the reaction layer. This is so-called non-local feedback control [36]. This method is investigated using sensory domains of various shapes and sizes.

In this research, the dynamics of rigidly rotating spiral waves in the light-sensitive $Ru(bpy)_3^{2+}$-catalyzed BZ reaction under local and non-local feedback control have been investigated as follows. The scope of this research including the detailed objectives are presented in Chapter 2. In Chapter 3, the properties of the BZ reaction are described and the dynamics of spiral waves and their control in this reaction is introduced. In Chapter 4, the materials and experimental methods are presented. Chapter 5 focuses on the results and discussion. Conclusions are drawn from all the results of this work in Chapter 6, and perspectives are also presented.

CHAPTER 2

OBJECTIVES

The aim of this research is to study the dynamics of a rigidly rotating spiral wave in the light-sensitive $Ru(bpy)_3^{2+}$-catalyzed BZ reaction. This system can be effectively controlled by applying an external illumination with an algorithm based on local or non-local feedback control. The objectives of this research are as follows:

1. To observe the dynamics of a rigidly rotating spiral wave under local feedback control. The hypocycloidal resonance attractors are studied and compared with the epicycloidal resonance attractors.

2. To investigate the dynamical response of the hypocycloidal resonance attractor on application of varying time delay (τ). The theoretical prediction is developed to analyze and explain the experimental results.

3. To observe the dynamics of the rigidly rotating spiral wave under the non-local feedback control derived from a square-shaped sensory domain and effect of size of the applied domain on the spiral wave dynamics.

CHAPTER 3

BACKGROUND AND LITERATURE REVIEW

Spontaneous pattern formation has been widely studied in many nonlinear systems [15, 16, 18, 20, 21, 23], especially in chemical oscillations [9]. The BZ reaction is one of the chemical oscillations which has been extensively studied. Patterns, such as target and spiral patterns, can be generated in the BZ reaction [6]. An intriguing example of these patterns is the spiral wave that has been observed, for example, in the light-sensitive $Ru(bpy)_3^{2+}$-catalyzed BZ reaction [33, 42]. The dynamics of spiral waves in this system can be effectively controlled by applying an external illumination [32, 33, 34, 36, 37]. This chapter presents an overview of the BZ reaction and an introduction to the dynamics of spiral waves in this system.

3.1 The Belousov-Zhabotinsky (BZ) reaction

3.1.1 Chemistry of the BZ reaction

Before the development of the BZ reaction, there were arguments that spontaneous temporal self-organization violated the Second Law of Thermodynamics, since the concentration of the reactants and products are increasing and decreasing with time while the free energy must monotonically decrease to the equilibrium value. However in the 1930s, Onsager, Prigogine, and others [1] realized that the laws of non-equilibrium thermodynamics [1, 2] could be applied to systems far from equilibrium. The free energy of the reaction is always decreasing since high free energy reactants are continuously converted to low free energy products. However intermediates can undergo oscillations on the way to equilibrium [43].

The origin of modern nonlinear chemical dynamics can be traced to Belousov [7], who discovered oscillating chemical reactions in the 1950s. The reaction was an inorganic

analog of the Krebs cycle, which is a key metabolic process in which a citric acid is an intermediate [7]. Later, in the 1960s, Zhabotinsky [8] studied intensively the same system and demonstrated that if the reaction mixture was left unstirred, spatial periodic variations of the intermediates can also occur. It was shown that the citric acid in the reaction can be replaced by malonic acid to obtain a better system, which did not produce a precipitate [8]. This reaction is called the Belousov-Zhabotinsky (BZ) reaction. The overall BZ reaction is the oxidative bromination by acidic bromate of an organic substrate such as malonic acid [44]:

$$2BrO_3^- + 3CH_2(COOH)_2 + 2H^+ \rightarrow 2BrCH(COOH)_2 + 3CO_2 + 4H_2O \quad (3.1)$$

The BZ reaction is catalyzed by an oxidation-reduction couple such as Ce^{4+}/Ce^{3+}, $Fe(phen)_3^{3+}/Fe(phen)_3^{2+}$ or $Ru(bpy)_3^{3+}/Ru(bpy)_3^{2+}$. The concentrations of some chemical intermediates can vary in time periodically [44]. During the oscillatory phase the ratio of the oxidized to reduced form of the catalyst and the concentrations of Br^-, and/or the other species can oscillate through hundreds or even thousands of cycles. The overall oxidation reaction then proceeds equilibrium. Figure 3.1 shows the temporal evolutions of $[Br^-]$ and $[Ce^{4+}]/[Ce^{3+}]$ ratio. After an initiation period, $[Ce^{4+}]/[Ce^{3+}]$ and $[Br^-]$ show oscillatory behaviour. The oxidation and reduction of this catalyst

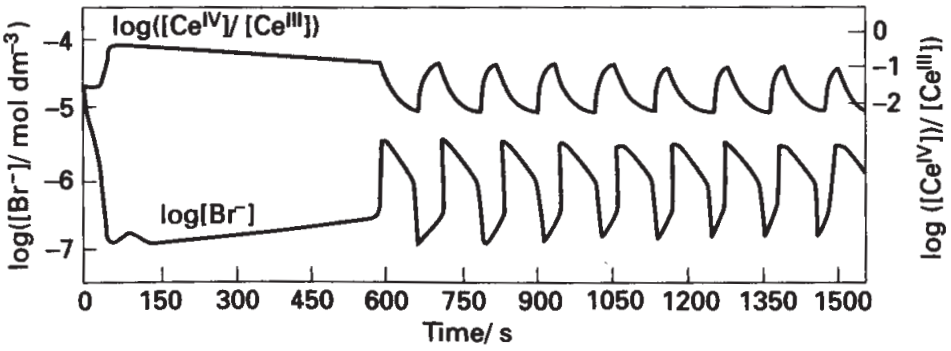

Figure 3.1: Potentiometric traces of log $[Br^-]$ and log $[Ce^{4+}]/[Ce^{3+}]$ in the BZ reaction (Redrawn from Field, Körös and Noyes in 1972). Initial conditions were $[CH_2(COOH)_2]_0$ = 0.032 M, $[KBrO_3]_0 = 0.063$ M, $[KBr]_0 = 1.5\times10^{-5}$ M, $[Ce(NH_4)_2(NO_3)_5]_0 = 0.001$ M, and $[H_2SO_4]_0 = 0.8$ M (from [45]).

causes the solution to change colour periodically from colourless to yellow [12].

3.1.2 FKN mechanism

The detailed mechanism for the BZ reaction was developed by Field, Körös, and Noyes in 1972 [45, 46, 47, 48]. This mechanism is called FKN mechanism and is used to account for the oscillations of the BZ reaction in terms of various chemical elements [12, 46, 47, 48]. A simple version of the FKN mechanism can be divided into three processes as indicated in Table. 3.1.

Table 3.1: FKN mechanism for the BZ reaction [46, 47, 48].

	Reaction	**Rate constant**
Process A		
	Reduction and exhaustion of Br^-	
$(A1)$	$BrO_3^- + Br^- + 2H^+ \rightarrow HBrO_2 + HOBr$	$k_{A1} = 2\ M^{-3}s^{-1}$
$(A2)$	$HBrO_2 + Br^- + H^+ \rightarrow 2HOBr$	$k_{A2} = 10^6\ M^{-2}s^{-1}$
$(A3)$	$3\cdot(Br^- + HOBr + H^+ \rightarrow Br_2 + H_2O)$	$k_{A3} = 8\times10^9\ M^{-2}s^{-1}$
	Bromination of organic substrate	
$(A4)$	$3\cdot(Br_2 + CH_2(COOH)_2 \rightarrow BrCH(COOH)_2 + Br^- + H^+)$	
(A)	$BrO_3^- + 2Br^- + 3CH_2(COOH)_2 + 3H^+ \rightarrow 3BrCH(COOH)_2 + 3H_2O$	
Process B		
	Radical generation and oxidation of Cat_{re}	
$(B1)$	$2\cdot(BrO_3^- + HBrO_2 + H^+ \rightarrow 2BrO_2^\bullet + H_2O)$	$k_{B1} = 10\ M^{-2}s^{-1}$
$(B2)$	$4\cdot(BrO_2^\bullet + Cat_{re} + H^+ \rightarrow HBrO_2 + Cat_{ox})$	$k_{B2} = 6\times10^5\ M^{-2}s^{-1}$
	$HBrO_2$ disproportion	
$(B3)$	$2HBrO_2 \rightarrow BrO_3^- + HOBr + H^+$	$k_{B3} = 2\times10^3\ M^{-1}s^{-1}$
(B)	$BrO_3^- + 4Cat_{re} + 5H^+ \rightarrow HOBr + 4Cat_{ox} + 2H_2O$	
Process C		
(C)	$2Cat_{ox} + HOBr + 2CH_2(COOH)_2 + BrCH(COOH)_2 + 2H_2O \rightarrow 2Cat_{re} + 3HOCH(COOH)_2 + 2Br^- + 4H^+$	

Process A is the reduction of BrO_3^- by Br^- through a series of oxygen atom transfers (2-electron reduction) producing HOBr and Br_2, and the subsequent bromination of $CH_2(COOH)_2$ by Br_2. It is dominant at high $[Br^-]$, but its net effect is only the removal of Br^-. When $[Br^-]$ falls below a critical value, $[Br^-] \leq (k_5/k_2)[BrO_3^-]$, the system shifts to Process B. The important mechanism in Process B is the autocatalytic generation of $HBrO_2$ with the concurrent oxidation of the metal catalyst. The reaction of $HBrO_2$ with BrO_3^- to yield the radical species $BrO_2^\bullet$ (Reaction $B1$)becomes competitive with removal of $HBrO_2$ by Br^- (Reaction $A2$). The oxidation of Cat_{re} to Cat_{ox} with the production of $[HBrO_2]$ arises from the single-electron oxidant $BrO_2^\bullet$ (Reaction $B2$). The autocatalytic production of $HBrO_2$ is eventually limited by the disproportional reaction (Reaction $B3$). The next step is the oxidation of $CH_2(COOH)_2$ and $BrCH(COOH)_2$ by Cat_{ox} in Process C, which reduces Cat_{ox} back to Cat_{re} and provides a negative feedback loop by the production of Br^-. Thus this process brings Process A back when $[Br^-]$ reaches a sufficiently high level. The three processes, which are proposed as essential components of the BZ reaction, take place successively to constitute one oscillation and the sequence is then repeated. When Br^- is consumed to a critical concentration in Process A, the autocatalysis in Process B takes place and the Br^- is regenerated in Process C. Thus oscillations may occur whenever Process B is linked with other processes.

3.1.3 Oregonator model

Based on the FKN mechanism, Field and Noyes also proposed a simplified version of the BZ reaction involving the behaviour of a three-variable scheme, called Oregonator model [46]. This model consists of five irreversible steps with six chemical components from the elementary reactions in the FKN mechanism as shown in Table. 3.2 [47, 49, 50].

Table 3.2: Comparison of the Oregonator model and the FKN mechanism [47, 49, 50].

	Oregonator model		**Comparison with FKN**
$(O1)$	$A + W \xrightarrow{k_1} U + P$	$k_1 = 2\ \mathrm{M^{-3}s^{-1}[H^+]^2}$	$(A1)$ slow reaction
$(O2)$	$U + W \xrightarrow{k_2} 2P$	$k_2 = 10^6\ \mathrm{M^{-2}s^{-1}[H^+]}$	$(A2)$ fast reaction; low[$HBrO_2$]
$(O3)$	$A + U \xrightarrow{k_3} 2U + 2V$	$k_3 = 40\ \mathrm{M^{-2}s^{-1}[H^+]}$	$(B1$ and $B2)$ autocatalysis of $HBrO_2$
$(O4)$	$2U \xrightarrow{k_4} A + P$	$k_4 = 2 \times 10^3\ \mathrm{M^{-1}s^{-1}}$	$(B3)$ limitation of [$HBrO_2$]
$(O5)$	$B + V \xrightarrow{k_5} fW$	$k_5 = 0.4\ \mathrm{M^{-1}s^{-1}}$	(C) regeneration of [Br^-]

$U \equiv HBrO_2$, $W \equiv Br^-$, $V \equiv Cat_{ox}$, $A \equiv BrO_3^-$, $P \equiv$ HOBr , and $B \equiv BrCH_2(COOH)_2$, the rate constants k_1 to k_5, and the stoichiometric factor f are the variables. $[A]$ and $[B]$ are held constant as is the hydrogen ion concentration (included in the rate constants). The product P, which goes on to brominate malonic acid, does not appear in the rate equations because only the features essential to the dynamical behaviour are included in this model [46, 47, 49, 51].

If the elementary steps of the model are all assumed to be irreversible [46, 47, 49], the kinetic behaviour of the Oregonator can be described by a system of the differential equations involving the concentrations of the three intermediates with respect to time as follows [47, 49]:

$$\begin{aligned} \frac{dU}{dt} &= k_1AW - k_2UW + k_3AU - 2k_4U^2, \\ \frac{dV}{dt} &= 2k_3AU - k_5BV, \\ \frac{dW}{dt} &= -k_1AW - k_2UW + fk_5BV. \end{aligned} \tag{3.2}$$

The concentrations are transformed into the dimensionless variables defined by [49]

$$\begin{gathered} u = \frac{2k_4}{k_3A}\,U, \quad w = \frac{k_2}{k_3A}\,W, \quad v = \frac{k_4k_5B}{(k_3A)^2}\,V, \quad t = k_5B(time), \\ \varepsilon = \frac{k_5B}{k_3A}, \quad \varepsilon' = \frac{2k_ck_4B}{k_2k_3A}, \quad \text{and} \quad q = \frac{2k_1k_4}{k_2k_3}\,. \end{gathered} \tag{3.3}$$

Substituting Eq. (3.3) into Eq. (3.2) yields the system of three differential equations as follows:

$$\begin{aligned} \frac{du}{dt} &= \frac{qw - uw + u(1-u)}{\varepsilon}, \\ \frac{dv}{dt} &= u - v, \\ \frac{dw}{dt} &= \frac{-qw - uw + fv}{\varepsilon'}. \end{aligned} \tag{3.4}$$

Equations (3.4) can be reduced to a two-variable system with only $\mathrm{d}u/\mathrm{d}t$ and $\mathrm{d}v/\mathrm{d}t$ equations. The small parameters ε' and ε may thus cause any oscillatory response to have the form of relaxation oscillations. When $\varepsilon' \ll \varepsilon \ll 1$, i.e., ε' is very small, the bromide ion concentration will always adjust rapidly to the instantaneous composition of the reacting mixture. Thus the $[\mathrm{Br}^-]$ will always remain close to a value such that the right-hand side is equal to zero ($dw/dt = 0$) [49, 52]:

$$w = \frac{fv}{q+u}\,. \tag{3.5}$$

Substituting Eq. (3.5) into Eq. (3.4), the resulting two-variable system is governed by the rate equations describing the chemical reaction without the diffusion terms:

$$\begin{aligned} \varepsilon\frac{du}{dt} &= u(1-u) - \frac{u-q}{u+q}fv &&= f(u,v), \\ \frac{dv}{dt} &= u - v &&= g(u,v). \end{aligned} \tag{3.6}$$

Reaction-diffusion BZ system

The reaction-diffusion BZ system consists of molecular transport through diffusion and chemical reaction. The diffusion term can be added to the Oregonator model in Eq. (3.6) to give [49]:

$$\begin{aligned} \frac{\partial u}{\partial t} &= \frac{1}{\epsilon}(u - u^2 - fv\frac{u-q}{u+q}) + D_u\nabla^2 u, \\ \frac{\partial v}{\partial t} &= u - v + D_v\nabla^2 v, \end{aligned} \tag{3.7}$$

where u and v describe the concentration of autocatalytic species ($HBrO_2$) and the oxidized form of the catalyst (Cat_{ox}), respectively. $f(u,v)$ and $g(u,v)$ represent the chemical kinetic reactions of state variables u and v. $\epsilon \ll 1$, where ϵ is proportional to the ratio of the diffusion rate with respect to the chemical reaction rate. D_u and D_v are the transport (diffusion) coefficients for u and v [43, 49]. The coupling between the diffusion and chemical reaction can lead to the spatial organization generating the chemical waves in the BZ reaction. [50]. Note that in the system used in this work the catalyst of the BZ reaction is immobilized in the silica hydrogel with the result that its diffusion coefficient $D_v = 0$. However, for aqueous solution, it has a finite value, which is generally taken to be equal to the diffusion coefficient of the autocatalytic species ($D_u = D_v$) [50, 53].

3.1.4 The light-sensitive catalyst $Ru(bpy)_3^{2+}$ in the BZ reaction

In the BZ reaction, the light-sensitive ruthenium bipyridyl complex ($Ru(bpy)_3^{2+}$) is used as a catalyst [32] for studying the effect of external forcing on spiral wave dynamics. The catalyst $Ru(bpy)_3^{2+}$ promotes the autocatalytic production of $HBrO_2$, which is the activator species in the BZ system. An applied illumination enhances the production of the inhibitor Br^-. The excitability of the medium depends on the externally applied illumination. For examples, a low light intensity corresponds to high excitability of the medium, whereas high light intensity corresponds to low excitability. This provides an experimentally accessible method to control spiral wave dynamics [32], since the light intensity influences parameters such as the wavelength, period of rotation and the diameter of the spiral core.

The photosensitive catalyst tris(2, 2′-bipyridine)ruthenium(II) complex ($Ru(bpy)_3^{2+}$) is a metal co-ordination compound. A ruthenium atom is bonded to three 2, 2′-bipyridine ligands in such a way that the metal is located at the centre of the octahedron arrangement of the nitrogen atoms of the ligands, as shown in Fig. 3.2. Upon light absorption,

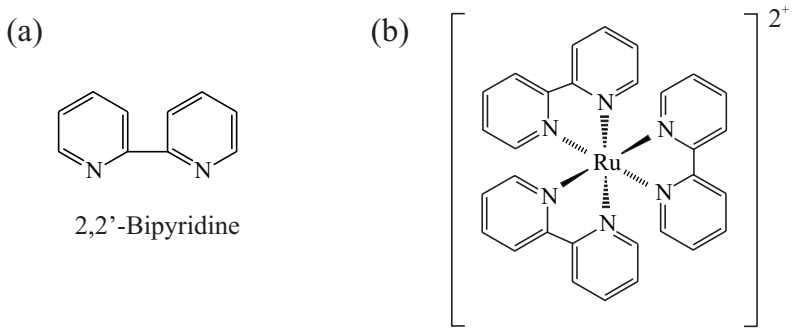

Figure 3.2: The structure of $Ru(bpy)_3^{2+}$ [32]: (a) the 2,2'-bipyridine and (b) the ruthenium ion is coordinated by three bipyridyl ligands to form $Ru(bpy)_3^{2+}$.

the $Ru(bpy)_3^{2+}$ complex becomes photochemically excited:

$$Ru(bpy)_3^{2+} + h\nu \quad \rightarrow \quad {}^*Ru(bpy)_3^{2+} \tag{3.8}$$

The exited state can relax to the ground state nonradiatively or radiatively in the form of photoluminescence, and has chemical properties, which differ from those of the ground state. The maximum absorption lies at $\lambda = 452$ nm [32].

Several mechanisms have been proposed to account for the light-sensitive $Ru(bpy)_3^{2+}$-catalyzed BZ reaction which shows a variety of photoinduced behaviours including photoinhibition (transitions from oscillations to steady states) [54], photoinduction (transitions from steady states to oscillations) [55, 56], and irregular oscillations [57] under a constant illumination of light. On the basis of the FKN mechanism (see Section 3.1.2), it is reasonable to consider that the inhibitory effects of illumination result from the formation of excess bromide ions due to the photochemical reaction of $Ru(bpy)_3^{2+}$ [54].

Kuhnert [32] has proposed that absorption of light can induce a dramatic change in the redox properties of $Ru(bpy)_3^{2+}$ and $^*Ru(bpy)_3^{2+}$. The excited state of this catalyst is able to reduce bromate to the inhibitory bromide directly via [32]:

$$6{}^*Ru(bpy)_3^{2+} + BrO_3^- + 6H^+ \quad \rightarrow \quad 6Ru(bpy)_3^{3+} + 3H_2O + Br^- \tag{3.9}$$

In the same manner, Jinguji *et al.* [54] had reported the inhibitory effect of light and explained the observation based on the FKN mechanism. The photoexcited $^*Ru(bpy)_3^{2+}$

serves to reduce the reactant BrO_3^- to Br^-, which is the primary autocatalysis inhibitor in the BZ reaction.

$$BrO_3^- + HBrO_2 + 2^*Ru(bpy)_3^{2+} + 3H^+ \rightarrow 2Ru(bpy)_3^{3+} + HBrO_2 + 2H_2O \quad (3.10)$$

Furthermore, the photochemical reduction of BrO_3^- to Br^- in the presence of oxygen has also been proposed by Reddy *et al.* [57]. They suggested a scheme involving the photochemical production of the autocatalyst $HBrO_2$ and the inhibitor Br^- to account for the illumination effect on the $Ru(bpy)_3^{2+}$-catalysed BZ reaction [54, 57].

Extended Oregonator model

An additional constant bromide flow ϕ observed under a constant illumination, is assumed and the velocity of the bromide release is proportional to the light intensity. The wave propagation in the medium can be simulated by the two-variable Oregonator model [46, 49] in Eq. 3.7 as follows [58]:

$$\begin{aligned} \frac{\partial u}{\partial t} &= \frac{1}{\epsilon}[u - u^2 - (fv + \phi)\frac{u - q}{u + q}] + D_u \nabla^2 u, \\ \frac{\partial v}{\partial t} &= u - v + D_v \nabla^2 v, \end{aligned} \quad (3.11)$$

where the photochemically produced bromide flow Φ is scaled to give the dimensionless variable $\phi = (2k_4/(k_3 A)^2)\Phi$ [49, 58].

3.2 Waves and patterns in chemical reactions

As previously mentioned, the coupling between diffusion and chemical reaction generates chemical waves in excitable media. The BZ reaction, which is an example of excitable media, supports experimental studies of the chemical waves. The spiral wave is one of the fascinating wave patterns in this reaction [9, 10, 11, 44]. The characteristic properties of spiral waves in the BZ reaction have been extensively studied both experimentally [9, 16, 24, 25, 26, 27, 59] and theoretically [10, 11, 28, 30, 31, 50, 60].

3.2.1 Chemical waves

Chemical fronts and waves are variations in concentrations of chemical species, or possibly in other state variables, which travel in space and occur in the nonlinear reactive systems far from equilibrium [44]. Travelling waves in the BZ reaction can be continuously generated by new waves being born and moving through the medium. The wave fronts of chemical activity may have various shapes depending on the geometry, such as plane waves in one dimension, target patterns and spiral waves in two dimensions, and scroll waves in three dimensions.

Chemical waves in one spatial dimension are easiest to explain and simulate numerically. The wave profile in space resembles the concentration with time profile for the homogenous reaction [48]. The waves in three dimensions are rather difficult to obtain experimentally and give rise to highly dramatic structures. For an intermediate case, the wave in two-dimensional system is the one that frequently occurs in nature, and that can be easily created in the laboratory [6, 44]. Moreover, the two-dimensional wave provides some of the most beautiful and interesting phenomena in chemistry.

In a uniform two-dimensional medium, the wave emanating from a point produces a circular front since it travels at the same velocity in all directions. In the presence of a periodic or continuous stimulation, it gives rise to a pattern of concentric circles,

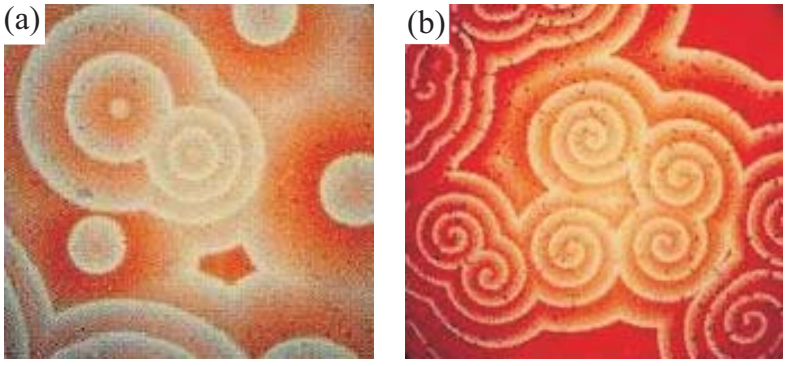

Figure 3.3: Patterns of the two-dimensional wave in the BZ reaction: (a) target patterns and (b) spiral waves (from [51]).

known as a target pattern [6, 44], as shown in Fig. 3.3(a). The spontaneous wave of the target pattern appears to depend on heterogeneitic in the medium, such as dust particles or defects on the surface. Spiral-shaped waves can be formed by the disruption of an expanding wave front, such as an air blast from a pipette onto the surface of the reaction solution [9, 6, 16], as shown in Fig. 3.3(b). The open ends of the circular wave are then the starting points of an evolution toward a structure composed of a pair of counterrotating spiral waves with highly regular geometry [44]. The rotating spiral wave is currently the subject of extensive experiments in the BZ reaction.

3.2.2 Properties of spiral waves in two dimensions

An interesting type of two-dimensional waves in excitable media is a rotating spiral wave. The spiral wave rotates around a core that shows unique forms of rotation [11]. These patterns of the rotation of the spiral core can be represented by a tip trajectory.

3.2.2.1 Motions of spiral tip

In the simplest case, the spiral wave rotating rigidly around a fixed circular path enclosing a central core region, as shown in Fig. 3.4(a), is called a rigid rotation [9]. The spiral tip moves around a circle with a constant rotation frequency f_0 and radius r_0.

More generally, the dynamics of spiral wave is described by a noncircular trajectory. Such two-frequency compound motion is referred to as meandering [9, 61]. The path of the spiral tip traces out a flowerlike pattern. Figure 3.4(b-c) show the spiral tip that describes a hypocycloid-like orbit with outward petals and an epicycloid-like orbit with inward petals, respectively [62, 63, 64]. A primary motion corresponds to the orbit of a spiral tip exhibiting simple rotation with frequency f_1 and radius r_1. The another rotation is a secondary motion with frequency f_2 and radius r_2. The hypocycloidal motion with outward petals is illustrated in Fig. 3.4(b), where the primary circle r_1 orbits the secondary circle r_2 in one direction with frequency f_2 and spins about its centre in the opposite direction with frequency f_1. On the other hand, the epicycloidal motion

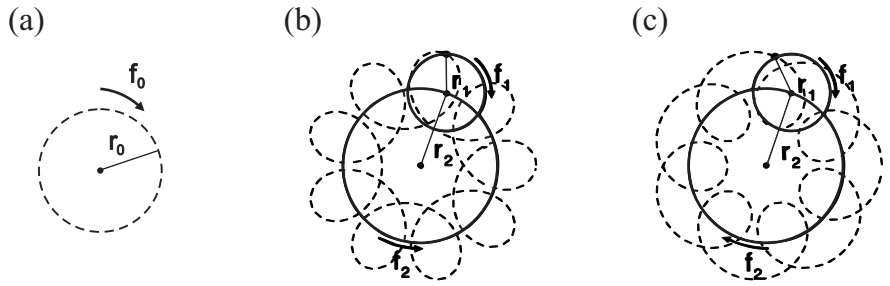

Figure 3.4: Orbits of the spiral tip for: (a) a rigid rotation, and two types of meandering motion with (b) outward petals (hypocycloid-like orbits) and (c) inward petals (epicycloid-like orbits) [63, 66]. Dashed line represents the motion of the spiral tip. The rigid rotation occurs with a frequency f_0 and a circular radius r_0. For meandering motion, the compound spiral tip is generated by superposing two circular motions (solid line) having radii r_1 and r_2, and rotation frequencies f_1 and f_2, respectively. Filled arrows indicate the rotation direction of the spiral tip and the spiral core with f_1 and f_2, respectively.

rotates in both directions in the same sense and was inward petals (see Fig. 3.4(c)).

Meandering rotations are observed more often than rigid rotation in experiments with the BZ reaction [24, 26, 65]. Rigid rotations can be observed in the limiting cases of very high or very low excitability or small refractoriness of a medium [62, 64]. For a given composition of the BZ reaction, the trajectories of the spiral tip depend on various parameters, which influence the excitability of the medium [26, 59, 63, 66]. For instance, the excitability is reduced by increasing the concentration of bromate at which the transition from rigidly rotating to meandering spiral waves occurs [26]. In the case of the photosensitive $Ru(bpy)_3^{2+}$-catalyzed BZ reaction, the transition from a meandering to a rigidly rotating spiral wave can be induced by increasing the illumination intensity (see Fig. 3.5). Moreover, the core radius of these rigidly rotating spirals significantly increases, as the light intensity is further increased [59].

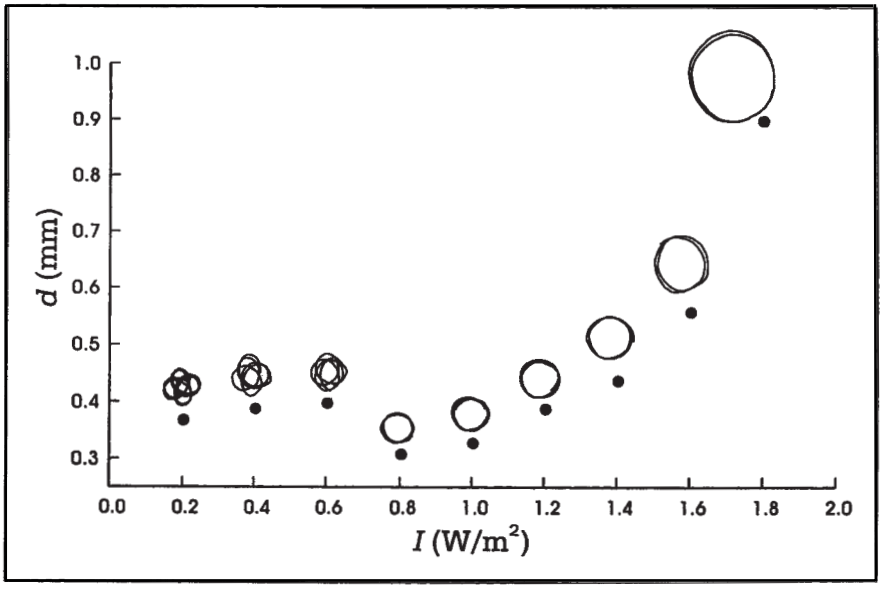

Figure 3.5: Transition from meandering to rigid rotation by variation of the light intensity in the $Ru(bpy)_3^{2+}$-catalyzed BZ reaction from 0.2-1.8 W m^{-2} (from [59]).

3.2.2.2 Theoretical analysis of rotating spiral waves

The kinematical description of the spiral wave can be used to explain the motion of curves with free ends. The curves evolve to a steadily rotating spiral wave [10] or a complicated meandering regime [10, 28]. The first kinematical model for the description of processes in excitable media was proposed by Wiener and Rosenblueth [67], who found that a curve rotating around an obstacle forms a spiral. It constitutes an involute of this obstacle and approaches the Archimedian spiral far from it [67, 68]. In this work, the rigidly rotating spiral wave is focused on because this motion can be characterized by the simplest approximations of its form and rotation frequency.

A description of a freely rotating spiral wave in an excitable medium is based on the assumption that the normal propagation velocity of a curved wave front is a linear function of its curvature. The curvature of any point on a wave front can be qualitatively characterized in terms of its *radius of curvature*—the radius of the circle that best fits the front in the neighbourhood of the point in question [43]. If the radius of curvature is

R, the curvature κ is defined as $1/R$. The curvature is considered positive and negative for a convex and a concave wave fronts, respectively. Thus a plane wave has $\kappa = 0$ [43]. The relationship between the velocity of the curved wave front and the curvature κ is given by the eikonal equation [43, 69]:

$$v = v_0 + D\kappa, \tag{3.12}$$

where v is the normal velocity of the wave front, v_0 is the velocity of the plane wave and D is the diffusion coefficient of the activator species in the medium. The value of the propagation rate of a curved front is substantially influenced by its curvature. This is a consequence of the diffusion of elements of the excitable medium [43].

Kinematical considerations

The kinematic motion of a circulating wave of excitation in a two-dimensional excitable medium was analyzed by Zykov *et al.* [28, 60]. During the steady circulation of an excitation wave, the form of the excited region remains unchanged in time and it performs a uniform rotational movement with a certain angular velocity ω about the centre of rotation [28].

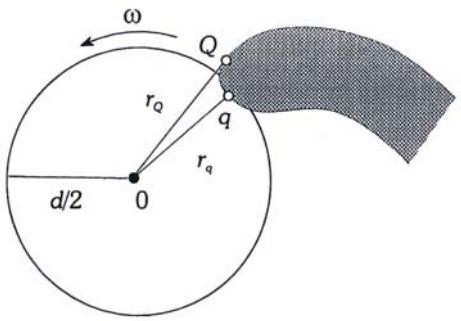

Figure 3.6: Diagram of a stationary rotating spiral wave, where d is the diameter of the spiral core and ω is the rotation frequency of the spiral tip. The circular path shows the trajectory of the spiral tip. Points q and Q on the contour line of the excitation wave (shaded area) correspond to the shortest and the tangential radius-vectors, r_q and r_Q, respectively (from [59]).

A Diagram of the rigidly rotating spiral wave is shown in Fig. 3.6. Points q and Q on the contour line of the excitation wave correspond to the shortest and the tangential radius vectors, r_q and r_Q, respectively. Each point of the contour line is involved in a visible rotatory motion that occurs at the speed $u = \omega r$ [28], where ω is the rotation frequency and r is the distance from the rotation centre. On the other hand, the real displacement of the wave front occurs in the normal direction with respect to the contour line due to the physical nature of travelling excitation waves [28, 59].

Point q does not move in the normal direction. Its location can be determined as the intersection of contour lines plotted at two close instants [59]. This corresponds to the definition of the spiral tip used in our experiments (see Section 4.3.5.1). The circle in Fig. 3.6 is the trajectory of the spiral wave tip determined as the intersection of contour lines plotted at two close instants separated by time step $\Delta t = 3.12$ s [59]. In the theoretical limit $\Delta t \to 0$ the spiral wave tip should coincide with point q [59].

Point Q also plays an important role in the kinematical description of the spiral wave, because its visible rotation around the centre coincides with the displacement in the normal direction to the wave front. The trajectory of the point Q can be considered as the boundary of a circular hole around which the spiral wave circulates. Under the assumption of constant normal propagation velocity $v = v_0$, it was shown that the shape of the spiral around such a hole represents the involute of the hole [9, 67].

3.3 Controlling of the spiral wave dynamics

Under the illumination, the $Ru(bpy)_3^{2+}$ catalyst of the BZ reaction becomes photochemically excitable. The excitability of the medium can be controlled by the applied light intensity, which influences the dynamics of the spiral wave. Thus, the light-sensitive $Ru(bpy)_3^{2+}$-catalyzed BZ system allows methods to control the spiral wave dynamics by an external illumination, for instance harmonic modulations of the illumination [33, 61, 70, 71] and feedback mechanism [34, 35, 36, 38]. The feedback algorithms

are based on collecting data on the activity level of the system and transforming this information to a spatially uniform modulation of the excitability of the medium.

3.3.1 Periodic forcing of the spiral wave

Periodic modulation of the external illumination can cause dramatic changes in the dynamics of a spiral wave. The induced variations of the trajectory, especially the shift of the spiral wave core, will accumulate over a period of time. Results from two types of periodic modulation have been reported: There are based on applying an external illumination with sinusoidal [33, 61, 70] and pulsatory [71] algorithms. In sinusoidal modulation, the intensity level of an applied illumination is given by $\phi(t) = \phi_0 + Asin(2\pi/T_m)$ [33, 61, 70]. A is amplitude and T_m is the modulation period T_m. Pulsatory modulation is achieved by the repetitive application of short light pulses with a selected duration and amplitude. The sequence of the light pulses is adjusted by varying the periods of the modulation T_m [71].

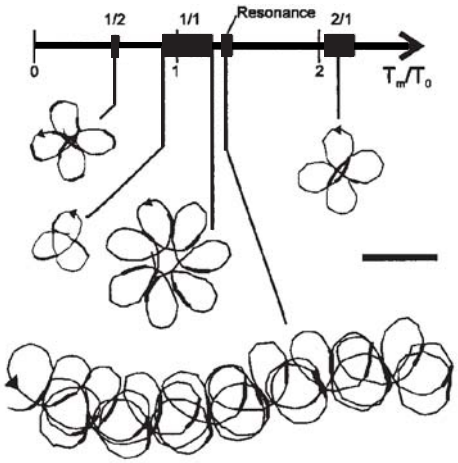

Figure 3.7: Observed bands of entrainment $(1/2, 1/1, 2/1)$ and resonance along the axis of normalized modulation period. Representative trajectories of the bands were shown. Thick segments of the trajectories indicate the application of light pulses. Scale bar: 0.5 mm (from [71]).

An interesting phenomenon under the periodic modulation of the applied light intensity, namely, entrainment occurs originally for a spiral with the meandering rotation

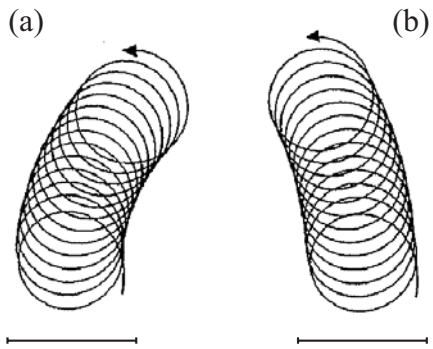

Figure 3.8: Resonance drift of the rigidly rotating spiral wave under the sinusoidal modulation computed from Eq. 3.11 with $\epsilon = 0.05, q = 0.02$, $f = 3.5$, $\phi_0 = 0.01$, and modulation amplitude $A = 0.0002$ in term $\phi(t) = \phi_0 + Asin(2\pi t/(T_m))$. Modulation period: (a) $T_m = 6.6$ and (b) $T_m = 6.7$. Scale bar: 10.0 (from [72]).

describing the hypocycloidal trajectory, if the stimulation period is chosen to be close to T_0 [33]. The unperturbed meandering tip is characterized by two rotation periods: the oscillation period T_0 is measured at its centre of the tip trajectory and another period T_∞ is measured at a point far from the centre [33, 71]. An entrainment band of an applied stimulating period T_m/T_0 was found, each characterized by a rational number r/s, where r is the number of lobes completed during s periods of external modulations [71]. The most pronounced entrainment bands are shown (labelled 1/2, 1/1 and 2/1) on the axis of the modulation period T_m (see Fig. 3.7). Within the entrainment bands, the trajectory describes hypocycloidal shapes, where the spiral tip is stimulated with modulation period T_m. Figure 3.7 shows entrained trajectories, which had been observed when applying pulsatory modulation of the light intensity [71].

Furthermore, the resonance condition is fulfilled, if the spiral is stimulated with the wave period T_∞ measured far from the centre [72]. In contrast to the case of the entrainment, no synchronization with the external signal occurs. This is natural because in this case the modulation period differs sufficiently from the period of one lobe, and consequently the phase of external pulses varies from lobe to lobe [71]. Under the pulsatory modulation of an illumination, the regime of a resonance drift

Far from the rotation centre, the meandering spiral resembles the rigidly rotating spiral: it has the form of the Archimedian spiral and rotates uniformly at a period T_∞ [72, 61]. Figure 3.8 shows the resonance drifts for the rigidly rotating spiral wave. Two different values of the frequency of external forcing ω_m are applied under sinusoidal modulation with $\omega_m > \omega_r$ and $\omega_m < \omega_r$, where ω_r is the frequency of the unperturbed spiral, as shown in Fig. 3.8(a-b), respectively. In both cases, the tip moves along a cycloid. The tip move around a circle with radius r_0, and then the tip moves along a motion of the centre of core on a large circle with radius R_c. The radius grows as the frequency of external force ω_m approaches the frequency ω_r. When $\omega_m = \omega_r$ (perfect resonance), the core centre moves with the constant velocity along a straight line. The velocity of the core motion is proportional to the amplitude of external forcing and its direction depends on the initial phase of the spiral wave [60, 72].

3.3.2 Feedback control mechanism

As previously mentioned in the section on periodic modulation, even small changes in the system dynamics, e.g., aging of the chemical medium, can change the wave period T_∞. The resonance regime cannot be maintained over long times without frequently adjusting the modulation period [71]. The feedback mechanism of the applied external illumination was introduced by adjusting the period of modulation to the measured wave period [34].

3.3.2.1 Local feedback control

Local feedback control was introduced to control the dynamics of a spiral wave by applying a light pulse of amplitude A and duration about 10 - 20% at the instant when the wave front passes a particular measuring point, or after some time delay. This mechanism had been investigated originally for a spiral with a meandering tip [34].

Under this feedback control two dynamical regimes called entrainment and resonance attractors have been observed [34]. The entrainment attractor occurs if the measuring

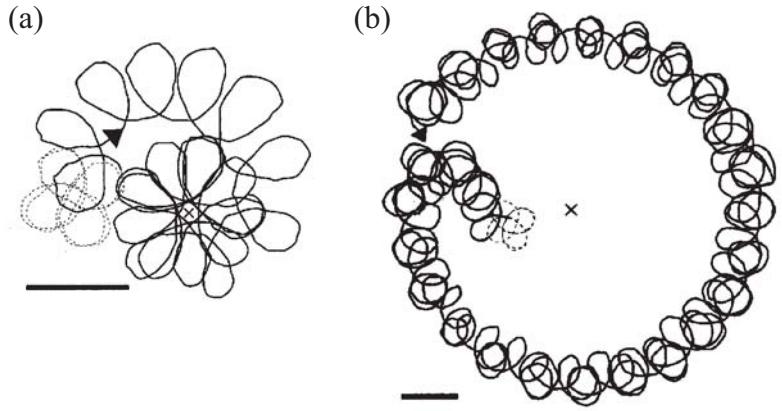

Figure 3.9: Two attractors observed in the light-sensitive BZ reaction forced by a sequence of short light pulses applied at every moment when a wave front passes through the measuring point (cross): (a) entrainment attractor, the distance between the centre of the unperturbed trajectory (dashed line) and the measuring point is $R_0 = 0.49$ mm, and (b) resonance attractor, the initial distance is $R_0 = 0.57$ mm. Scale bar: 0.5 mm (from [34]).

point is located close to the centre of the unperturbed trajectory as shown in Fig. 3.9(a) ($R_0 \approx 1/3$ of the spiral wavelength [34, 71]). As the period of the external modulation approaches T_0, and the tip moves on a hypocycloid in perfect synchrony with the external signal. The regime of the entrainment attractor exhibits the properties of entrained frequencies as it occurs in similar systems with periodic modulation (see Section 3.3.1) [33, 72]. The increase in the number of lobes with time delay can be interpreted as an effect of the phase of the applied stimulus, and corresponds to the variety of the trajectories induced by different phase relationships within an entrainment band [33]. For larger R_0, the tip is found to describe a resonance attractor as shown in Fig. 3.9(b). The average period of the triggered external stimuli is close to T_∞ corresponding to the resonance drift under the periodic modulation (see Section 3.3.1). There is no strict synchronization as obtained in the case of the entrainment attractor [71]. Both regimes are stable with respect to a small shift of the measuring point, which always constitutes the symmetry centre of attractor orbits [34].

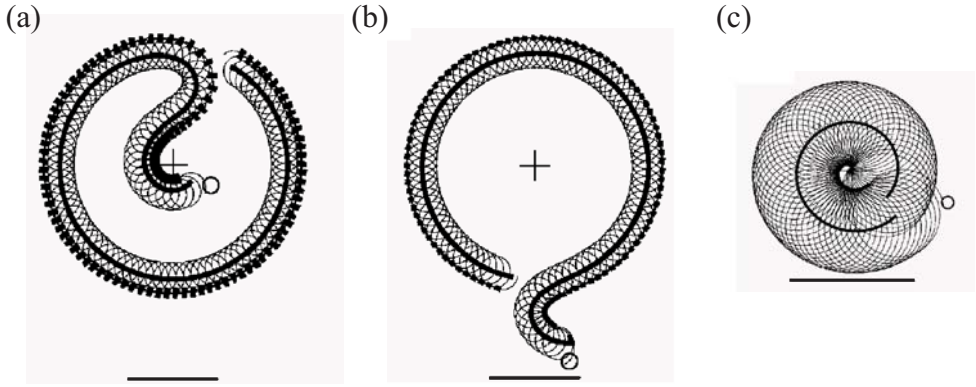

Figure 3.10: Trajectories of the spiral wave tip (thin solid line) computed with the Oregonator model (Eq. 3.11): (a), (b) with $\tau = 0$, $A = 0.004$, and $D = 0.3$ for different initial distances $R_0 = 5.5$ and 39.0, respectively; and (c) with $\tau = 0$, $A = 0.003$, and $D = 0.1$. Scale bar: 10. The small open circles indicate the initial location of the spiral wave tip. Thick segments correspond to the application of impulses (from [40]).

More recently, this kind of local feedback control was also applied to rigidly rotating spiral wave [35, 40, 41] characterized by one rotation period. In this case, only the resonance attractor was observed and most of trajectories of this attractor were epicycloids with their petals directed inwards as shown in Fig. 3.10(a-b). Epicycloidal resonance attractors have been observed both in experiments [35] and numerical simulation [40]. However, it was reported in the numerical study [40] that very small resonance attractors may assume a hypocycloidal shape, i.e., with the outward directed petals as shown in Fig. 3.10(c). This latter case has not yet been investigated in the laboratory, and we will show that, in fact, hypocycloidal resonance attractors exist for rigidly rotating spiral waves and that their occurrence depends sensitively on the initial conditions chosen for the feedback signal. Thus, the latter case will be shown in the present work (see Section 5.1).

Theoretical analysis of the resonance attractor

A theory for explaining the features of the resonance attractor which starts with a rigidly rotating spiral was proposed by Karma *et al.* [40]. The main idea is to describe

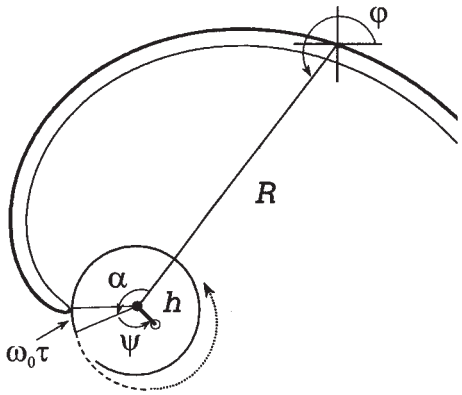

Figure 3.11: A spiral wave rotating around a circular core at the time when the wave front (thick solid line) passes through the measuring point (thin cross). The application of the illumination impulse induces a shift of the spiral core centre (filled circle) to the new position (open circle) resulting in a shifted steady-state circular trajectory of the spiral tip (dotted curve). The trajectory of the spiral wave during some intermediate process is shown by a dashed curve (from [35]).

the dynamics of the spiral core in terms of an iterative map that gives the new location of the core after each applied pulse. The position of the core centre in polar coordinates (R, φ) with the origin at the measuring point is shown in Fig. 3.11. The shape of the spiral front can be given by the function $\Theta(r)$, where (r, Θ) is the polar coordinate system with the origin at the core centre and $\Theta = 0$ corresponds to the location of the spiral tip.

Application of the pulse induces the displacement of the core centre as shown in Fig. 3.11. The displacement h of the core centre after application of the ith pulse is indicated as a short straight solid line. The direction of this displacement is determined by the angle ψ which is measured with respect to the line connecting the core centre and the position of the spiral wave tip at the instant when the ith pulse is applied. The distance R is measured between the spiral core and the measuring point. The angle α describes a rotation around the spiral core. This angle is measured from the line connecting the core centre and the measuring point to the line from the core centre to the starting pulse. α_i, R_i, and φ_i denote the value of these variables evaluated at the

time t_i at which the ith external impulse is applied. It is straightforward to derive the following map describing the motion of the core centre [35, 40]:

$$\alpha_i = \omega_0\tau - \Theta(R_i), \tag{3.13}$$

$$R_{i+1}^2 = R_i^2 + h^2 - 2R_i h\cos(\psi + \alpha_i), \tag{3.14}$$

$$\varphi_{i+1} = \varphi_i + \arcsin[(h/R_{i+1})\sin(\psi + \alpha_i)]. \tag{3.15}$$

The system of Eqs. (3.13)- (3.15) analyzed under the assumptions $h/R_i \ll 1$ and $\mid \psi \mid -\pi/2 \ll 1$ becomes accurate in the limit of a small amplitude and short impulse. In this case, Eqs. (3.14) - (3.15) become

$$R_{i+1} = R_i + h\sin(\psi)\sin(\alpha_i), \tag{3.16}$$

$$\varphi_{i+1} = \varphi_i - h\sin(\psi)\cos(\alpha_i)/R_{i+1}. \tag{3.17}$$

An analysis of the map Eqs. (3.13)- (3.14) and Eq. 3.16 shows that a more accurate analysis is accomplished by using the original map [40]. Indeed, the analysis of this map yields,

$$\omega_0\tau = \Theta(R_s) \pm \arccos[h/(2R_s) - \psi + 2m\pi], \tag{3.18}$$

when m is a positive integer. Linear stability analysis shows that several stable branches corresponding to Eq. 3.18 are plotted in Fig. 3.12. In the case $\psi > 0$, one part of each curve in Fig. 3.12 with $R_s > r_Q$ is associated with a negative slope. This part corresponds to a stable motion for any odd k. The another part with $R_s < r_Q$ corresponds to a positive slope and is stable for any even k. All stable (unstable) steady states of Eqs. (3.13) and (3.16) are shown as solid (dotted) lines in Fig. 3.12. For $\psi < 0$, the opposite situation is true and all dotted (solid) lines in Fig. 3.12 correspond to stable (unstable) attractors. It is important to emphasize that the dotted (solid) line corresponding to a given unstable steady-state k for $\psi > 0$ ($\psi < 0$) plays the role of a separatrix between the basins of attraction of the stable attractors $k-1$ and $k+1$. The set of these separatrices determines that the attractor is selected from an arbitrary

initial condition. It can be noted that the thin horizontal line in Fig. 3.12 corresponds to $R_s = r_q$. If the distance between the spiral core centre and the measuring point is smaller than r_q, the wave front never traverses the measuring point and no light impulse is generated. Thus, in this case, the attractor is simply the unperturbed rigid rotation of the spiral wave around a circular core [35, 40].

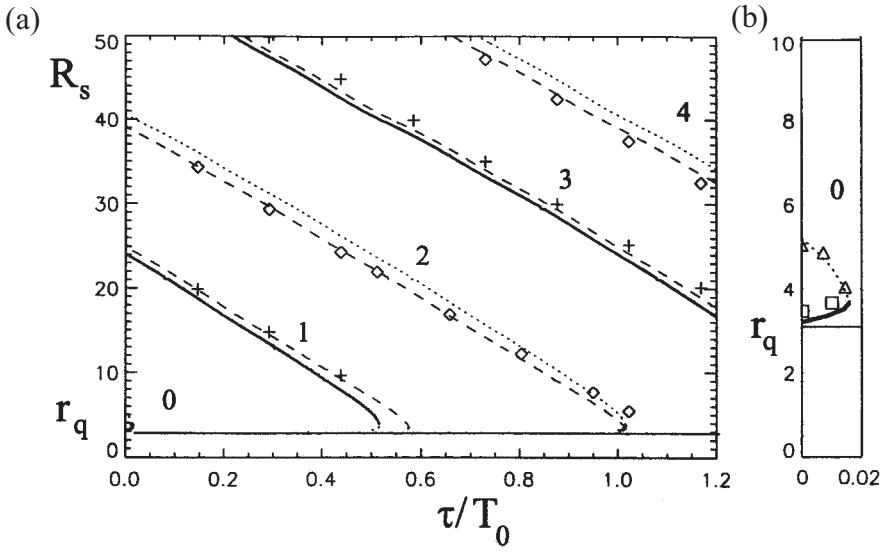

Figure 3.12: (a) Structure of the resonance attractor for $\psi > 0$. The radius R_s of the stable attractors (solid curves) and the unstable separatrixes (dotted curves) are plotted as a function of the time delay τ. The dashed curves correspond to the improved prediction of Eq. (3.18) and the thin solid line indicates the smallest possible size of the resonance attractor. (b) Magnification of (a) near the origin by the use of a different scale (from [40]).

3.3.2.2 Non-local feedback control

In non-local feedback control, the feedback signal is proportional to the integral of the wave activity over a region known as the sensory domain. To introduce a non-local coupling, the illumination intensity of the feedback control is expressed as [36]

$$I(t) = I_0 + k_{fb}[B(t-\tau) - B_0], \tag{3.19}$$

where I_0 is a background intensity, k_{fb} is a feedback gain, τ is the time delay and

$$B(t) = \frac{1}{A}\int_A w \; ds. \tag{3.20}$$

where $B(t)$ is the average of the absorption w over the sensory domain and A is the area of the sensory domain. The constant B_0 is the time-averaged value of $B(t)$ for the case of a stationary rotation [38].

The evolution of the rigidly rotating spiral wave within a circular domain under non-local feedback was studied experimentally by Kheowan *et al.* [36, 73]. An example of these investigations is shown in Fig. 3.13, where the domain diameter is fixed at $d = \lambda$. The spiral wave core is initially placed at the centre of domain as shown in Fig. 3.13(a). The rotation follows a drift of the core first towards the boundary of the integration area, and finally along a circular pathway with a radius of 0.65λ. If the spiral wave core was placed outside the integration domain, as shown in Fig. 3.13(b), the spiral wave tip after some transient process approaches the same asymptotic circular pathway as in the previous case. Both experiments suggest that this asymptotic trajectory can be considered as an attractor for this dynamical system under such a feedback [36].

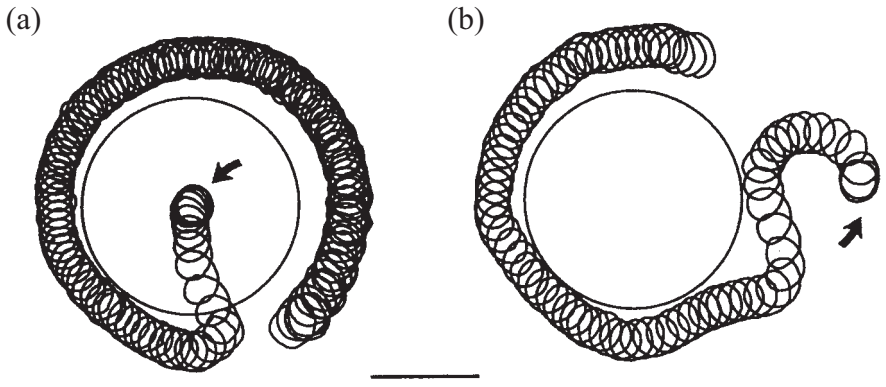

Figure 3.13: (a) and (b) Trajectories of the spiral wave tip under positive feedback ($k_{fb} = 0.5, \tau = 0$) observed for different initial locations of the spiral wave core (arrows): (a) at the centre and (b) outside of integration area (circle). Scale bar: 1 mm (from [36]).

The spiral wave dynamics under a feedback signal computed by integrating the wave activity over a circular domain exhibits very interesting properties. These include the simultaneous characteristics of global and local feedback control. Indeed, the stabilization and the destabilization of a rigidly rotating spiral was observed under a global feedback, whereas the resonance attractor was a specific property of the local feedback control [36]. On the other hand, the existence of an attractor outside the integration domain is, of course, not possible under global feedback. The role of feedback parameters such as the sign of the gain, the time delay and the various sizes of the domain has been investigated further [73, 36].

The size of the excitable domain is an essential control parameter affecting the stability of the rigidly rotating spiral or the radius of the resonance attractor [36, 73]. The shape of the sensory domain can also have a great impact on the dynamics of spiral waves under the non-local feedback control. In the present work, a square-shaped sensory domain will be applied to study experimentally the rigidly rotating spiral wave under non-local feedback control.

CHAPTER 4

MATERIALS AND METHOD

An investigation of spiral wave dynamics in the laboratory has been studied by using the light-sensitive $Ru(bpy)_3^{2+}$-catalyzed BZ reaction. This system allows effective control of the excitability and therefore the control of the dynamics of spiral waves in the system by an external illumination [32, 34, 36]. One of the important properties of the spiral wave is the motion of spiral tip. In this work, the dynamical properties of spiral waves including the spiral tip trajectory were monitored by using the method of two-dimensional photometry used in previous studies [33, 34, 59, 74].

4.1 Chemicals

All chemicals used in this work were reagent-grade chemicals obtained from various sources as shown in Table 4.1. All solutions were prepared by using deionized-distilled water (Barnstead, Nano pure, Ultra pure water system), and filtered through 20-25 μm Whatman filters and stored in separate containers.

Table 4.1: List of chemicals and suppliers.

Chemicals	**Formula**	**%Purify**	**Suppliers**
tris(2, 2′-bipyridyl) ruthenium(II) chloride hexahydrate	$Ru(bpy)_3Cl_2{\cdot}6H_2O$	98.0	Acros organics
Sodium Silicate	Na_2SiO_3	-	Riedel-de haën
Sodium Bromate	$NaBrO_3$	99.0	Fluka
Sodium Bromide	NaBr	99.0	Fluka
Malonic Acid	$CH_2(COOH)_2$	98.0	Fluka
Sulphuric Acid	H_2SO_4	96.6	J.T.Baker

4.1.1 The $Ru(bpy)_3SO_4$ salt and sodium waterglass

The light-sensitive $Ru(bpy)_3^{2+}$ is used as a catalyst. It is not commercially available, thus the $Ru(bpy)_3SO_4$ salt is prepared by precipitation from $Ru(bpy)_3Cl_2{\cdot}6H_2O$ in H_2SO_4 [75]. 2.5 g of $Ru(bpy)_3Cl_2{\cdot}6H_2O$ powder was dissolved in 40 ml of water and 5 M H_2SO_4 added to 100 ml. After H_2SO_4 was added, the suspension particles softly coagulated into an orange-red precipitate of $Ru(bpy)_3SO_4$. After 3 hours it was filtered off and dried at 50°C for 2 days. Subsequently, the solid $Ru(bpy)_3SO_4$ was dissolved in 100 ml of 0.025 M H_2SO_4. The concentration of $Ru(bpy)_3SO_4$ was determined by measuring the absorption at $\lambda = 460$ nm ($\varepsilon_{Ru(II)} = 13400\ M^{-1}\,cm^{-1}$) [76] using a UV/VIS spectrophotometor (PerkinElmer, Lambda800, U.S.A).

15% Sodium silicate, commonly known as sodium waterglass was prepared by dissolving 15 g of sodium silicate powder in 100 ml water. The suspension was heated and stirred until sodium silicate completely dissolved. After cooling to room temperature the volume of water evaporated off during heating was added and then the sodium waterglass solution was filtered.

4.1.2 BZ stock solutions

The stock solutions used for the BZ reaction are listed in Table 4.2. The analytical balance is capable of measuring weights to ±0.01 mg (TC-254, Denver Instrument Company).

Table 4.2: List of the stock solutions.

Stock solutions	Dissolve
1 M $NaBrO_3$	15.089 g in 100 ml H_2O
1 M NaBr	10.290 g in 100 ml H_2O
4 M $CH_2(COOH)_2$	41.624 g in 100 ml H_2O
5 M H_2SO_4	27.590 ml in 100 ml H_2O

4.2 Preparation of the BZ reaction

The following sections include procedures for the preparation of the BZ reaction, which is used to observe the dynamics of spiral waves. To eliminate hydrodynamic convection in the system, a gel medium is used instead of aqueous solution. The $Ru(bpy)_3SO_4$ catalyst is immobilized in the gel.

4.2.1 Preparation of gels with the $Ru(bpy)_3SO_4$ catalyst

A silica-gel matrix was prepared from sodium silicate, commonly known as sodium waterglass. The concentration of $Ru(bpy)_3SO_4$ catalyst was fixed at 4.2 mM in the gel. The proportional volume of $Ru(bpy)_3SO_4$, H_2SO_4 and H_2O to sodium waterglass is 2:1. The time of gelation is controlled by the concentration of H_2SO_4. Decreasing the H_2SO_4 concentration causes an increase in gelation time. For example, the volume of chemical used in this work was prepared from:

0.214 ml	0.0194 M $Ru(bpy)_3SO_4$,
0.032 ml	5 M H_2SO_4,
0.084 ml	H_2O,
0.670 ml	15% sodium waterglass.

At first $Ru(bpy)_3SO_4$ solution, H_2SO_4, and water were mixed. This solution was slowly added drop by drop with continuous stirring into 0.67 ml of 15% sodium waterglass solution, and then 0.71 ml of the mixture was poured on a flat glass petri dish. After gelation the gel was neutralized by covering it with 2.13 ml of 0.1 M H_2SO_4 for 30 minutes. Subsequently, the H_2SO_4 solution was poured out, and then the gel layer was washed several times with water. The gel was covered with water for a few minutes before starting an experiment, in order to prevent desiccation. The gels were kept at an ambient temperature of $25\pm1^{\circ}C$.

The thickness of the gel was controlled by the method detailed in Appendix A. The thickness of the gel layer was 0.30 ± 0.02 mm, which was measured by using a micrometer

(Mitutoyo, series129, Japan). This thickness was chosen in order to make any 3D effects negligible.

4.2.2 Initiation of the BZ reaction

The BZ stock solutions were used to prepare two different BZ solutions as described in Table 4.3. The concentration of BZ-solution II is only half of BZ-solution I. BZ-solution II was added after pouring BZ-solution I onto the gel. This solution has a reaction time of more than 3 hours [34, 72].

Table 4.3: List of BZ solutions.

2.5 ml of BZ-solution I		**10 ml of BZ-solution II**	
1.00 ml	1 M $NaBrO_3$	2.00 ml	1 M $NaBrO_3$
0.21 ml	4 M $CH_2(COOH)_2$	0.42 ml	4 M $CH_2(COOH)_2$
0.45 ml	H_2O	5.90 ml	H_2O
0.39 ml	5 M H_2SO_4	0.78 ml	5 M H_2SO_4
0.45 ml	1 M NaBr	0.90 ml	1 M NaBr

It should be noted that the NaBr was added to the both solutions last of all. During addition of NaBr, the solution must be placed in a fume hood because of the formation of bromine gas. The colour of the solution changes to yellow because in acid solution bromate is oxidized by bromide:

$$5Br^- + BrO_3^- + 6H^+ \rightarrow 3Br_2 + 3H_2O$$

The bromination of malonic acid occurs via Br_2 (see Eq. (A4)): After a few minutes the colour of the solution changes back to colourless.

To start the reaction 0.71 ml of the BZ-solution I was put on top of the gel layer, in which the $Ru(bpy)_3SO_4$ catalyst has been immobilized. After a few minutes the BZ-solution I diffused into the gel, and the concentration of all chemicals in this solution was one half of their initial concentrations, the same concentration as BZ-solution II.

10 ml of the BZ-solution II was then added onto the gel layer in order to increase the volume of the system. In this way the life-time of the excitable system is increased and the aging process is slowed down. After several minutes an equilibrium between the solution and gel was established, with the following initial concentrations (disregarding the bromination of malonic acid):

$Ru(bpy)_3^{2+}$	4.20 mM,
$NaBrO_3$	0.20 M,
$CH_2(COOH)_2$	0.17 M,
H_2SO_4	0.39 M,
NaBr	0.09 M.

Subsequently, spontaneous waves can occur because of small inhomogeneities in the system, and propagate through the gel layer. Such an inhomogeneity was created by carefully pouring the solutions onto the gel at the edge of the petri dish. This generated a single wave front and this wave was broken up to create a pair of spirals, so that one spiral was selected to generate in the petri dish (see Section 4.3.3). The silica hydrogel with the immobilized $Ru(bpy)_3^{2+}$ catalyst covered by the BZ solution as kept at an ambient temperature of $25 \pm 1°C$.

4.3 Experimental method

The dynamics of spiral wave in the petri dish can be analyzed with a sufficiently high spatial and temporal resolution by using the method of two-dimensional (2D) spectrophotometry [33, 34, 59, 74]. The experimental apparatus is shown schematically in Fig. 4.1.

4.3.1 Illumination manipulation

A video projector (Sony, VPL-CX10, Japan) with an ultra-high performance (UHP) lamp (120 W) was used to illuminate the BZ reaction in a petri dish. The illumination

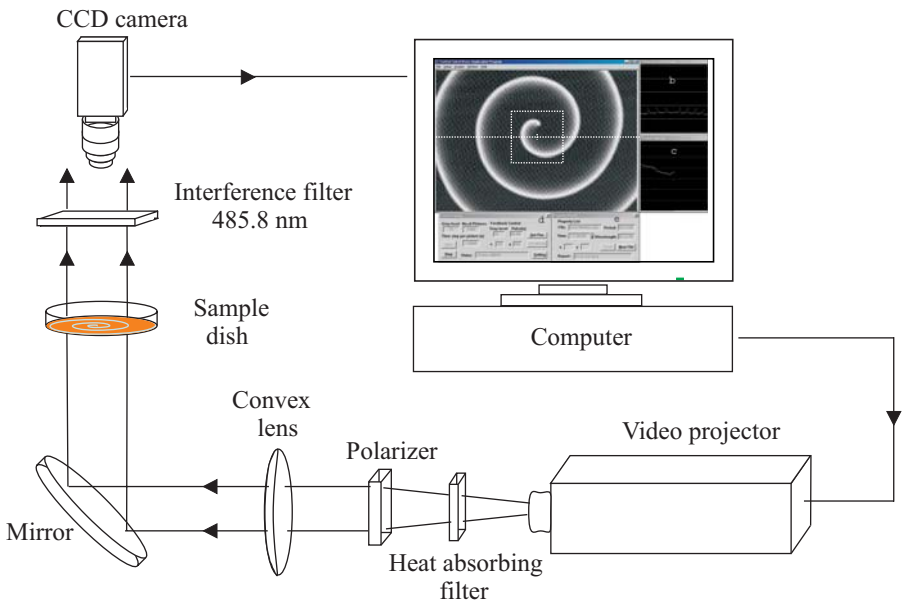

Figure 4.1: Schematic diagram of experimental apparatus.

light was filtered with a heat absorbing filter to eliminate heating from the light source. After that, the intensity of illumination was adjusted by using a pair of polarizers. In addition, to improve the homogeneity of the illumination, the light beam was made parallel by using a plano-convex lens with focal length $f = 200$ mm (PCX lens, 75 mm diameter). This convex lens was placed in front of a mirror at a distance about 100 mm. All the reaction medium was illuminated from below by using the video projector, the intensity of which was controlled by a computer. The light intensity was measured by using a powermeter (Newport, 1815-C, USA) with a detector (Newport, UV-818) placed at the centre of the petri dish. The illumination intensity was subdivided into 256 values between the minimum and maximum of possible light intensity (grey level 0 = dark, grey level 255 = bright). These values were entered into a C-program in order to control the video projector and to create a desired light intensity.

4.3.2 Data acquisition

The oxidation waves appearing in this gel were monitored by using a charge-coupled-device (CCD) camera (Hamamatsu, H 3077-71, Japan) with a 55 mm objective (Com-

putar product, TEC-M55). The oxidized waves appeared as blue-green waves with an orange background of the reduced catalyst. However, the contrast was rather poor. In order to enhance this contrast an interference filter at a wavelength of 485.8 nm ($\triangle\lambda$ = 10.2 nm) was placed in front of the camera. This wavelength is close to the maximum difference between the extinction coefficients of the reduced and oxidized catalyst. A sequence of spiral wave images were acquired every 0.08 s with the CCD camera for immediate processing (see Section 4.3.4). These images covered an area of 7.17×7.17 mm^2 (256×256 pixels) of the reactive layer. The image data was stored every 1 s by the computer via the frame grabber (Data Translations, DT3155). This time interval was sufficiently small for the data evaluation software to detect the spiral tip trajectory as described in Section 4.3.5.1.

4.3.3 Creation of the spiral wave

A few minutes after the experiment had been started, the oxidation waves spontaneously began to emerge at the edge of the petri dish. A cold light source of high illumination intensity (Hayashi brand, LA-150TX) with a light spot (diameter, 1 cm) was used to break a propagating wave front in the middle of the petri dish. After that, the open ends of the wave began to form a pair of spirals. One of the spirals was suppressed with the light spot to leave a single spiral in the centre of the dish. This was done by slowly moving the light spot along the wave front towards the boundary of the dish. Then the single spiral remaining in the middle of the dish was selected as an initial condition for all of the experiments. The petri dish can be placed at a desired location by using a micromanipulator, which is used to adjust the position in three dimensions.

4.3.4 Feedback-controlled mechanism

The control methods are based on collecting data on the activity level of the system and transforming this information to a spatially uniform modulation of the excitability of the medium. The activity level of this medium can be measured at one point (local

feedback) [34, 35] as described in Section 4.3.4.1, or within a given domain (non-local feedback) [36] as explained in Section 4.3.4.2.

4.3.4.1 Local feedback control

Under the local feedback algorithm, the spiral wave is disturbed by a sequence of short light pulses. Each stimulus was applied at an instant corresponding to the passage of the wave front through a particular measuring point, or after some time delay (τ). The light pulse was characterized by the following parameters. The background intensity, I_0, was fixed for all experiments at 0.06 mW/cm^2. The pulse duration was also fixed at 5 s, which was about 12.7% of the wave period. During the pulse the total light intensity, I, was either increased (positive pulse, $I > I_0$) or decreased (negative pulse, $I < I_0$) with respect to the background intensity. The time required for the video projector to change the light intensity was less than 0.08 s, which was determined from the shortest detectable time of the CCD camera. The amplitude, A, was in the range -0.05 to 0.09 mW/cm^2. Examples of typical pulses are shown in Fig. 4.2.

To realize the desired feedback mechanism the intensity of the transmitted light of the oxidized catalyst at the particular measuring point was determined on-line for immediate processing by the computer. The threshold value for the detection of the

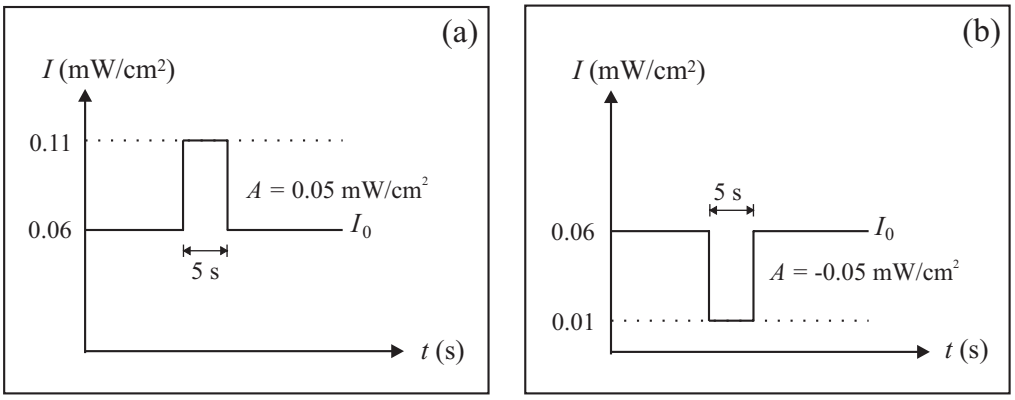

Figure 4.2: Typical pulse forms with background intensity $I_0 = 0.06$ mW/cm^2: (a) Positive pulse with amplitude, $A = 0.05$ mW/cm^2 and (b) negative pulse with $A = -0.05$ mW/cm^2. Pulse duration: 5 s.

wave front is defined as $0.6\times(I_{max} - I_{min}) + I_{min}$, where the maximum ($I_{max}$) and minimum ($I_{min}$) of the grey levels are obtained from a horizontal stripe (512×5 pixels). This band crossed the centre of the medium horizontally. The grey level at the measuring point was determined by averaging the grey level from 3×3 pixels around the measuring point. While the wave front is passing through the measuring point, the grey level reaches the threshold value. Thus the light pulses are created directly at that moment. After that, the grey level will reach this threshold value again when the wave back passes through the measuring point. In order to prevent a second light pulse in the wave back, a reset value is applied to avoid a double detection of the same wave. The reset value is defined as $0.4\times(I_{max} - I_{min}) + I_{min}$. The next pulse can be applied only if the grey level at the measuring point first falls below the reset value.

4.3.4.2 Non-local feedback control

The non-local feedback control can be investigated by choosing the feedback signal to be proportional to the average wave activity taken over a sensory domain that covers only a part of the reaction layer. The dynamics of spiral wave under such non-local feedback control have been observed with various shape of sensory domain, such as circular [36, 77, 78] and elliptical [78]. In this work, the effect of geometry on the spiral wave dynamics is studied further by using a square-shaped sensory domain. The illumination intensity of the feedback control is expressed as in Eq. 3.19 (Section 3.3.2.2). $B(t)$ was calculated by using

$$B(t) = \frac{1}{n}\sum_{i=1}^{n} G_i(t), \qquad i = 1, 2, ..., n, \tag{4.1}$$

where $0 \leq G_i \leq 255$ is the grey level of a given pixel, and n is the total number of pixels in the domain. Note that a higher grey level corresponds to a larger concentration of the oxidized form of the catalyst. The intensity of the feedback illumination $I(t)$ is controlled by a feedback gain k_{fb} and the value of $B(t)$. The constant B_0 is measured as the average grey level for one period of rotation of the spiral wave placed as close

as possible to the centre of the square domain. This value B_0 was determined at the beginning of each experiment. A background intensity of $I_0 = 0.07$ mW/cm^2 was used for all experiments.

Note that the effect of aging leads to slight changes in the integrated transmitted light intensity, as well as changes in certain spiral parameters such as wavelength and period. Therefore, the amplitude of the modulation decreases due to the aging effect. It was compensated for by adjusting the feedback gain. The gain k_{fb} was slightly increased with time (0.004 every 1 min) to keep the averaged amplitude of the modulation approximately constant for 2 hours of experimental time.

4.3.5 Data evaluations

The images obtained from the experiments are further processed in order to improve the quality of the pictures and to determine the location of the spiral tip. For this purpose, a program written in IDL (Interactive Data Language), a computer language for interactive analysis and visualization of scientific data, was used for the image processing and the data evaluation as developed in previous studies [33, 34, 35].

4.3.5.1 Image processing

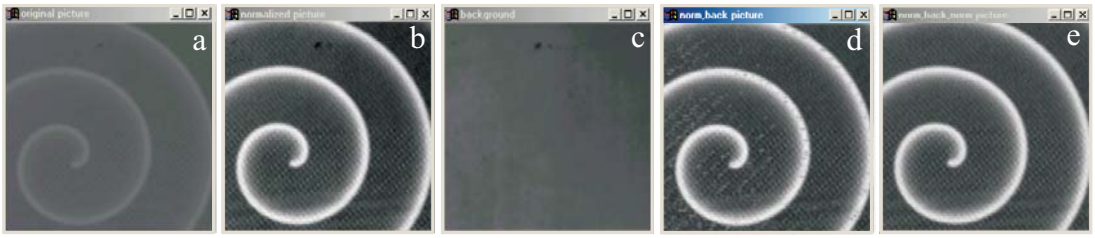

Figure 4.3: Normalization and background subtraction: a) original picture, b) normalized picture, c) background, d) picture after background subtraction, and e) repeated normalization.

The images were stored as two-dimensional arrays (byte-format), where the light intensity was divided into 256 different grey scale levels for each pixel of image. An original image is presented in Fig. 4.3(a). Because of the different illumination intensities

of the images, the brightness distribution of the each image is not always the same. Therefore, the quality of the picture is enhanced by applying the image processing procedures that attempt to improve the contrast in the image. As a first step of the processing, the original image was normalized by scaling the grey levels in the range from 0 to 255 (0 for black and 255 for white). The maximum (I_{max}) and minimum (I_{min}) of the grey levels of the original picture are determined. The grey levels of each pixel (I_{ij}) are scaled as follows [75]:

$$I'_{ij} = (I_{ij} - I_{min})\frac{255}{I_{max} - I_{min}}, \tag{4.2}$$

where i and j are the coordinates of the pixel. The normalized image shows that the contrast of the original image is emphasized as illustrated in Fig. 4.3(b). However, the image quality is not good enough for automatic evaluation because of the inhomogeneity of the image background due to impurities in the gel, such as dust particles, gas bubbles, and/or scratches on the petri dish. For automatic evaluation of the spiral tip position the background should be homogeneous, so that the contour line of the oxidation waves will not be deformed. With the histogram method the background of each image was determined as shown in Fig. 4.3(c). Then the next step is to subtract the background from the normalized images as presented in Fig. 4.3(d). Finally, this image was normalized again as shown in Fig. 4.3(e). Subsequently, the images were ready to be used for evaluation of the spiral tip location [34, 35, 75].

4.3.5.2 Detection of the spiral wave tip trajectory

The spiral tip trajectory is investigated to determine the core structure of the spiral wave and to characterize the dynamics of the spiral wave. The location of the spiral tip was detected automatically by means of an image processing program as used in previous work [34, 35, 75]. This program allows the determination of the tip trajectory objectively for a long period of experimental time and the quantitative analysis of a vast number of the experiments. The method was based on the overlay of appropriate

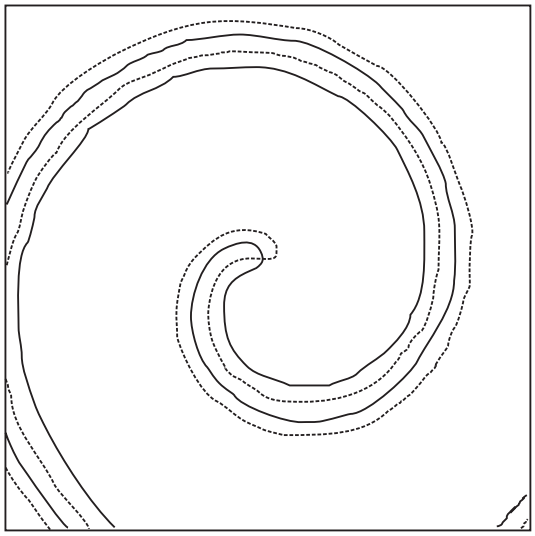

Figure 4.4: Overlay of two contour lines of a spiral wave extracted from two consecutive frames of images (time interval 3 s). The tip was defined as the intersection of the two contour lines. The first and the second consecutive contour lines are shown by solid and dashed curves, respectively.

contour line of the spiral wave extracted from two consecutive frames of the images. The time interval between the two images is 3 s. The intersection point of the two contour lines is defined as the actual tip location as shown in Fig. 4.4. It corresponds to the point where the concentration of the oxidized catalyst has not changed between the two frames of observation and is therefore considered as the momentary centre of rotation.

In order to improve the quality of the pictures, the single frame is smoothed by averaging over 10 pixels before starting the determination of the contour lines. The threshold value of pixel grey level for determination of contour lines is defined as follows: $0.6\times(I_{max} - I_{min}) + I_{min}$. The second contour line (dashed curved in Fig. 4.4) is determined with this threshold value. The intensity difference of images along with the two contour lines is calculated by the computer program. The position of the spiral tip is the pixel coordinate at the same grey level in which the intensity difference is zero. In addition, the spiral tip x, y-coordinates are saved as an ASCII file. The trajectory of

the tip was obtained as the temporal sequence of these tip locations.

The investigation of the spiral wave dynamics in the light-sensitive $Ru(bpy)_3^{2+}$-catalyzed BZ reaction is summarized in the following procedure:

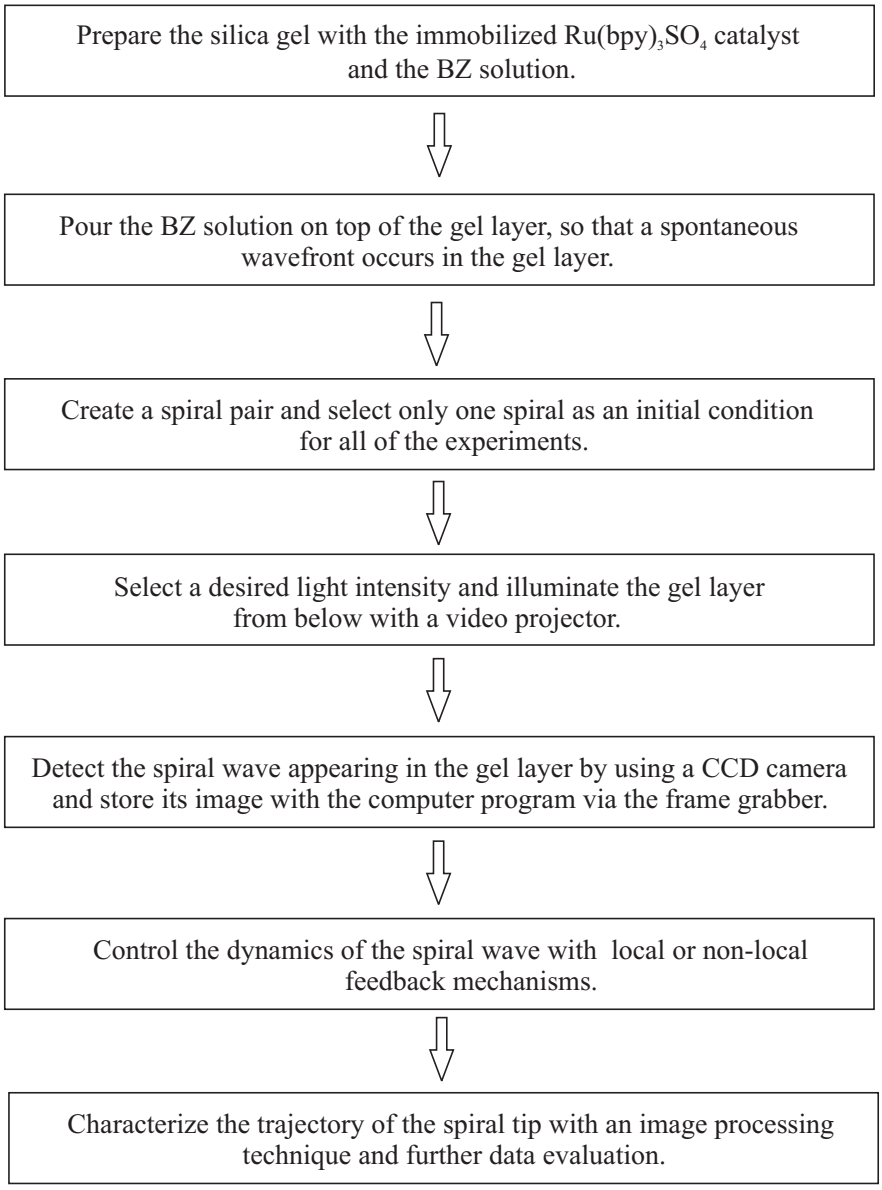

Figure 4.5: Schematic diagram of the experimental procedure.

CHAPTER 5

RESULTS AND DISCUSSION

In this chapter, the dynamics of rigidly rotating spiral wave in the light-sensitive $Ru(bpy)_3^{2+}$-catalyzed BZ reaction under the feedback mechanism is investigated . The presentation is divided into two parts. The first part is concerned with the experimental finding, which is obtained from the investigation of the rigidly rotating spiral wave dynamics under local feedback control. The dynamical features under the application of time delays are also presented. The experimental results are discussed and compared with an earlier developed theory [40]. The second part is devoted to the observations of non-local feedback control within the square-shaped sensory domain of the reaction layer. These observations are carried out for various sizes of the square-shaped sensory domain. A broad spectrum of the dynamical responses which results in various shapes of the spiral tip trajectories is reported.

5.1 Dynamical properties of rigidly rotating spiral wave under local feedback control

For a given background light intensity $I_0 = 0.061 \pm 0.001$ mW/cm^2, the spiral tip rotates rigidly around a closed circle with a diameter of 0.36 ± 0.03 mm. The unperturbed rotation period is $T_u \approx 37-41$ s, which was determined as the average time during which two consecutive wave fronts reached a predefined detection point. The spiral wavelength is $\lambda = 1.92 \pm 0.10$ mm, which was measured as the average length of the normal vector connecting two consecutive wave fronts. An example of the rigidly rotating spiral wave under the background illumination is shown in Fig. 5.1.

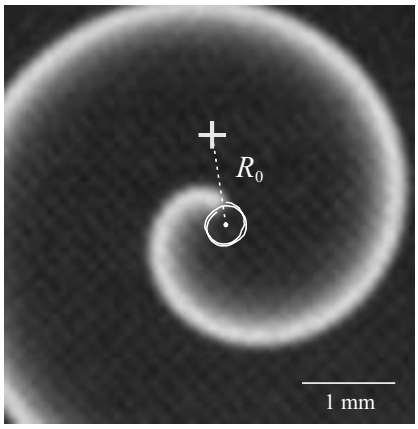

Figure 5.1: Tip trajectory of a spiral wave. Circular orbits of the spiral tip are observed at a constant light intensity $I_0 = 0.061$ mW/cm^2. A momentary location of the spiral wave is shown (shaded curve). The tip trajectory is described by a white solid line. R_0 (dotted line) is the initial distance between the core centre of the unperturbed spiral and the measuring point (cross).

5.1.1 Hypo- and epicycloidal resonance attractors

When the wave front passes through the measuring point in the reaction layer, the sequence of the short light pulses is triggered. The experimental results show that the trajectory is hypocycloidal as shown in Fig. 5.2(a-b). Thus hypocycloidal resonance attractor is found to occur when the measuring point is located very close to the core centre of the unperturbed spiral (see Fig. 5.2(a)), i.e., $R_0 \leq 0.15\lambda$. In this example, the spiral wave tip asymptotically approaches a five-lobed hypocycloidal trajectory with its centre of symmetry coinciding with the measuring point (see Fig. 5.2(b)). The ratio of the rotation period at the measuring point to the unperturbed period, T_{mp}/T_u, is 0.867 ± 0.035, and the ratio of the attractor radius to the spiral wavelength, R_s/λ, is 0.117 ± 0.003 (see Fig. 5.3(a-b), respectively). Both ratios are plotted as a function of time, where triangles represent the data points of the hypocycloidal attractor. The average values of T_{mp}/T_u and R_s/λ are calculated from the data obtained 10 min after starting the experiment. After a transient process, the hypocycloidal attractor remains approximately a stable trajectory that the shape is not changed. The light pulses (indicated by thick segments) appear in the inner part of the loopy trajectory, and

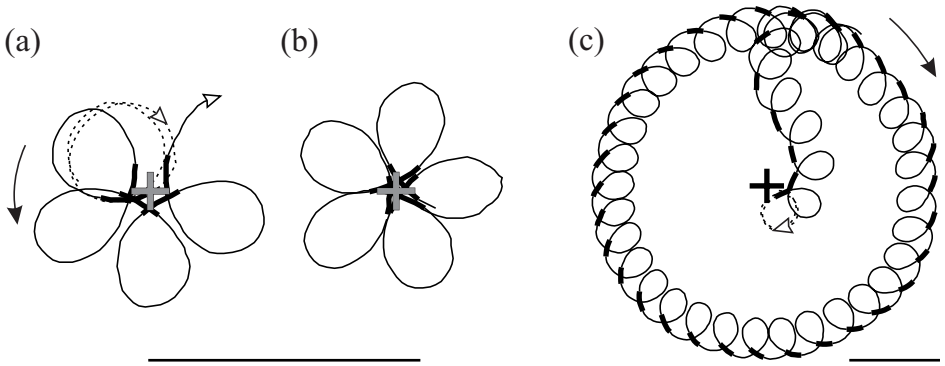

Figure 5.2: Hypocycloidal (a-b) and epicycloidal (c) resonance attractors of the rigidly rotating spiral. Initial distance between measuring point and unperturbed core centre, R_0: (a-b) 0.093λ and (c) 0.155λ. $I_0 = 0.061$ mW/cm^2; $A = 0.050$ mW/cm^2. (a) Transient state of trajectory in (b), which is the stationary attractor several spiral rotations after starting the feedback. Thick segments indicate application of light pulses. The location of the measuring point is shown by a cross. The dotted line depicts the unperturbed spiral tip trajectory. Open and filled arrows indicate the rotation direction of the spiral tip and the spiral core, respectively. The radius of an attractor R_s is defined as the averaged value of the radius of the inner and outer part of the loopy trajectory. Scale bar: 1 mm.

the drift direction of the spiral core is opposite to that of the tip rotation (arrows in Fig. 5.2(a)).

For $R_0 > 0.15\lambda$, the light pulses induces a drift of the spiral core away from the measuring point and finally along circular orbits centred at this point. The spiral tip describes an epicycloidal orbit with inward directed petals, where $T_{mp}/T_u = 1.098 \pm 0.050$ and $R_s/\lambda = 0.805 \pm 0.032$ (circles in Fig. 5.3(a-b), respectively). The attractor radius of the epicycloidal attractors is larger than the hypocycloidal one by a further of 6.88 ± 0.18. The light pulses occur when the tip moves along the outer part of the loopy trajectory (Fig. 5.2(c)). The sense of rotation is the same as for the spiral tip around the spiral core as indicated by the arrows in Fig. 5.2(c). In Table 5.1, some characteristic properties of both types of the hypo- and epicycloidal resonance attractors are compared with each other.

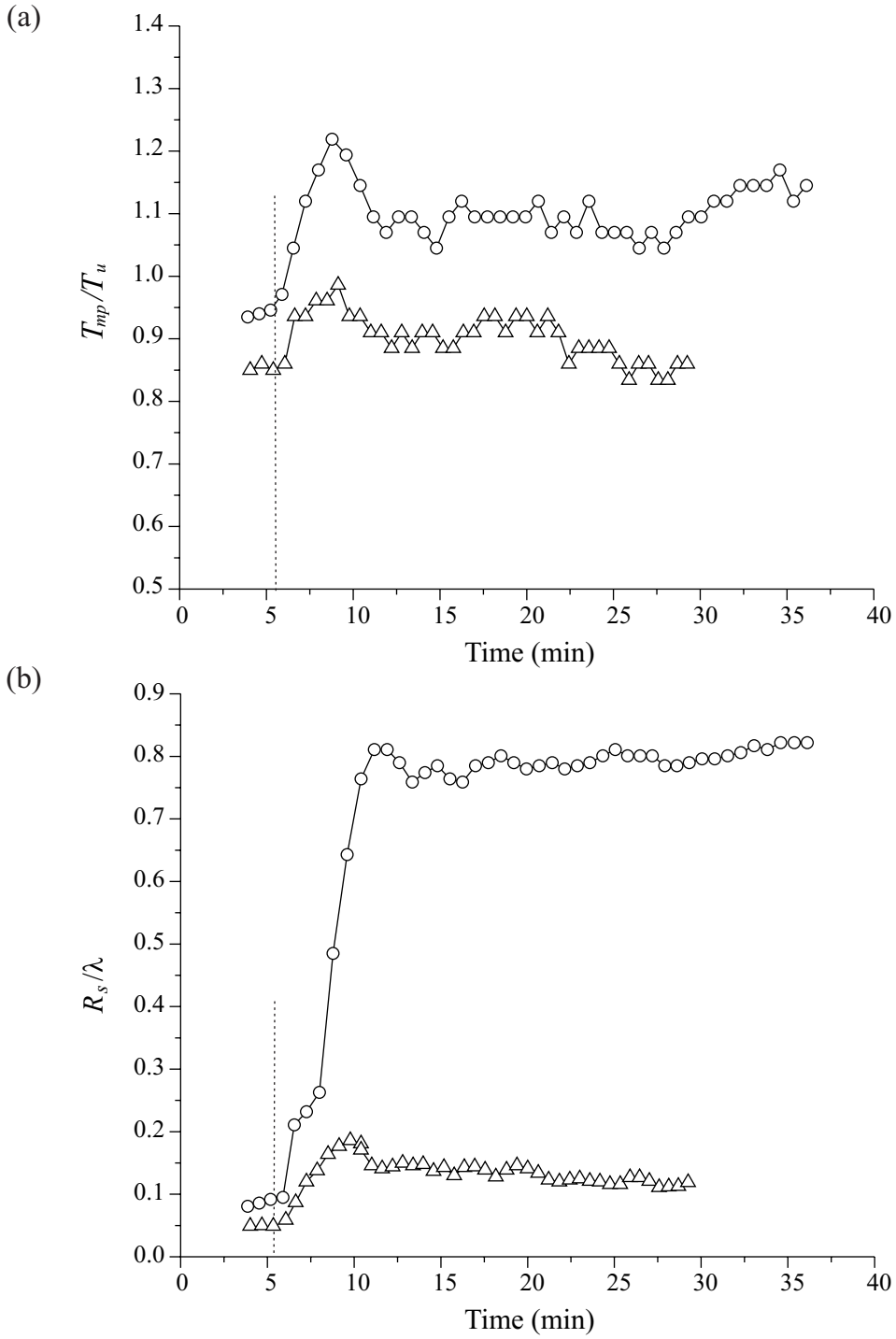

Figure 5.3: The temporal evolution of the ratio of (a) the rotation period at the measuring point to the unperturbed period, T_{mp}/T_u, and (b) the attractor radius to the spiral wavelength, R_s/λ. Circles and triangles correspond to the epi- and hypocycloidal trajectories, which are shown in Fig. 5.2(a-c), respectively. Dashed line represents the starting of feedback control at time = 6 min.

Table 5.1: Characteristic properties of the hypo- and epicycloidal resonance attractors.

Characteristic Property	Hypocycloidal Attractor	Epicycloidal Attractor
1. rotation direction of tip and core	opposite	coincide
2. rotation period, T_{mp}	$< T_u$	$> T_u$
3. attractor size	small	large
4. pulse interval location	inner part of the trajectory	outer part of the trajectory

Tip trajectories corresponding to near-resonance conditions of both attractors remind one of the resonance drift induced by periodic external forcing of a rigidly rotating spiral wave [60]. If T_{mp} and T_u are exactly equal, perfect resonance is expected, with the core centre moving along a straight line. But the period of modulation induced by the local feedback mechanism is just near-resonance, i.e., either $T_{mp} > T_u$ or $T_{mp} < T_u$, and so the trajectory is either epi- or hypocycloidal.

Interestingly, most of the properties of the hypocycloidal resonance attractor shown in Table 5.1, which refer to the rigidly rotating spiral wave, are very similar to those of the entrainment attractor for meandering spirals [34, 71], although the dynamics of the rigidly rotating and meandering spirals differ significantly by the fact that their movement is composed of either one (spatially uniform) or two (not spatially uniform) rotation frequencies.

To be noticed is the difference in the modulation period. For rigid rotation it is equivalent to the rotation period at the measuring point T_{mp}, where $T_{mp} < T_u$ for the hypocycloidal resonance attractor. On the other hand, for the entrainment attractor of meandering spirals, it is equal or very close to the period T_0 at the centre of the unperturbed hypocycloidal trajectory.

5.1.2 Hypocycloidal resonance attractor with an application of time delays

Intriguing properties of the hypocycloidal attractors and the epicycloidal attractors are demonstrated by introducing time delays τ into the feedback loop for two cases: (i) $\tau \leq T_u$ and (ii) the prolonged time delay $\tau > T_u$.

5.1.2.1 Effect of time delays $\tau \leq T_u$

In this section, the dynamics of the hypo- and epicycloidal resonance attractors is observed, when $\tau \leq T_u$. Examples for positive ($A = 0.043 \pm 0.005$ mW/cm^2) and negative pulse feedback ($A = -0.031 \pm 0.003$ mW/cm^2) are shown in Fig. 5.4. Starting with $\tau = 0$ in Fig. 5.4(a), the radius of the hypocycloidal resonance attractor increases with τ. This growth is accompanied by an increase in the number of lobes in the trajectory, i.e., 5, 6, and 7 lobes for $\tau/T_u = 0$, 0.026, 0.053, respectively. If the delay reaches a certain value ($\tau/T_u = 0.067$), a transition from the hypocycloidal to the epicycloidal regime takes place. In the range $0.067 \leq \tau/T_u \leq 0.679$ only this regime is observed, although a very small R_0 is chosen. Note that the radius of the epicycloidal attractor decreases with τ in agreement with previous findings [35, 40]. At $\tau/T_u = 0.679$, however, this radius becomes so small, that the measuring point is finally located inside the spiral core and no light pulse is triggered any more. Then a further increase of τ brings the dynamics of the system back to the hypocycloidal regime, where the size of the attractor orbits increases with τ ($0.775 \leq \tau/T_u \leq 0.989$). Hypocycloidal attractor becomes again unstable at $\tau/T_u = 1.038$, and consequently the dynamics switches, once more, to the epicycloidal regime.

Examples of the hypocycloidal resonance attractors observed for negative pulse feedback are shown in Fig. 5.4(b) in the range $0.300 \leq \tau/T_u \leq 0.560$. Here, the pulses (indicated by thick segments) occur in the outer part of the loopy hypocycloidal trajectory in contrast with the finding for the positive pulse feedback (see Figs. 5.2(a-b) and 5.4(a)), where the pulses appear in the inner part. However, the time delay plays a

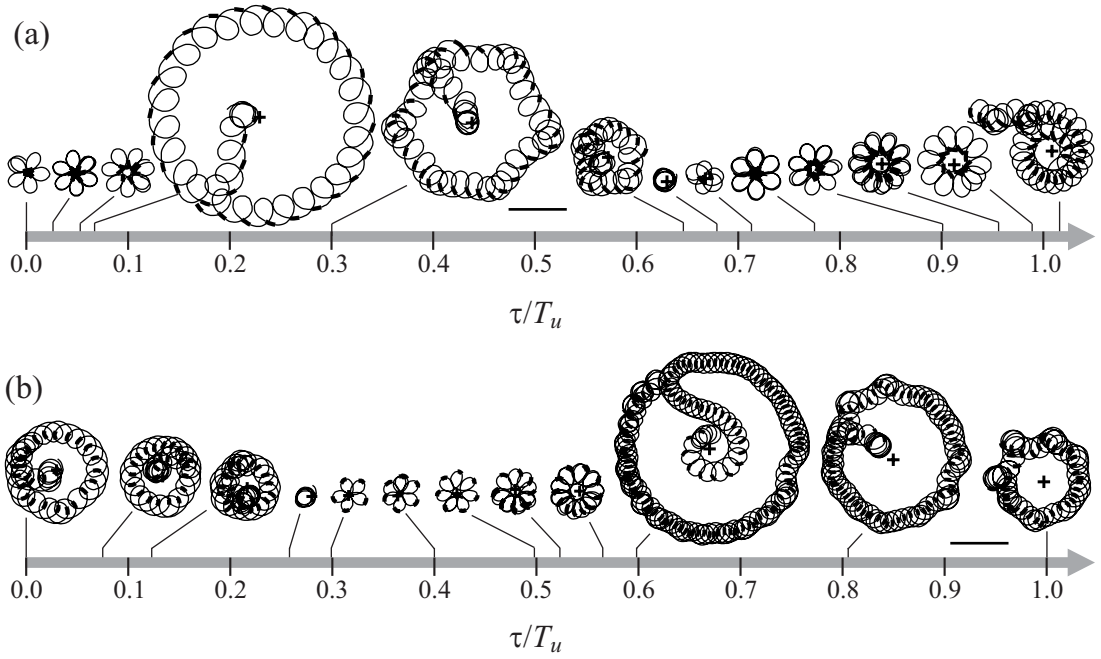

Figure 5.4: Trajectories of the spiral tip under variation of the time delay τ. (a) Positive pulses with amplitude $A = 0.043$ mW/cm^2 and (b) negative pulses with $A = -0.031$ mW/cm^2, where $I_0 = 0.61$ mW/cm^2. The measuring point (cross) is initially placed close to the unperturbed spiral core ($R_0 \leq 0.15\lambda$), except for the two orbits in (b) at $T_{mp}/T_u = 0.805$ and 1. Thick segments correspond to the application of light pulses. Scale bar: 1 mm.

similar role here, i.e., the radius of the hypocycloidal attractor increases with increasing τ. In the range $0 \leq \tau/T_u \leq 0.219$, only the epicycloidal regime is observed, where its radius decreases with increasing τ. Until $\tau/T_u = 0.258$, the radius of the orbits becomes so small and the transition from the epicycloidal to hypocycloidal regime occurs. This feature is similar to the trajectories observed under positive pulse feedback, as previously mentioned. Then the dynamics of the system is return to the epicycloidal regime once again at $\tau/T_u = 0.598$ (see Fig. 5.4(b)).

Figure 5.5 shows the relation between the rotation period at the measuring point T_{mp} and time delay τ, which are scaled by T_u, for the hypo- and epicycloidal resonance attractors. The ratio T_{mp}/T_u for the hypocycloidal attractors increases with increasing τ. On the other hand, the ratio T_{mp}/T_u for the epicycloidal attractors is approximately constant for all τ. The ratio T_{mp}/T_u, although under application of time delays, are

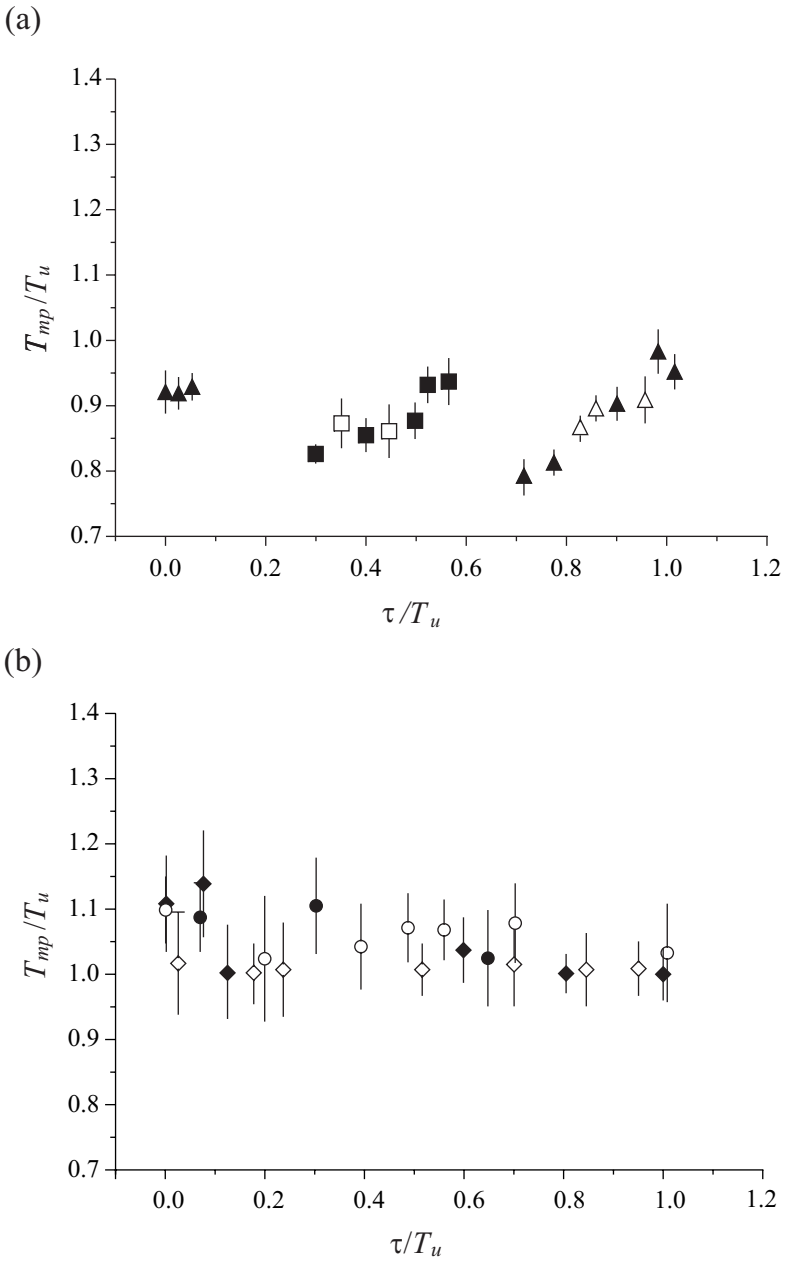

Figure 5.5: The ratio T_{mp}/T_u as a function of time delay τ for: (a) hypocycloidal resonance attractor with positive ($A = 0.041$ mW/cm^2) (triangles) and negative pulses ($A = -0.031$ mW/cm^2) (squares), and (b) epicycloidal resonance attractor with positive ($A = 0.051$ mW/cm^2) (circles) and negative pulses ($A = -0.030$ mW/cm^2) (diamonds). Filled symbols (triangles, squares, diamonds and circles) correspond to the trajectories shown in Fig. 5.4.

less than 1 and greater than 1 for hypo- and epicycloidal attractors, respectively (in agreement with the results reported in Section 5.1.1).

5.1.2.2 Effect of prolonged time delays

The experimental results are carried out with prolonged time delay and under the various intensities of the light pulses. The experimental results show that strong deviations of the hypocycloidal attractor from circular orbits are observed.

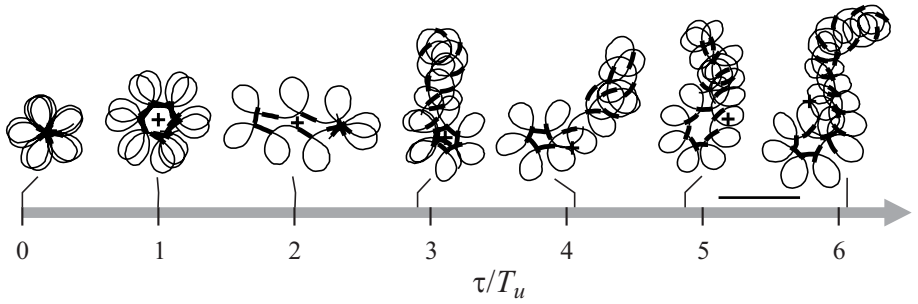

Figure 5.6: Trajectories of the spiral wave tip under application of large time delays τ, where $I_0 = 0.062 \pm 0.001$ mW/cm^2, $A = 0.091 \pm 0.001$ mW/cm^2. Thick segments correspond to the application of light pulses. The location of the measuring point is shown by a cross. Scale bar: 1 mm.

Further instabilities of the hypocycloidal attractors for positive pulses with $A = 0.091 \pm 0.001$ mW/cm^2 are observed when a prolonged time delay ($\tau/T_u > 1$) is introduced as shown in Fig. 5.6. A clear deviation from a circular symmetric attractor appears for $\tau/T_u \approx 2$ (extended hypocycloid). With increasing $\tau/T_u \approx 2.85$ deviations become more pronounced. Apparently, the trajectories share a similar feature: they consist of a 'head' (circular, outward loops) and a 'tail' (extended, inward loops). The length of the tail increases with τ. In the range of τ/T_u about 0 to 2.85, the measuring point is still located at the centre of the attractors and/or the circular orbits. For a larger time delay $\tau/T_u \approx 4.06$, the measuring point is located close to a part of the circular orbits.

Additional experiments of the hypocycloidal attractors with prolonged time delays are observed under negative pulse feedback with $A = -0.030 \pm 0.003$ and $A = -0.049 \pm 0.002$ mW/cm^2 as shown in Fig 5.7(a-b), respectively. In Fig. 5.7(a), the hypocycloidal attractor describes a circular symmetric attractor in the range of τ/T_u

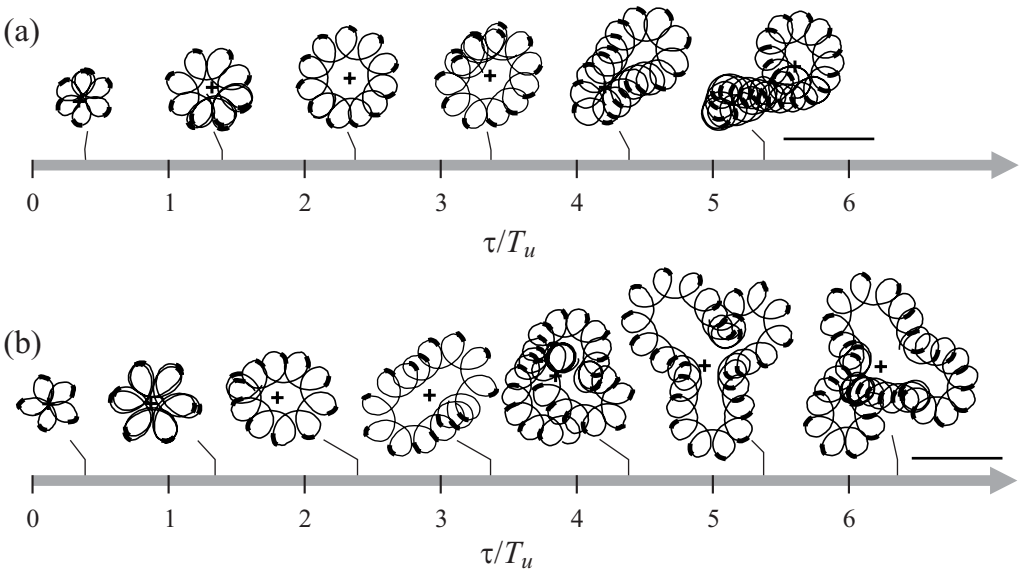

Figure 5.7: Effect of pulse intensity on the trajectories of the spiral wave tip observed for large time delays τ with negative pulses (a) $A = -0.030 \pm 0.003$ mW/cm^2 and (b) $A = -0.049 \pm 0.002$ mW/cm^2, where $I_0 = 0.062 \pm 0.001$ mW/cm^2. Thick segments indicate application of light pulses. The location of the measuring point is shown by a cross. Scale bar: 1 mm.

around 0.4 to 2.38. Until $\tau/T_u \approx 3.35$, the extended hypocycloid appears. When the time delay is increased to $\tau/T_u \approx 4.45$, the trajectory is strongly deformed. These trajectories are quite similar to those observed for positive pulses (Fig. 5.6). For larger pulse amplitude in Fig. 5.7(b), the circular trajectory appears for τ/T_u around 0.39 to 2.39 and the extended hypocycloid appears for $\tau/T_u \approx 3.37$. With further increasing $\tau/T_u \approx 4.38$, the deviations become more pronounced. The trajectories describe a deformed hypocycloidal shape with a three-bulge shape. Note that the measuring point is still located close to the centre of the attractors although these trajectories are strongly distorted.

5.1.3 Comparison of theoretical predictions and discussion

In order to explain the features of the hypo- and epicycloidal resonance attractors the dynamics of the spiral wave core in terms of an iterative map that yields the new location of the core after each applied pulse is considered (see Section 3.3.2.1 [40]). Then this

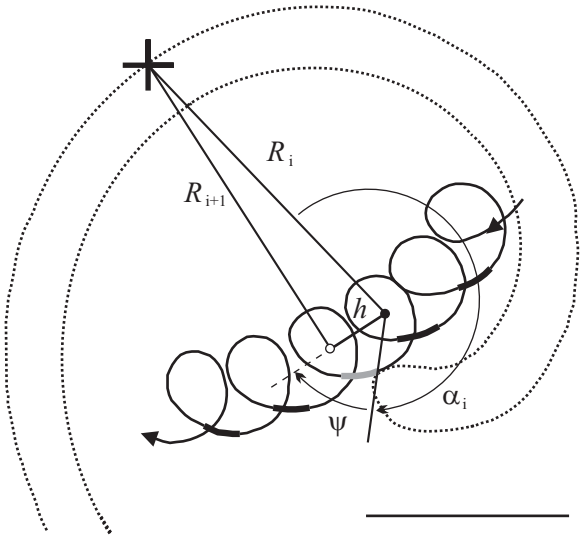

Figure 5.8: Shift of the spiral wave core due to one light pulse (grey thick line) in the pulse sequence (time delay $\tau = 0$ and amplitude $A = 0.05$ mW/cm^2. The thin loopy line represents a part of the trajectory for the epicycloidal attractor as shown in Fig. 5.2(c). The contour line (dotted line) of a spiral wave is shown at the instant, when its front passes through the measuring point (cross). The locations of the core centre before the ith and the $(i+1)$th pulse are shown as a filled and an open circles, respectively. Thick segments indicate application of the light pulses. Scale bar: 1 mm.

theory is applied to describe the experimental results. Each light pulse induces the displacement of the core centre. Based on the sketch of Fig 3.11 (Section 3.3.2.1), the spiral tip trajectories are drawn as schematically shown in Fig. 5.8.

The displacement h of the core centre after application of the ith pulse is indicated as a grey solid line in Fig. 5.8. The direction of this displacement is determined by the angle ψ. This angle is measured with respect to the line connecting the core centre and the location of the spiral wave tip at the instant when the ith pulse is applied. The rotation of the spiral tip around the core centre is specified by the angle α, which is measured from the line connecting the core centre to the measuring point. This angle also determines the orientation of the whole spiral wave shown by the dotted curve in Fig. 5.8.

The dependence of the attractor radius R_s (scaled by λ) on the time delay τ (scaled by T_u) is summarized in Fig. 5.9. The characteristics of the epicycloidal resonance

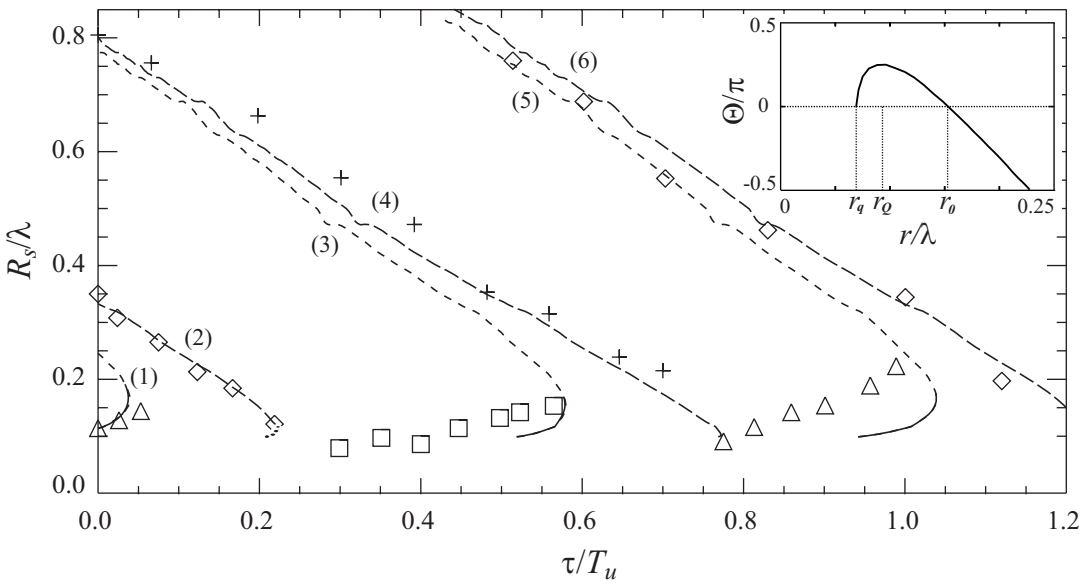

Figure 5.9: Attractor radius R_s for different delay times τ: diamonds and crosses, epicycloidal attractors with negative ($A = -0.030$ mW/cm^2) and positive pulse ($A = 0.051$ mW/cm^2); triangles and squares, hypocycloidal attractors with positive ($A = 0.041$ mW/cm^2) and negative pulse ($A = -0.031$ mW/cm^2), where $I_0 = 0.061$ mW/cm^2. Solid and short-dashed curves are prediction of $R_s(\tau)$ from Eqs. (1) and (2) for stable and unstable hypocycloidal attractors, respectively, with $h_n = 0.215 \pm 0.003$ mm, $\psi_n = 4.00 \pm 0.11$ rad for negative, and $h_p = 0.328 \pm 0.005$ mm, $\psi_p = 0.91 \pm r0.07$ rad for positive pulse. Similarly, long-dashed and dotted curves are prediction of $R_s(\tau)$ for stable and unstable epicycloidal attractors, respectively. Each branch (labelled (1)-(6)) of the dependency $R_s(\tau)$ is computed by substituting the different values of h, ψ and m in equations as follows: (1) h_p, ψ_p and $m = 0$ in Eq. (2), (2) h_n, ψ_n and $m = 1$ in Eq. (1), (3) h_n, ψ_n and $m = 1$ in Eq. (2), (4) h_p, ψ_p and $m = 1$ in Eq. (1), (5) h_p, ψ_p and $m = 1$ in Eq. (2), and (6) h_n, ψ_n and $m = 2$ in Eq. (1). *Inset*: function $\Theta(r)$ specifying the experimentally observed shape of the spiral wave front. $\Theta(r)$ increases with r in the vicinity of the core radius r_q, reaches a maximum at $r = r_Q$, and becomes negative for $r > r_0$.

attractors shown in this graph (diamonds and crosses for negative and positive pulses, respectively) agree well with previous studied [35, 40].

According to Section 3.3.2.1, a theoretical analysis has previously shown [40] that several stationary solutions of the attractor radius R_s exist for each value of the time delay τ, and that the following equations should be satisfied:

$$\frac{\tau}{T_u} = \frac{\Theta(R_s) - \arccos(h/(2R_s)) - \psi}{2\pi} + m, \tag{5.1}$$

$$\frac{\tau}{T_u} = \frac{\Theta(R_s) + \arccos(h/(2R_s)) - \psi}{2\pi} + m, \tag{5.2}$$

where m is a positive integer. The function $\Theta(r)$ (see insert of Fig. 5.9) and the values of h and ψ are measured quantities (cf. [35]). The size of the resonance orbit can then be predicted at any time delay τ by substituting these data into Eqs. (5.1) and (5.2). Linear stability analysis shows that Eq. (5.1) describes stable solutions and Eq. (5.2) corresponds to unstable ones [40].

In order to apply this theory to the experimental results, the function $\Theta(r)$ and the values of h and ψ are determined as follows. The image of the unperturbed spiral wave shown in Fig 5.1 was used to determine a contour line and the plotted function $\Theta(r)$ (see insert of Fig. 5.9). The values of the core displacement with the epicycloidal resonance attractors give the following data: $h_p = 0.328 \pm 0.005$ mm and $\psi_p = 0.91 \pm 0.07$ rad for positive pulses with the given amplitude $A = 0.05$ mW/cm^2, and $h_n = 0.215 \pm 0.003$ mm and $\psi_n = 4.00 \pm 0.11$ rad for negative pulses with $A = -0.04$ mW/cm^2. These values are obtained by the epicycloidal attractors corresponding to the trajectory in Figs. 5.2(c) and 5.4(a), where $\tau = 0$. The computed results are shown in Fig. 5.9, where each branch of the dependency $R_s(\tau)$ was obtained for different values of h, ψ and m.

In Fig. 5.9, there are mostly long-dashed branches and short-dashed branches. The short-dashed curves were computed from Eq. (5.2), with a positive sign in front of $\arccos(h/(2R_s))$. Since the change of slope of the $\Theta(r)$ curve in the interval from r_q to r_0 implies a switching of stability [40], there is an unstable portion of these curves (short-dashed) and a stable one (solid). Consider the shortest branch close to the ordinate of Fig. 5.9 ($\tau/T_u \leq 0.05$). The experimental results suggest that with positive pulses there exist only hypocycloidal attractors in this interval, whereas epicycloidal ones will not be stable. In a similar manner, the existence of other sets of hypocycloidal resonance attractors observed in experiments (all squares and triangles in Fig. 5.9) can be explained with other branches computed according to Eq. (5.2). Note that there are very small unstable branches (e.g., dotted arc-shaped segment at $\tau/T_u \approx 0.2$) connected to the lower end of each stable branch of epicycloidal resonance attractors, as reported

earlier [40].

As previously reported in Section 5.1.1, the hypocycloidal attractor is observed for $R_0 < 0.15\lambda$, whereas for larger values $R_0 > 0.15\lambda$ only the epicycloidal attractor occurs. However, R_0 must not be too small, i.e., it must be larger than the core radius, r_q. Otherwise, with the measuring point located inside the core no light pulse is triggered. According to [40] the hypocycloidal resonance attractor is reached for the interval $r_q < R_0 < r_0$. In the experiments of the present work, $r_q = 0.070\lambda$ and $r_0 = 0.152\lambda$ (see inset of Fig. 5.9). Hence, the boundary value $R_0 < 0.15\lambda$ is in good agreement with theoretical expectations [40].

The agreement between the experimental data and the theoretical prediction decreases for large time delay. A possible reason for this is the relaxation and delayed response of the spiral wave in experiments following the application of a light pulse [79]. The features of the pronounced deviations of the attractors are not explained in the theoretical prediction. However, the observed deviations are reproduced. These results show instabilities of the hypocycloidal resonance attractor for a long time delay.

5.2 A rigidly rotating spiral wave under non-local feedback control derived from a square-shaped sensory domain

The observations of the rigidly rotating spiral wave under non-local feedback are focused on the effects of the domain size. The background intensity I_0 is fixed at $I_0 = 0.070 \pm 0.020$ mW/cm^2 as an initial condition for all experiments. At this illumination intensity, the spiral tip rotates rigidly around a circular path with a diameter of 0.384 ± 0.014 mm, the rotation period of the unperturbed spiral wave $T_u = 43.38 \pm 1.35$ s, and the spiral wavelength $\lambda = 2.11 \pm 0.14$ mm. The constant B_0, the feedback gain k_{fb}, and the side length d of the controlled square-shaped domain are specified as initial parameters for each experiment.

Figures 5.10 and 5.11 show the effect of the domain sizes on the dynamics of the rigidly rotating spiral wave under non-local feedback control. The domain sizes are

changed with various side lengths d. For the side length of the domain significantly smaller than the spiral wavelength ($d = 0.5\lambda$), the spiral leaves the centre of the sensory domain, where its circular core was initially placed (arrow in Fig. 5.10(a)), by drifting outwards until it makes a turn to follow a circular path with a radius of about 0.76λ. This motion resembles that observed in earlier reported experiments applying a small size, circular-shaped sensory domain [36].

For a domain size equal to the spiral wavelength ($d = \lambda$), the spiral core first drifts away from the domain centre as shown in Fig. 5.10(b), then it approaches a stable trajectory describing a square-shaped pathway. The square-shaped trajectory with a side length of about 1.33λ is rotated by about 45° with respect to the domain. Note that the drift velocity of the spiral wave core changes periodically: it is slower at the corners and faster at the sides of the trajectory.

Figure 5.10(c) shows the trajectory of the spiral tip in an experiment with a still larger feedback domain, $d = 1.25\lambda$. In this case, the spiral tip is initially placed close to the domain boundary. The feedback control induces first a drift towards the centre and subsequently towards the middle region of the adjacent side of the domain. This

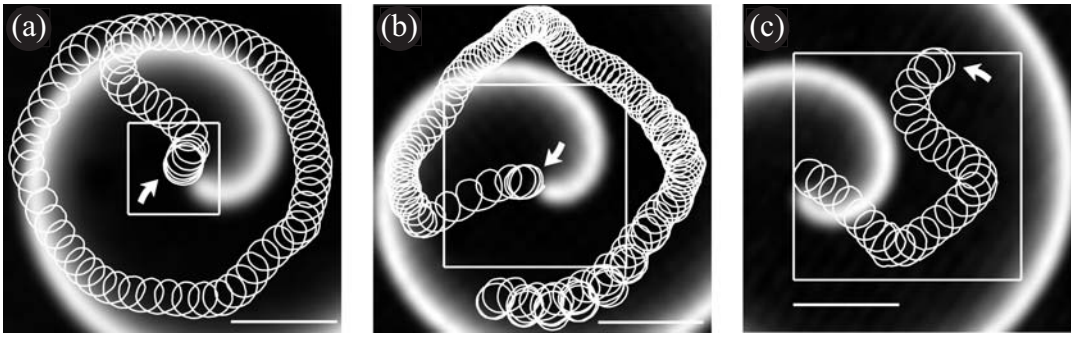

Figure 5.10: Experimental trajectories of a spiral wave tip subjected to non-local feedback control for different sizes of the sensory domain: (a) $d = 0.5\lambda$ (λ = the spiral wavelength) with $B_0 = 24$, $k_{fb} = 0.2$, (b) $d = 1.0\lambda$ with $B_0 = 24.5$, $k_{fb} = 0.8$, and (c) $d = 1.25\lambda$ with $B_0 = 19$, $k_{fb} = 0.45$. $I_0 = 0.07$ mW/cm^2 for all experiments. The domains and the initial spiral core locations are indicated by squares and thick arrows, respectively. The spiral images are shown for the start of the trajectory in (a) and (b) and the end of the trajectory in (c). Scale bar: 1 mm.

process occurs several times and consequently the spiral tip is caught inside the square, bouncing from and to the "virtual walls".

When the domain is further increased to $d \geq 1.45\lambda$, the trajectory is qualitatively changed as shown in Fig. 5.11. The spiral wave core is initially placed close to the centre of the domain $d = 1.45\lambda$ (see Fig. 5.11(a)). The trajectory is approximately a small square. For a larger feedback domain $d = 1.5\lambda$, the spiral wave core is initially placed outside the domain (see Fig. 5.11(b)). The spiral core is attracted towards a trajectory describing a large square with rounded corners. The drift velocity is slower at the corners. Its orientation coincides with that of the domain, in contrast with the trajectories in Fig. 5.10(b) and 5.10(c), which are rotated by about 45° with respect to the domain.

Figures 5.10 and 5.11 indicate that increasing the size d of the feedback domain has a pronounced effect on the shape and size of the spiral tip trajectory. For a rather small size ($d = 0.5\lambda$), the trajectory describes a circular shape. The circular trajectory transforms to a square for $d = \lambda$ (see Figs. 5.10(a-b) and 5.11(a)). The size of the

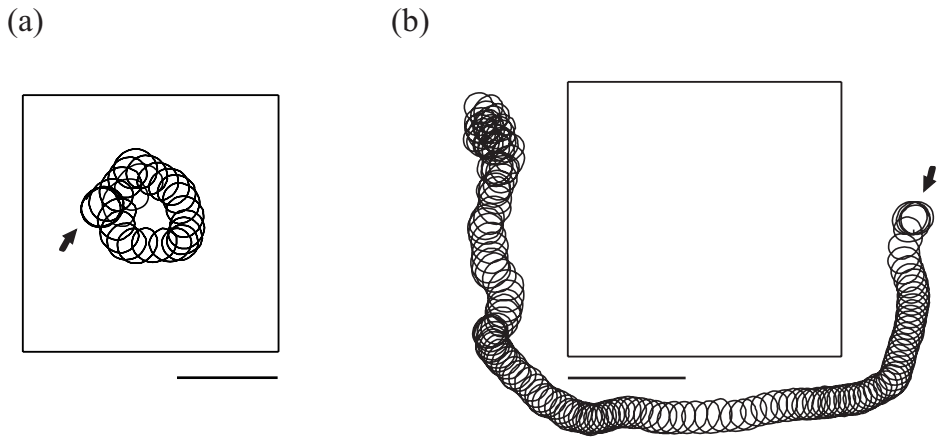

Figure 5.11: Experimental trajectories of a spiral wave tip observed for different sizes of the sensory domain: (a) $d = 1.45\lambda$ with $B_0 = 19.5$, $k_{fb} = 0.2$ and (b) $d = 1.5\lambda$ with $B_0 = 22$, $k_{fb} = 0.8$. $I_0 = 0.70$ mW/cm^2 for all experiments. The domains and the initial spiral core locations are indicated by squares and thick arrows, respectively. Scale bar: 1 mm.

square-shaped trajectories decrease with increasing the domain size (see Fig. 5.10(b-c)). For further increasing the domain $d = 1.50\lambda$, a large square-shaped trajectory with rounded corners is observed, where the spiral wave core is initially placed outside the domain.

CHAPTER 6

CONCLUSIONS AND OUTLOOK

Feedback algorithms are an effective way to control the dynamics of spiral waves which are observed in an excitable layer of the BZ reaction with the light-sensitive $Ru(bpy)_3^{2+}$ catalyst. The light-sensitive $Ru(bpy)_3^{2+}$-catalyzed BZ reaction has proven to be a suitable laboratory system for investigating local and non-local feedback control by means of time-dependent illumination. The systematic study of spiral wave dynamics under local and non-local feedback control demonstrates a variety of dynamical responses.

Local feedback control results in a drift of the spiral core along circular orbits, which appear to be an attractor. There are two types of resonance attractors that can be observed for a rigidly rotating spiral wave under local feedback control: hypocycloidal and epicycloidal resonance attractors. The dynamical features of both attractors is just near-resonance, i.e., either $T_{mp} > T_u$ or $T_{mp} < T_u$, where T_{mp} is the rotation period at the measuring point and T_u is the unperturbed rotation period, corresponding to either epi- or hypocycloidal shape. A control parameter that defines the boundary between the two types of the resonance attractors, is the initial distance R_0 between the measuring point and the initial location of the spiral core. In fact, the hypocycloidal attractor is observed for $R_0 < 0.15\lambda$, whereas for larger values $R_0 > 0.15\lambda$ only the epicycloidal attractor occurs.

The type, size and stability of the hypo- and epicycloidal resonance attractor can be changed by introducing a time delay into the feedback loop. With increasing time delay τ, the radius of the hypo- and epicycloidal resonance attractors increases and decreases, respectively. An experimental study of the dependence of their radius R_s on time delay is in good agreement with the theoretical predictions. The agreement

between the experimental data and the theoretical prediction decreases for large time delay. The attractor shapes deviate strongly from circular symmetry and then becomes quite irregularly shape if the time delay in the feedback loop becomes relatively long. To study further instabilities of the hypocycloidal resonance attractor for such long delays is an interesting challenge for future work.

Rigidly rotating spiral wave dynamics is also studied under a non-local feedback algorithm for while the illumination intensity is proportional to the average wave activity within a square-shaped sensory domain of the reaction layer. The investigations show a broad spectrum of dynamical responses most of which result in square-shaped trajectories of the spiral tip, including reflection at the virtual walls. In certain ranges of increasing d the size of the square trajectory is reduced. Then, the size of the feedback domain plays an important role in the pronounced effect on the shape and the size of the spiral tip trajectory. Experiments also show that the trajectories act like the attractors: the spiral tip always approaches them independently from its initial position. Then, the size and shape of a sensor by which we collect information about the activity level of a dynamical system turns out to be crucial in determining the size and shape of the spatio-temporal attractor governing the behaviour of the system under feedback control.

A study of the spiral wave dynamics in the BZ reaction can lead to a useful description of biological systems wih excitable behaviour. The feedback algorithms are an effective method to manipulate spatio-temporal patterns of nonlinear dynamics, especially spiral waves in excitable media. If a way can be found to modulate the excitability, this method can be transferred to control such dynamics in other types of spatially extended systems, e.g., in cardiac muscle [18] and neuronal tissue [80] or in context of intracellular calcium dynamics [81].

REFERENCES

[1] Nicolis G and Prigogine I. Self-organization in nonequilibrium systems. New York: John Wiley&Sons; 1977.

[2] Haken H. Synergetics: an introduction nonequilibrium phase transition and self organization in physics, chemistry and biology. Berlin: Springer-Verlag Berlin Hrifrlberg; 1977.

[3] Turing AM. The chemical basis of morphogenesis. Phil. Trans. R. Soc. 1952; B237: 37-72.

[4] Richard Fitzhugh. Impulses and physiological states in theoretical models of nerve membrane. Biophys. J. 1961; 1: 445-466.

[5] Kondo S. and Asai R. A reaction-diffusion wave on the skin of the marine angelfish *Pomacanthus*. Nature 1995; 376: 765-768.

[6] Zaikin AN and Zhabotinsky AM. Concentration wave propagation in two-dimensional liquid phase self-oscillating system. Nature 1970; 225: 535-537.

[7] Belousov BP. A periodic reaction and its mechanism. In: Oscillations and travelling waves in chemical systems, edited by Field, R.J. and Burger, M. New York: John Wiley&sons; 1985: 605-613.

[8] Zhabotinsky AM. Periodical oxidation of malonic acid in solution (a study of the Belousov reaction kinetics). Biofizika. 1964; 9: 306-311.

[9] Winfree AT. Spiral Waves of Chemical Activity. Science 1972; 175: 634-636.

[10] Mikhailov AS. Foundations of Synergetics I Distributed active systems. Berlin: Springer-Verlag; 1994.

[11] Meron E. Pattern formation in excitable media. Phys. Rep. 1992; 218: 1-66.

[12] Murray JD. Mathematical biology. Berlin: Springer-Verlag; 1989.

[13] Ball P. The self-made tapestry: pattern formation in nature. New York: Oxford university press Inc. 1999.

[14] Shibata M and Bureš J. Reverberation of cortical spreading depression along closed path ways in rat cerebral cortex. J. Neurophysiol. 1972; 35: 381-388.

[15] Gorelova NA and Bures J. Spiral waves of spreading depression in the isolated chicken retina. J. Neurobiol. 1983; 14: 353-363.

[16] Müller SC, Plesser T, and Hess B. The structure of the core of the spiral wave in Belousov-Zhabotinskii reaction. Science 1985; 230: 661-663.

[17] Krinsky VI. Mathematical models of cardiac arrhythmias (spiral waves). Pharmac. Ther. B 1978; 3: 539-555.

[18] Davidenko JM, Pertsov AV, Salomonsz R, Baxter W and Jalife J. Stationary and drifting spiral waves of excitation in isolated cardiac muscle. Nature 1992; 355: 349-351.

[19] Newell PC. Attraction and adhesion in the slime mold Dictyostelium. In: J.E. Smith (ed.) Fungal Differentiation: A Contemporary Synthesis. Mycology Series 43. New York: Marcel Dekker; 1983.

[20] Foerster P, Müller SC, and Hess B. Curvature and spiral geometry in aggregation patterns of Dictyostelium discoideum. Development 1990; 109: 11-16.

[21] Jakubith S, Rotermund HH, Engel W, von Oertzen A and Ertl G. Spatiotemporal concentration patterns in a surface reaction: propagating and standing waves, rotating spirals and turbulence. Phys. Rev. Lett. 1990; 65: 3013-3016.

[22] Nettesheim S, von Oertzen A, Rotermund HH and Ertl G. Reaction diffusion patterns in the catalytic CO-oxidation on Pt(110): Front propagation and spiral waves. J. Chem. Phys. 1993; 98: 9977-9985

[23] Mair T and Müller SC. Travelling NADH and proton waves during oscillatory glycolysis in vitro. J. Biol. Chem. 1996; 271: 627-630.

[24] Jahnke W, Skaggs WE, and Winfree AT. Chemical vortex dynamics in the Belousov-Zhabotinskii reaction and in the two-variable Oregonator model. J. Phys. Chem. 1989; 93: 740-749.

[25] Plesser T, Müller SC, and Hess B. Spiral wave dynamics as a function of proton concentration in the ferroin-catalyzed Belousov-Zhabotinskii reaction. J. Phys. Chem. 1990; 94: 7501-7507.

[26] Skinner GS and Swinney HL. Periodic to quasiperiodic transition of chemical spiral rotation. Physica D 1991; 48: 1-16.

[27] Nagy-Ungvarai Z, Ungvarai J, and Müller SC. Complexity in spiral wave dynamics. Chaos 1993; 3: 15-19.

[28] Zykov VS. Simulation of wave processes in excitable media. Manchester: Manchester University Press; 1987.

[29] Lugosi E. Analysis of meandering in Zykov kinetics. Physica D 1989; 40: 331-337.

[30] Karma A. Meandering transition in two-dimensional excitable media. Phys. Rev. Lett. 1990; 65: 28242827.

[31] Barkley D. Linear stability analysis of rotating sprial waves in excitable media Phys. Rev. Lett. 1992; 68: 2090-2093.

[32] Kuhnert L. A new optical photochemical memory device in a light-sensitive chemical active medium. Nature 1986; 319: 393-394.

[33] Steinbock O, Zykov VS, and Müller SC. Control of spiral-wave dynamics in active media by periodic modulation of excitability. Nature 1993; 366: 322-324.

[34] Grill S, Zykov VS, and Müller SC. Feedback-controlled dynamics of meandering spiral waves. Phys. Rev. Lett. 1995; 75: 3368-3371.

[35] Kheowan O, Zykov VS, Rangsiman O, and Müller SC. Transition between orbits of resonance attractors for spiral waves. Phys. Rev. Lett. 2001; 86: 2170-2173.

[36] Kheowan O, Chan CK, Zykov VS, Rangsiman O, and Müller SC. Spiral wave dynamics under feedback derived from a confined circular domain. Phys. Rev. E. 2001; 64: 35201.

[37] Agladze KI, Davydov VA, and Mikhailov AS. Observation of a helical wave resonance in an excitable distributed medium. JETP Lett. 1987; 45: 767-770.

[38] Zykov VS, Mikhailov AS, and Müller SC. Controlling spiral waves in confined geometrices by global feedback. Phys. Rev. Lett. 1997; 78: 3398-3401.

[39] Sakurai T., Mihaliuk E., Chirila F., and Showalter, K. Design and control of wave propagation patterns in excitable media Science 2002; 296: 2009-2012.

[40] Karma A and Zykov VS. Structure of the resonance attractor for spiral wave in excitable media. Phys. Rev. Lett. 1999; 83: 2453-2456.

[41] Zykov VS, Kheowan O, Rangsiman O, and Müller SC. Instabilities of the resonance attractor for spiral wave in an excitable medium. Phys. Rev. E. 2002; 65: 026206.

[42] Braune M and Engel H. Compound rotation of spiral waves in active media with periodically modulated excitability. Chem. Phys. Lett. 1993; 211: 534-540.

[43] Epstein IR and Pojaman JA. An introduction to nonlinear chemical dynamics. New York: Oxford University Press; 1998.

[44] Ross J, Müller SC, and Vidal C. Chemical waves. Science. 1988; 240: 460-465.

[45] Field RJ, Körös E, and Noyes RM. Oscillations in chemical systems II: Through analysis of temporal oscillation in the Bromate-Cerium-Malonic acid system. J. Am. Chem. Soc. 1972; 94: 8649-8664.

[46] Field RJ and Noyes RM. Oscillations in chemical systems. IV. Limit cycle behaviour in a model of a real chemical reaction. J. Chem. Phys. 1974; 60: 1877-1884.

[47] Gray P and Scott S. Chemical oscillations and instabilities: non-linear chemical kinetics. Oxford: Claredon Press; 1990.

[48] Stephen KS. Oscillations, waves, and chaos in chemical kinetics. Oxford, Oxford University Press; 1994.

[49] Tyson JJ and File PC. Target pattern in a realistic model of the Belousov-Zhabotinskii reaction. J. Chem. Phys. 1980; 73: 2224-2237.

[50] Keener JP and Tyson JJ. Spiral waves in the Belousov-Zhabotinskii reaction. Physica D. 1986; 21: 307-324.

[51] Epstein IR and Showalter K. Nonlinear chemical dynamics: oscillations, patterns, and chaos. J. Phys. Chem. 1996; 100: 13132-13147.

[52] Kapral R and Showalter K. Chemical Waves and Patterns. Dordrecht: Kluwer Academic Publishers; 1995.

[53] Yamaguchi T, Kuhnert L, Nagy-Ungvarai Zs, Müller SC, and Hess B. Gel System for the Belousov-Zhabotinskii Reaction. J. Phys. Chem. 1991; 95: 5831-5837.

[54] Jinguji M, Ishihara M, and Nakazawa T. Primary process of illumination effect on the $Ru(bpy)_3^{2+}$-catalyzed Belousov-Zhabotinskii reacttion. J. Phys. Chem. 1992; 96: 4279-4281.

[55] Srivastava PK, Mori Y, and Hanazaki I. Photo-inhibition of chemical oscillation in the $Ru(bpy)_3^{2+}$-catalyzed Belousov-Zhabotinskii reaction. Chem. Phys. Lett. 1992; 190: 279-284.

[56] Hanazaki I, Mori Y, Sekiguchi T, and Rábai G. Photo-response of chemical oscillators. Physica D 1995; 84: 228-237.

[57] Ram Reddy MK, Szlaivik Z, Nagy-Ungvarai Zs, and Müller SC. Influence of light on the inorganic part of the ruthenium-catalyzed Belousov-Zhabotinsky Reaction. J. Phys. Chem. 1995; 99: 15081-15085.

[58] Krug HJ, Pohlmann L, and Kuhnert L. Analysis of modified complete Oregonator accounting for oxygen sensitive and photo-sensitive of Belousov-Zhabotinsky systems. J. Phys. Chem. 1990; 94: 4862-4866.

[59] Kheowan O, G*áspár* V, and Zykov VS, and Müller SC. Measurements of kinematical parameters of spiral waves in media of low excitability. Phys. Chem. Chem. Phys. 2001; 3: 4747-4752.

[60] Davydov VA, Zykov VS, and Mikhailov AS. Kinematic of autowave structures in excitable media. Sov. Phys. Usp. 1991; 34: 665-684.

[61] Schrader A, Braune M, and Engel H. Dynamics of spiral waves in excitable media subjected to external periodic forcing. Phys. Rev. E 1995; 52: 98-108.

[62] Jahnke W and Winfree AT. A survey of spiral-wave behaviours in the Oregonator model. Int. J. Bifur. and Chaos 1991; 1: 445-446.

[63] Li G, Ouyang Q, Petrov V, and Swinney HL. Transition from simple rotating chemical spirals to meandering and travelling spirals. Phys. Rev. Lett. 1996; 77: 2105-2108.

[64] Winfree AT. Variety of spiral wave behaviour: An experimentalist's approach to the theroy of exctiatble media. Chaos. 1991; 1: 303-334.

[65] Braune M and Engel H. Compound rotation of spiral waves in a light-sensitive Belousov-Zhabotinsky medium. Chem. Phys. Lett. 1993; 204: 257-264.

[66] Barkley D. Euclidean symmetry and the dynamics of rotating sprial waves. Phys. Rev. Lett. 1994; 72: 164-167.

[67] Wiener N. and Rosenblueth A. The mathematical formulation of the problem of conduction of impulses in a network of connected excitable elements. Arch. Inst. Cardiol. Mex. 1946, 16: 205-265

[68] Müller SC, Plesser T, and Hess B. Two-dimensional spectrophotometry of spiral wave propagation in the Belousov-Zhabotinsky reaction Physica D. 1987; 24: 87-96.

[69] Foerster P, Müller SC, and Hess B. Curvature and propagation velocity of chemical waves. Science. 1988; 241: 685-687.

[70] Braune M, Schrader A, and Engel H. Entrainment and Resonance of spiral waves in active media with periodically modulated excitability. Chem. Phys. Lett. 1994; 222: 358-362.

[71] Grill S, Zykov VS, and Müller SC. Spiral wave dynamics under pulsatory modulation of excitability. J. Phys. Chem. 1996; 100: 19082-19088.

[72] Zykov VS, Steinbock O, and Müller SC. External forcing of spiral waves. Chaos 1994; 4: 509-518.

[73] Kheowan O, Zykov VS, and Müller SC. Transition from local to global feedback control of spiral wave dynamics. Phys. Chem. Chem. Phys. 2002; 4: 1334-1338.

[74] Steinbock O and Müller SC. Chemical spiral rotation is controlled by light-induced artificial cores. Physica A 1992; 188: 61-67.

[75] Kheowan O. Dynamics of spiral waves under feedback control in the light-sensitive Belousov-Zhabotinsky reaction. Ph.D. Thesis, Mahidol University; 2001.

[76] Kuhnert L and Krug HJ. Kinetic of chemical waves in the acidic bromate-malonic acid-$Ru(bpy)_3^{2+}$ system in comparison with ferroin system J. Phys. Chem. 1987; 91: 730-733.

[77] Zykov VS and Engel H. Resonance attractors of spiral waves in excitable media under global feedback control. Phys. Rev. E 2002; 66: 016206.

[78] Zykov VS, Bordiougov G, Brandtstädter H, Gerdes I, and Engel H. Global control of spiral wave dynamics in an excitable domain of circular and elliptical shapes. Phys. Rev. Lett. 2004; 92: 018304.

[79] Ram Reddy MK, Dahlem M, Zykov VS, and Müller SC. The effect of an illumination jump on wave propagation in the Ru-catalyzed Belousov-Zhabotinsky reaction. Chem. Phys. Lett. 1995; 236: 111-116.

[80] Dahlem M.A. and Müller S.C. Self-induced of spiral-shaped spreading depression waves in chicken retina Exp. Brain. Res. 1997; 115: 319-324.

[81] Falcke M, Li Y, Lechleiter JD, and Camacho P. Modeling the dependence of the period of the intracellular Ca^{2+} waves on SERCA expression. Biophys. J. 2003; 85: 1474-1481.

APPENDIXES

APPENDIX A

METHOD FOR CONTROLLING THE THICKNESS OF THE GEL LAYER

The BZ reaction is carried out in a gel layer, which has a thickness of about 0.3 mm. In order to control the thickness of the gel layer at this particular value, we employ a supplementary tool comprising of a circular plastic ring and a press plate. The solution of the gel was poured inside the ring, which is fixed in the petri dish, and the press plate was immediately placed on top of this solution. Then the solution spreads all over the area inside of the ring. After gelation, the press plate was taken off. The thickness of the gel layer is the same as the thickness of the circular ring. The thickness of the plastic ring is 0.30 $\pm$ 0.02 mm with an inside diameter of 5.5 cm and an outside diameter of 6.5 cm (see Fig. A.1(a)). The ring was glued to the petri dish using silicone-paste (Baysilones-paste, GE Bayer Silicones). To avoid the gel sticking to the press plate, it was covered with plastic film (Nescofilm, Karlan).

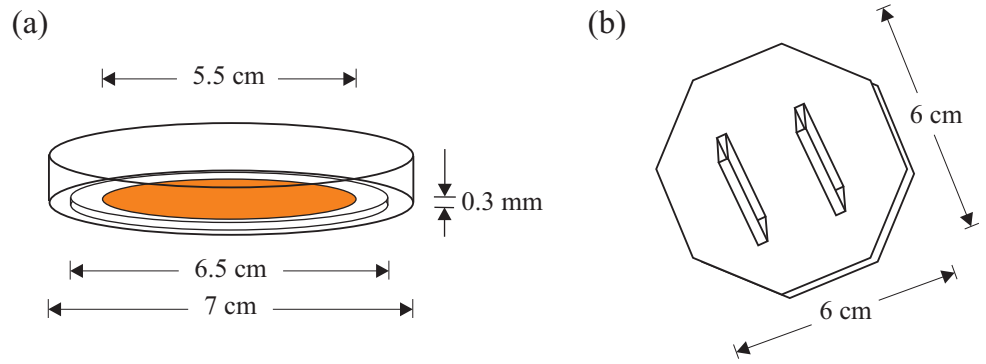

Figure A.1: A supplementary tool for controlling the thickness of the gel layer. (a) The circular plastic ring was put inside the petri dish and (b) the press plate with an octagonal shape, 6×6 cm, made from a plexiglass.

PUBLICATION I: SPIRAL WAVE DYNAMICS CONTROLLED BY A SQUARE-SHAPED SENSORY DOMAIN

On-Uma Kheowan, Supichai Kantrasiri, Chananate Uthaisar,

Vilmos Gáspár and Stefan C. Müller

Chemical Physics Letters 389 (2004) 140 – 144

Available online at www.sciencedirect.com
SCIENCE DIRECT®
Chemical Physics Letters 389 (2004) 140–144
CHEMICAL PHYSICS LETTERS
www.elsevier.com/locate/cplett

Spiral wave dynamics controlled by a square-shaped sensory domain

On-Uma Kheowan [a,*], Supichai Kantrasiri [a], Chananate Uthaisar [a], Vilmos Gáspár [b], Stefan C. Müller [c]

[a] Department of Chemistry, Mahidol University, Rama 6 Road, Bangkok 10400, Thailand
[b] Institute of Physical Chemistry, University of Debrecen, P.O. Box 7, H-4010 Debrecen, Hungary
[c] Institut für Experimentelle Physik, Otto-von-Guericke-Universität, Universitätsplatz 2, D-39106 Magdeburg, Germany

Received 6 February 2004; in final form 17 March 2004

Abstract

Spiral waves rotating rigidly in a thin layer of the light-sensitive Belousov–Zhabotinsky (BZ) reaction are subjected to a time-dependent uniform illumination. A non-local feedback algorithm computes the illumination intensity to be proportional to the average wave activity within a square-shaped sensory domain. The investigations show a broad spectrum of dynamical responses which results in square- and cross-shaped trajectories of the spiral tip, including reflections at the virtual walls. The geometry of the sensory domain is crucial in determining size and shape of the tip trajectories. A theoretical approach is proposed to explain the observed phenomena.

Controlling the evolution of complex processes in time and space is a major research issue of nonlinear dynamics [1,2]. It is important for many dynamical phenomena including the formation of spatio-temporal patterns in chemical reactions like the CO oxidation on platinum surfaces [3,4] or the Belousov–Zhabotinsky (BZ) reaction [5,6]. Some of the effective control methods have been applied to chemical waves propagating in excitable media, such as external (periodic) forcing [7–9]. Methods involving a time-delayed feedback [2], require more complex algorithms [10,11] that are based on collecting data on the activity level of the medium.

In this report we investigate spiral waves rotating in an excitable layer of the BZ reaction. The activity level in this medium can be measured at one point (local feedback) [9,12], in a given domain (non-local feedback) [13,14] and at all points (global feedback) [10]. Of both theoretical and practical interest is the effect of shape and size of the applied 'sensory domain' on the dynamics of rotating spiral waves under feedback control. We apply square-shaped domains and find a broad spectrum of dynamical responses, including square-shaped and cross-shaped trajectories of the spiral tip. Numerical simulations using the light-sensitive Oregonator model [15,16] reproduce this behaviour. We suggest that the feedback method introduced in this work offers an efficient tool for controlling also the dynamics of other excitable media.

We study spiral wave dynamics in thin layers of the BZ reaction with the light-sensitive $Ru(bpy)_3^{2+}$ catalyst [17]. This catalyst promotes the autocatalytic production of $HBrO_2$, the activator species of the BZ system. The applied illumination enhances the production of the bromide ion, an inhibitor species, and thus decreases the system's excitability which, in turn, results in slowing down the wave activity in the medium. This provides an experimentally accessible method to control spiral wave dynamics, in that the light intensity influences parameters such as the wavelength and the diameter of the spiral core.

In our experiments, the $Ru(bpy)_3^{2+}$ catalyst was immobilized in a silica gel matrix [18] (thickness 0.3 mm, diameter 5 cm) at a concentration of 4.2 mM. The reactants and their concentrations (disregarding bromination of malonic acid) were: $NaBrO_3$ (0.20 M), malonic acid (0.17 M), H_2SO_4 (0.39 M) and NaBr (0.09 M) [12]. The experiments were carried out at an ambient

* Corresponding author. Fax: +662-2458332.
E-mail address: scokw@mucc.mahidol.ac.th (O.-U. Kheowan).

0009-2614/$ - see front matter © 2004 Elsevier B.V. All rights reserved.
doi:10.1016/j.cplett.2004.03.077

temperature of 25 ± 1 °C. We created a spiral wave by using a spot (diameter, 1 cm) of intense light from a cold light source to break a propagating wave front (this creates two wave ends) and suppressing one of the open ends with the light spot to leave a single spiral in the center of the dish [12]. The reaction layer was uniformly illuminated from below with a video projector controlled by a computer via a frame grabber. The oxidation waves were observed in transmitted light by a CCD camera and stored on a computer. The main features of spiral rotation, the trajectory of spiral tip, is determined by a special computer procedure given in [9].

In our non-local feedback algorithm, the illumination intensity applied to the reaction layer is given by Kheowan et al. [13]

$$I(t) = I_0 + k_{\mathrm{fb}}[B(t) - B_0], \tag{1}$$

where I_0 is a constant background intensity. $B(t)$ is the average grey level of the pixels in the square-shaped sensory domain

$$B(t) = \frac{1}{n}\sum_{i=1}^{n} G_i(t), \tag{2}$$

where $0 \leqslant G_i \leqslant 255$ is the grey level of a given pixel, and n is the total number of pixels in the domain. Note that a larger grey level corresponds to higher concentration of the oxidized form of the catalyst (bright fronts). The intensity of the feedback illumination $I(t)$ is controlled by the gain k_{fb}, and the value of $B(t)$. The constant B_0 is the $B(t)$ averaged over one period of a spiral placed in the center of the square domain and illuminated with background intensity I_0.

The effects of such non-local feedback on a rigidly rotating spiral wave are shown in Fig. 1. For a side length d of the domain significantly smaller than the spiral wavelength λ ($d = 0.5\lambda$), the spiral leaves the center of the sensory domain, where its circular core was initially placed (arrow in Fig. 1a), by drifting outwards until it makes a turn to follow a circular path with a radius of about 0.76λ. This motion resembles that observed in earlier reported experiments applying a small size, circular-shaped sensory domain [13].

For a domain size equal to the spiral wavelength ($d = \lambda$), the spiral core first drifts away from the domain center (Fig. 1b), then it approaches a stable, square-shaped trajectory with a side length of about 1.33λ, which is rotated by about 45° with respect to the domain. Note that the drift velocity of the spiral wave core changes periodically: it is slower at the corners and faster at the sides of the trajectory.

Fig. 1c shows the trajectory of the spiral tip in an experiment with a still larger feedback domain, $d = 1.25\lambda$. In this case, the spiral tip was initially placed close to the domain boundary. The feedback control induces first a drift towards the center and subsequently towards the middle region of the adjacent side of the domain. This process occurs several times and consequently the spiral tip is caught inside the square, bouncing from and to the 'virtual walls'. Fig. 1a–c indicate that increasing the size d of the feedback domain has a pronounced effect on the shape and size of the spiral tip trajectory. In certain ranges of increasing d, the size of the square trajectory is reduced. Experiments also show that the trajectories act like attractors: the spiral tip always approaches them independently from its initial position.

We complemented the experiments by numerical simulations using the Oregonator model [15], extended by a term $\phi = \phi(t)$ accounting for the effect of bromide ion produced due to the illumination [16]:

$$\frac{\partial u}{\partial t} = \frac{1}{\epsilon}\left[u - u^2 - (fv + \phi)\frac{u - q}{u + q}\right] + \nabla^2 u, \tag{3}$$

$$\frac{\partial v}{\partial t} = u - v. \tag{4}$$

Here, the variables u and v describe the evolution of the concentration of the autocatalytic species $HBrO_2$ and

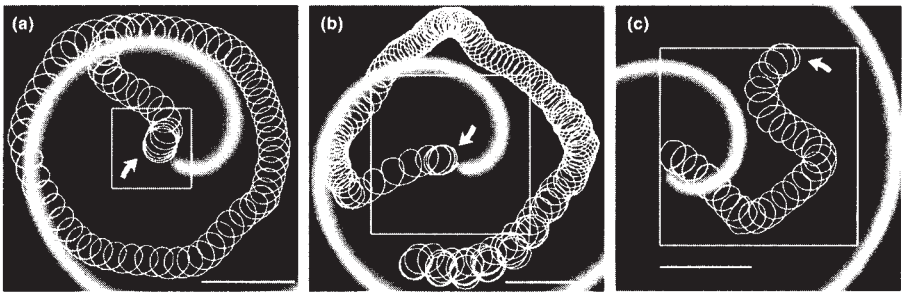

Fig. 1. Experimental trajectories of a spiral wave tip subjected to the feedback control Eqs. (1) and (2) for different sizes of the sensory domain: (a) $d = 0.5\lambda$ (λ = spiral wavelength) with $B_0 = 24$, $k_{\mathrm{fb}} = 0.2$, (b) $d = 1.0\lambda$ with $B_0 = 24.5$, $k_{\mathrm{fb}} = 0.8$, and (c) $d = 1.25\lambda$ with $B_0 = 19$, $k_{\mathrm{fb}} = 0.45$. $I_0 = 0.70$ mW cm^2 for all experiments. The domains and the initial spiral core locations are indicated by squares and thick arrows, respectively. The spiral images are shown for the start of the trajectory in (a) and (b) and the end of the trajectory in (c). Scale bar: 1 mm.

the oxidized form of the catalyst, respectively. Due to the immobilization of the catalyst, variable v does not diffuse in this model. The parameters $\varepsilon = 0.05$, $q = 0.002$ and $f = 3.5$ are kept constant. Non-local feedback is introduced into the model by varying the value of $\phi(t)$ according to [10]

$$\phi(t) = \phi_0 + k_{\mathrm{fb}}[\tilde{B}(t) - \tilde{B}_0], \tag{5}$$

$$\tilde{B}(t) = \frac{1}{S}\int_s v\mathrm{d}s, \tag{6}$$

where ϕ_0 is constant ($=0.01$). The integral $\tilde{B}(t)$ takes into account the effect of the average wave activity in the square-shaped sensory domain S. The constant $\tilde{B}_0$ refers to this integral averaged over one period of a spiral placed in the domain center with constant production term $\phi(t) = \phi_0$.

Fig. 2a shows the result of calculations based on Eqs. (3)–(6) with $d = \lambda$ (41 s.u.) and $k_{\mathrm{fb}} = 0.1$. The spiral core was initially located at the center of the sensory domain. Switching on the feedback control induces the drift of the spiral core first outwards from the center and then along a square-shaped trajectory, in good agreement with the experimental results (Fig. 1b). In the parts of the trajectory labeled 1 and 4 the center of the core drifts approximately along a straight line. In part 2 the trajectory starts to bend and to slow down and then turns by 90° in part 3. Corresponding changes in the illumination intensity $\phi(t)$ are shown in Fig. 2b. The feedback algorithm is turned on at $t = 20$ (after about 3 rotations) resulting in large amplitude oscillations of the ϕ values. To show a slight shift in the phase of this oscillation, black dots have been plotted on the abscissa at an interval equal to the oscillation period measured at the part of the trajectory labeled 1. Using these 'stroboscopic' dots, the phase shift, for example, between points labeled 1 and 4 can be determined as 0.54π, which agrees well with the angle difference of the drift directions (90°) at points 1 and 4 of the square-shaped trajectory in Fig. 2a.

The oscillations in $\phi(t)$ are due to corresponding changes of the value of the integral in Eq. (6), which we analyze by considering unperturbed spirals (without feedback) placed inside and outside the quadratic sensory domain. The location of the spiral tip is indicated by black circles labeled with letters P–S, as indicated in the quadratic insert of Fig. 2c. These black circles depict

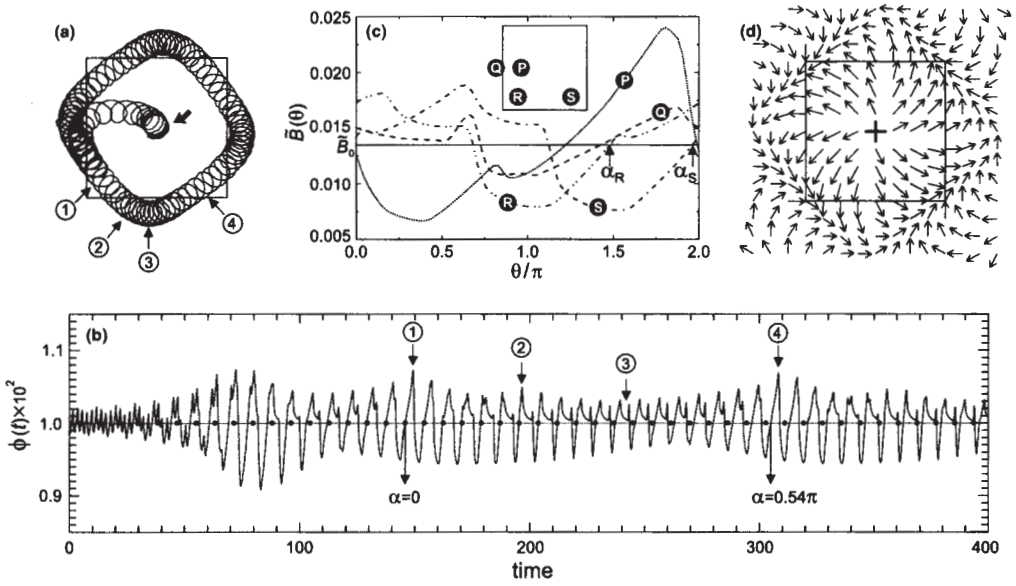

Fig. 2. Spiral wave simulated by Eqs. (3)–(6) under feedback control derived from a square domain with $d = \lambda$. The computations were performed by the explicit Euler method, using a five-point approximation of the Laplacian on a 384×384 array with a grid spacing $\Delta x = 0.5$ and time step triangle $t = 0.001$. (a) Trajectory of spiral wave tip under a feedback control with $k_{\mathrm{fb}} = 0.10$. (b) Value of $\phi(t)$ corresponding to the trajectory in (a). The feedback was switched on at time = 20. α is the rotation phase. (c) Analysis of integral (Eq. (6)) as a function of the rotation angle θ of the spiral wave (without feedback) for different locations of the spiral wave core. Each curve is labeled by letters that correspond to those in the square domain (inset) and indicate the location of the spiral core. $\tilde{B}_0$ is the average value of $\tilde{B}(\theta)$ for one rotation of a spiral placed at the domain center. Rotation phases given by arrows are: $\alpha_R = 1.48$, $\alpha_S = 1.97$. (d) Flow map of spiral core trajectory. Arrows indicate the velocity and the direction of the drift. Distance between data points is $1/8\lambda$. The direction of each vector is determined from the difference between the phase of $\tilde{B}$ at that point (arrow tail) and a reference phase (in this case $\pi/4$). Its modulus is calculated as the integral of $|\tilde{B}(\theta)-\tilde{B}_0|$ over one period of the rotation angle θ.

the locations of the spiral core along the trajectory in Fig. 2a. For example, points R and S in the insert correspond to the parts of the trajectory in Fig. 2a, labeled 1 and 4, respectively.

The $\tilde{B}$-values are calculated and plotted in Fig. 2c for one rotation of the spiral ($0 \leqslant$ rotation angle $\theta \leqslant 2\pi$), without feedback. Here, $\tilde{B}$ can be written as a function of the rotation angle $\theta(t)$, which is proportional to time t, i.e. $\tilde{B} = \tilde{B}(\theta)$. The horizontal line in this graph corresponds to $\tilde{B}_0$, as specified in the caption. Curves $\tilde{B}(\theta)$ oscillate with different shape and amplitude for different locations P–S. Considering the extrema of these curves $\tilde{B}(\theta)$, their high values at location P result in a large perturbation and therefore, a fast drift of the spiral wave core, as observed in Fig. 2a. Around location Q, corresponding to one of the corners of the square-shaped trajectory in Fig. 2a, the values of these extrema drop, therefore, the drift around the corners is slow. In order to explain the direction of the drift, the phase of curve $\tilde{B}(\theta)$ must be characterized. Note that all shown curves cross the reference line, $\tilde{B}(\theta) = \tilde{B}_0$, with a positive slope only once during a rotation period. In order to further characterize these curves, the value of the rotation angle at the intersections is defined as the rotation phase α. One can see that the shapes of the $\tilde{B}(\theta)$ curves at locations R and S (with drift directions that are perpendicular to each other) are similar, but their phases differ by about 0.5π (compare α_R and α_S in Fig. 2c). This corresponds well to the phase shift of 0.54π in the feedback signal in parts 1 and 4 of Fig. 2b.

For a more detailed analysis, the local values of $\tilde{B}(\theta) = \tilde{B}_{x,y}(\theta)$ were determined on a finer grid of core locations (x, y). This provides the possibility to construct a flow map shown in Fig. 2d. As described in the caption, this flow map is based on phases representing the drift directions. The integral of $|\tilde{B}(\theta)-\tilde{B}_0|$ over one period is taken as a measure for the magnitude of the perturbation and represents the drift velocity. Most of the flow vectors are attracted towards a square trajectory, on which they are caught in a counterclockwise motion, in agreement with the observed attractor in Fig. 2a.

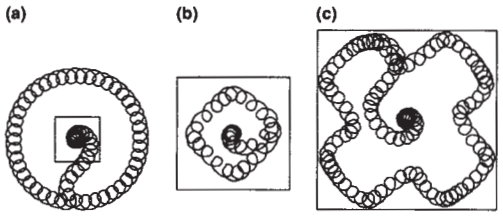

Fig. 3. Simulation results of the spiral wave dynamics under a feedback control derived from different sizes of the domain: (a) $d = 0.5\lambda$, $k_{fb} = 0.10$, (b) $d = 1.25\lambda$, $k_{fb} = 0.20$, and (c) $d = 2\lambda$, $k_{fb} = 0.50$. Trajectories (a) and (b) correspond to experiments shown in Fig. 1a and c, respectively.

The dynamics of such an attractor changes with the size of the integration domain. For a rather small domain ($d = 0.5\lambda$) one obtains a circular attractor (Fig. 3a), similar to that of Fig. 1a. Here, the four-fold geometry of the sensory domain is not reflected in the shape of the trajectory. For domains larger than the spiral wavelength, the size of the attractor decreases, as shown in Fig. 3b where $d = 1.25\lambda$. The 90° turns of the drift direction close to the virtual walls agree with the experimental observation (Fig. 1b). An interesting cross-shaped trajectory is created by further increasing the domain (Fig. 3c).

Our experimental and numerical results demonstrate that the considered nonlocal feedback algorithm is highly efficient to control spiral wave dynamics. The method can be transferred to control such dynamics in other types of spatially extended systems, e.g. in cardiac [19] and neuronal tissue [20] or in the context of intracellular calcium dynamics [21]. The size and shape of a sensor by which we collect information about the activity level of a dynamical system turns out to be crucial and decisive on determining the size and shape of the spatio-temporal attractor governing the behaviour of the system under feedback control.

Acknowledgements

The authors acknowledge the contribution of R. Csillag to the preliminary experiments and thank U. Storb for useful discussions. O.K., S.K. and C.U. thank the Postgraduate Education and Research Program in Chemistry funded by the Royal Thai Government for financial support. O.K. thanks the Thailand Research Fund and V.G. thanks OTKA T038071 for financial support.

References

[1] H.G. Schuster (Ed.), Handbook of Chaos Control, Wiley-VCH, Weinheim, 1999.
[2] K. Pyragas, Phys. Rev. E 66 (2002) 26207.
[3] S. Jakubith, H.H. Rotermund, W. Engel, A. von Oertzen, G. Ertl, Phys. Rev. Lett. 65 (1990) 3013.
[4] M. Kim, M. Bertram, M. Pollmann, A. von Oertzen, A.S. Mikhailov, H.H. Rotermund, G. Ertl, Science 292 (2001) 1357.
[5] A.T. Winfree, Science 175 (1972) 634.
[6] A.L. Lin, M. Bertram, K. Martinez, H.L. Swinney, A. Ardelea, G.F. Carey, Phys. Rev. Lett. 84 (2000) 4240.
[7] K.I. Agladze, V.A. Davydov, A.S. Mikhailov, JETP Lett. 45 (1987) 767.
[8] O. Steinbock, V.S. Zykov, S.C. Müller, Nature 366 (1993) 322.
[9] S. Grill, V.S. Zykov, S.C. Müller, Phys. Rev. Lett. 75 (1995) 3368.
[10] V.S. Zykov, A.S. Mikhailov, S.C. Müller, Phys. Rev. Lett. 78 (1997) 3398.
[11] T. Sakurai, E. Mihaliuk, F. Chirila, K. Showalter, Science 296 (2002) 2009.

[12] O. Kheowan, V.S. Zykov, O. Rangsiman, S.C. Müller, Phys. Rev. Lett. 86 (2001) 2170.
[13] O. Kheowan, C.K. Chan, V.S. Zykov, O. Rangsiman, S.C. Müller, Phys. Rev. E 64 (2001) 35201.
[14] V.S. Zykov, G. Bordiougov, H. Brandtstädter, I. Gerdes, H. Engel, Phys. Rev. Lett. 92 (2004) 18304.
[15] W. Jahnke, A.T. Winfree, J. Bifur. Chaos 1 (1991) 445.
[16] H.J. Krug, L. Pohlmann, L. Kuhnert, J. Phys. Chem. 94 (1990) 4862.
[17] V. Gáspár, Gy. Bazsa, M.T. Beck, Z. Phys. Chem. (Leipzig) 264 (1983) 43.
[18] T. Yamaguchi, L. Kuhnert, Zs. Nagy-Ungvarai, S.C. Müller, B. Hess, J. Phys. Chem. 95 (1991) 5831.
[19] J.M. Davidenko, A.V. Pertsov, R. Salomonsz, W. Baxter, J. Jalife, Nature (London) 355 (1992) 349.
[20] M. Dahlem, S.C. Müller, Exp. Brain Res. 115 (1997) 319.
[21] M. Falcke, Y. Li, J.D. Lechleiter, P. Camacho, Biophys. J. 85 (2003) 1474.

PUBLICATION II: HYPOCYCLOIDAL RESONANCE ATTRACTOR FOR RIGIDLY ROTATING SPIRAL WAVES

On-Uma Kheowan, Chananate Uthaisar, Supichai Kantrasiri, and Stefan C. Müller

Chemical Physics Letters 399 (2004) 506 − 511

Available online at www.sciencedirect.com
SCIENCE DIRECT®
Chemical Physics Letters 399 (2004) 506–511
CHEMICAL PHYSICS LETTERS
www.elsevier.com/locate/cplett

Hypocycloidal resonance attractor for rigidly rotating spiral waves

On-Uma Kheowan [a,*], Chananate Uthaisar [a], Supichai Kantrasiri [a], Stefan C. Müller [b]

[a] *Department of Chemistry, Mahidol University, Rama 6 Road, Bangkok 10400, Thailand*
[b] *Institut für Experimentelle Physik, Otto-von-Guericke-Universität, Universitätsplatz 2, D-39106 Magdeburg, Germany*

Received 7 September 2004; in final form 12 October 2004
Available online 5 November 2004

Abstract

Rigidly rotating spiral waves are investigated in the light sensitive excitable Belousov–Zhabotinsky reaction under local feedback control. Each light pulse is applied at a moment that corresponds to the passage of the wave front through a particular measuring point. For a small distance between the measuring point and the initial location of the spiral core, a resonance attractor with hypocycloidal shape is observed, whereas for a larger distance an epicycloidal resonance attractor occurs. The size of the attractor can be changed by introducing a time delay. Experimental and numerical results are compared with an earlier developed theory on the resonance attractor.

Controlling the dynamics of spiral waves is important for many excitable media including chemical systems like the Belousov–Zhabotinsky (BZ) reaction [1–6], or biological systems like cardiac tissue [7–10]. One effective control method is a local feedback algorithm. It has been suggested that this method can be applied to eliminate spiral waves in cardiac tissue [8], i.e., if certain properties of the medium are varied with the period of rotation of a spiral wave, the spiral wave will be subjected to a drift and can be eliminated at the boundary of the medium. Such a local feedback has been realized in the laboratory by disturbing spiral waves in the light-sensitive version of the BZ reaction [11] with a sequence of short light pulses [12–18]. Each stimulus was applied at an instant corresponding to the passage of the wave front through a particular measuring point. This local feedback mechanism was investigated originally for spirals with a 'meandering' tip describing a hypocycloidal trajectory that is characterized by two rotation periods: T_0, as measured at the center of the trajectory and T_∞, as determined far away from it [14].

* Corresponding author. Fax: +66 2 3547151.
E-mail address: scokw@mucc.mahidol.ac.th (O.-U. Kheowan).

0009-2614/$ - see front matter © 2004 Elsevier B.V. All rights reserved.
doi:10.1016/j.cplett.2004.10.046

Under this feedback control two dynamical regimes, called entrainment attractor and resonance attractor, have been observed [14]. The entrainment attractor occurs if the measuring point is located close to the center of the unperturbed trajectory (initial distance R_0 about 1/3 of the spiral wavelength [14,15]). The period of external modulation becomes $T_m \approx T_0$, and the tip moves on a hypocycloid in perfect synchrony with the external signal. For larger R_0, the tip is found to move on the resonance attractor. At this larger distance, the average period of the triggered external stimuli is close to T_∞, and no strict synchronization as in the case of the entrainment attractor is obtained. Both regimes are stable with respect to a small shift of the measuring point, which always constitutes the symmetry center of these attractor orbits [14].

More recently, this kind of local feedback control was also applied to rigidly rotating spiral waves [16–18], characterized by only one rotation period. In this case, only the resonance attractor was observed and mostly the trajectories of this attractor are epicycloids, i.e., their petals are directed inwards. However, it was reported in a numerical study [16] that very small resonance attractors may assume a hypocycloidal shape, i.e., with

outward directed petals. This latter case has not yet been investigated in the laboratory, and we show in this Letter that, in fact, hypocycloidal resonance attractors exist for rigidly rotating spiral waves and that their occurrence depends sensitively on the initial conditions chosen for the feedback signal. We investigate their dynamical features under the application of time delays. The results are corroborated by numerical simulations and compared with theoretical predictions.

The reaction was carried out in a petri dish (diameter, 5.5 cm) containing a thin layer (thickness, 0.30 mm) of silica gel [17]. The light sensitive $Ru(bpy)_3^{2+}$ catalyst was immobilized in the gel at a concentration of 4.2 mM. The BZ solution without catalyst was poured on top of the gel. After several minutes an equilibrium between liquid and gel was established and the following concentrations of reactants were reached: 0.20 M $NaBrO_3$, 0.17 M malonic acid, 0.39 M H_2SO_4, and 0.09 M NaBr. The gel and the solution were kept at a constant temperature of 25 ± 1 °C.

A wave front was broken with a spot (diameter, 1 cm) of intense light from a cold light source. As a consequence, the open ends of the wave begin to form a pair of spirals. One spiral was suppressed with the light spot to leave a single spiral in the center of the dish. This procedure defined the initial condition for all of the experiments. The gel in the petri dish was illuminated from below with a video projector and controlled by a computer. The pictures of the appearing oxidation waves were observed in transmitted light ($\lambda = 485$ nm), detected by a CCD camera and stored with a computer program. The spiral rotation was characterized by considering the trajectory of the spiral tip detected with image processing techniques, as specified in [3,14,17].

For a given background light intensity $I_0 = 0.061 \pm 0.001$ mW/cm^2, the spiral tip rotates rigidly around a closed circle with a diameter of 0.36 ± 0.03 mm. The unperturbed rotation period is $T_u = 39.41 \pm 2.14$ s and the spiral wavelength is $\lambda = 1.92 \pm 0.10$ mm. The rigid rotation is disturbed by a sequence of short light pulses (amplitude A, duration 5 s), applied at the moment, when the wave front passes through a preselected measuring point, or after some time delay τ. During the pulse the total light intensity I is either increased (positive pulse, $I > I_0$) or decreased (negative pulse, $I < I_0$).

The hypocycloidal resonance attractor is found to occur if the measuring point is located very close to the core center of the unperturbed spiral (Fig. 1a), i.e. $R_0 \leqslant 15\lambda$. In this example the spiral wave tip asymptotically approaches a five-lobed hypocycloidal trajectory with its symmetry center coinciding with the measuring point (Fig. 1b). The ratio of the rotation period at the measuring point (T_{mp}) to the unperturbed period, T_{mp}/T_u, is 0.867 and the ratio of the attractor radius to the spiral wavelength, R_s/λ is 0.117. The light pulses

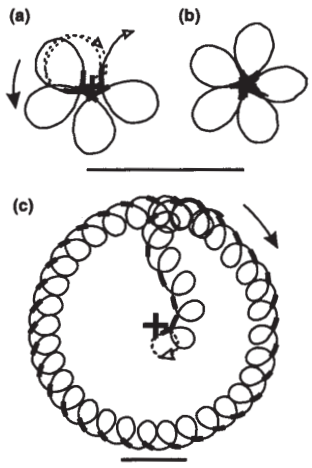

Fig. 1. Hypocycloidal (a–b) and epicycloidal (c) resonance attractors of the rigidly rotating spiral. Initial distance between measuring point (cross) and unperturbed core center, R_0: (a–b) 0.093λ and (c) 0.155λ. $I_0 = 0.061$ mW/cm^2; $A = 0.050$ mW/cm^2. (a) Transient state of trajectory in (b), which is the stationary attractor several sprial rotations after starting the feedback. Thick segments indicate application of light pulses. The dotted line depicts the unperturbed spiral tip trajectory. Open and filled arrows indicate the rotation direction of the sprial tip and the spiral core, resp. The radius of an attractor R_s is defined as the average of inner and outer radius of the looping trajectory. Scale bar: 1 mm.

appear in the inner part of the loopy trajectory, and the drift direction of the spiral core is opposite to that of the tip rotation.

For $R_0 > 0.15\lambda$, the spiral tip describes an epicycloidal orbit centered at the measuring point, and we find $T_{mp}/T_u = 1.098$, $R_s/\lambda = 0.805$. The light pulses occur when the tip moves along the outer part of the loopy trajectory. The sense of rotation is the same for the spiral core and the spiral tip.

The dynamics of the hypocycloidal attractor was further studied after introducing a time delay τ into the feedback loop. Examples for positive ($A = 0.040$ mW/cm^2) and negative pulse feedback ($A = -0.031$ mW/cm^2) are shown in Fig. 2. Starting with $\tau = 0$ in Fig. 2a, the radius of the hypocycloidal resonance attractor increases with τ. This growth is accompanied by an increase of the number of lobes in the trajectory, i.e., 5, 6, and 7 lobes for $\tau/T_u = 0$, 0.026, 0.053, respectively. If the delay reaches a certain value ($\tau/T_u = 0.067$), a transition from the hypo- to the epicycloidal regime takes place. In the range $0.067 \leqslant \tau/T_u \leqslant 0.679$ only this regime is observed, although a very small R_0 was chosen. Note that the radius of the epicycloidal attractor decreases with τ in agreement with previous findings [16,17]. At $\tau/T_u = 0.679$, however, this radius becomes so small, that the measuring point is finally located inside the spiral core and no light pulse is triggered any more. Then a further increase of τ brings the

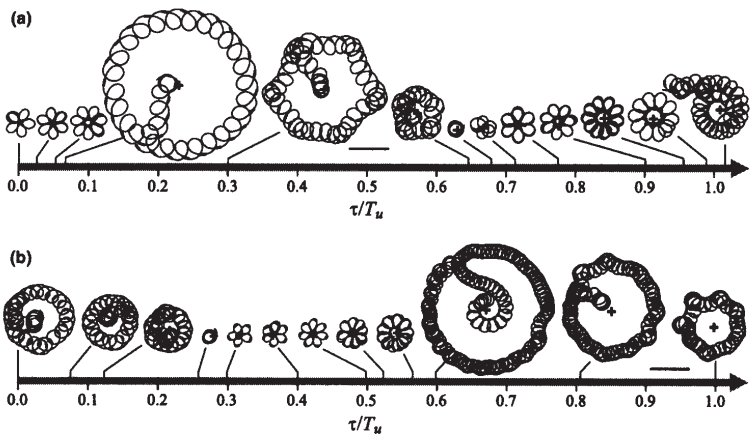

Fig. 2. Trajectories of the spiral tip under variation of the time delay τ: (a) positive pulse feedback with amplitude $A = 0.043$ mW/cm^2; (b) negative pulse feedback with $A = -0.031$ mW/cm^2, where $I_o = 0.061$ mW/cm^2. The measuring point (crosses) was initially placed close to the unperturbed spiral core ($R_0 \leqslant 0.15\lambda$), except for the two orbits in (b) at $T_{mp}/T_u = 0.805$ and 1. Thick segments correspond to the application of light pulses. Scale bar: 1 mm.

dynamics of the system back to the hypocycloidal regime, where the size of the attractor orbits increases with τ ($0.775 \leqslant \tau/T_u \leqslant 0.989$). Hypocycloidal attractor becomes again unstable at $\tau/T_u = 1.038$, consequently the dynamics switches, once more, to the epicycloidal regime.

Examples of hypocycloidal resonance attractors observed for negative pulse feedback are shown in Fig. 2b in the range $0.3 \leqslant \tau/T_u \leqslant 0.56$. Here, the pulses (indicated by thick segments) occur in the outer part of the hypocycloidal trajectory in contrast with the finding for positive pulse feedback (see Figs. 1a and 2a), where the pulses appear in the inner part. However, the time delay plays a similar role here, i.e., the radius of the attractor increases with τ.

Further instabilities of the hypocycloidal attractors are observed, when a prolonged time delay ($\tau/T_u > 1$) is introduced (Fig. 3). A clear deviation from a circular symmetric attractor appears for $\tau/T_u = 2$ (extended hypocycloid, Fig. 3c). With increasing τ deviations become more pronounced: Apparently, the trajectories in Fig. 3d–f share a similar feature: they consist of a 'head' (circular, outward loops), and a 'tail' (extended, inward loops). The length of the tail increases with τ.

The dependence of the attractor radius R_s on the time delay τ is summarized in Fig. 4. The characteristics of the epicycloidal resonance attractors shown in this graph (diamonds and crosses) agree well with previous studies [16,17]. The new results for the hypocycloidal resonance attractor are represented by squares and triangles (see caption).

A theoretical analysis has previously shown [16] that several stationary solutions of the attractor radius R_s

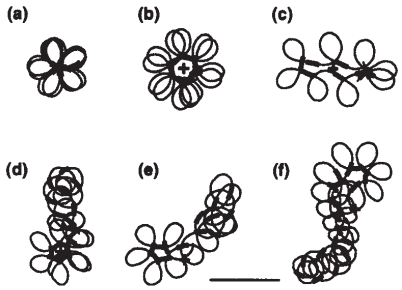

Fig. 3. Trajectories of the spiral wave tip observed for large time delays τ, where $I_0 = 0.062$ mW/cm^2, $A = 0.091$ mW/cm^2: (a) $\tau/T_u = 0$; (b) $\tau/T_u = 1$; (c) $\tau/T_u = 2$; (d) $\tau/T_u = 3$; (e) $\tau/T_u = 4$; (f) $\tau/T_u = 6$. Thick segments correspond to the application of light pulses. Scale bar: 1 mm.

exist for each value of the time delay τ and that the following equations should be satisfied:

$$\frac{\tau}{T_u} = \frac{\Theta(R_s) - \arccos(h/(2R_s)) - \psi}{2\pi} + m, \quad (1)$$

$$\frac{\tau}{T_u} = \frac{\Theta(R_s) + \arccos(h/(2R_s)) - \psi}{2\pi} + m, \quad (2)$$

where m is a positive integer. The function $\Theta(r)$ (see inset of Fig. 4) and the values h and ψ are measured quantities (cf. [17]). The size of the resonance orbit can then be predicted at any time delay τ by substituting these data into Eqs. (1) and (2). Linear stability analysis shows that Eq. (1) describes stable orbits and Eq. (2) unstable ones [16]. The computed results are shown in

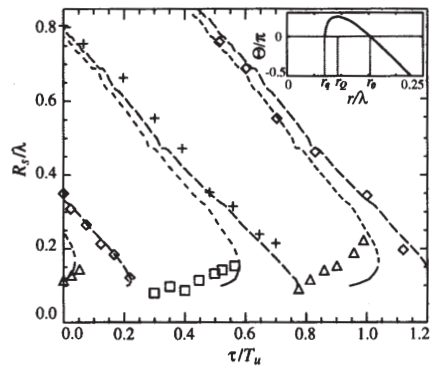

Fig. 4. Attractor radius R_s for different delay times τ: diamonds and crosses, epicycloidal attractors with negative ($A = -0.030$ mW/cm^2) and positive pulse ($A = 0.051$ mW/cm^2); triangles and squares, hypocycloidal attractors with positive ($A = 0.041$ mW/cm^2) and negative pulse ($A = -0.031$ mW/cm^2), where $I_0 = 0.061$ mW/cm^2. Solid and short-dashed curves are prediction of $R_s(\tau)$ from Eqs. (1) and (2) for stable and unstable hypocycloidal attractors, resp, with $h_n = 0.215 \pm 0.003$ mm, $\psi_n = 4.00 \pm 0.11$ rad for negative, and $h_p = 0.328 \pm 0.005$ mm, $\psi_p = 0.91 \pm 0.07$ rad for positive pulse. Similarly, long-dashed and dotted curves are prediction of $R_s(\tau)$ for stable and unstable epicycloidal attractors, resp. *Inset:* function $\Theta(r)$ specifying the experimentally observed shape of the spiral wave front. $\Theta(r)$ increases with r in the vicinity of the core radius r_q, reaches a maximum at $r = r_Q$, and becomes negative for $r > r_0$.

Fig. 4, where each branch of the dependency R_s was obtained for a fixed value of m.

In this figure there are mostly long-dashed branches and mostly short-dashed branches. The mostly short-dashed curves were computed from Eq. (2), with a positive sign in front of $\arccos(h/(2R_s))$. Since the change of slope of the $\Theta(r)$ curve in the interval from r_q to r_0 implies a switching of stability [16], there is an unstable portion of these curves (short-dashed) and a stable one (solid). Consider the shortest branch close to the ordinate of Fig. 4 ($\tau/T_u \leqslant 0.05$). Our experimental results suggest that with positive pulses there exist only hypocycloidal attractors in this interval, whereas epicycloidal ones will not be stable. In a similar manner, the existence of other sets of hypocycloidal resonance attractors observed in experiments (all squares and triangles in Fig. 4) can be explained with other branches computed according to Eq. (2). Note that there are very small unstable branches (e.g., dotted arc-shaped segment at $\tau/T_u \approx 0.2$) connected to the lower end of each stable branch of epicycloidal resonance attractors, as reported earlier [16].

Some of these results were complemented by numerical simulations using Oregonator model [19,20] extended by a term $\phi = \phi(t)$ that accounts for the effect of bromide ions produced by the illumination [21]:

$$\frac{\partial u}{\partial t} = \frac{1}{\varepsilon}\left[u - u^2 - (fv + \phi)\frac{u - q}{u + q}\right] + D_u \nabla^2 u, \tag{3}$$

$$\frac{\partial u}{\partial t} = u - v. \tag{4}$$

Here, the variables u and v correspond to the concentration of the autocatalytic species $HBrO_2$ and the oxidized form of the catalyst, respectively. Due to the immobilization of the catalyst, variable v does not diffuse in this model. The parameters $\varepsilon = 0.05$, $q = 0.002$, $f = 3.5$ and $D_u = 1$ are kept constant.

A series of trajectories of the spiral wave tip simulated under local feedback control is shown in Fig. 5a. These simulation results are consistent with the epi- and hypocycloidal resonance attractors observed experimentally (see Fig. 2a). A numerical study of the dependence of their radius R_s on τ, as shown in Fig. 5b, is in good agreement with the theoretical predictions. There is, however, some discrepancy with the experimental findings (see Fig. 4). In the experiments hypocycloidal resonance attractors are observed in a quite extended range of delay times, whereas the corresponding intervals in theory and simulations are comparatively narrow. This disagreement becomes more pronounced as τ increases. A possible reason for this is the relaxation and delayed response of the spiral wave in experiments following the application of a light pulse [22].

Our experimental results show that there are two types of resonance attractors that can be observed for a rigidly rotating spiral wave under local feedback control: an epi- and a hypocycloidal one. Type, size and stability of the attractor can be changed by introducing a time delay into the feedback loop. In Table 1 some of the characteristic properties are compared with each other.

Tip trajectories corresponding to near-resonance conditions of the two attractors remind one of the resonance drift induced by periodic external forcing of rigidly rotating spiral waves [23]. If T_{mp} and T_u are exactly equal, the perfect resonance is expected, with the core center moving along a straight line. But the period of modulation induced by the local feedback mechanism is just near-resonance, i.e., either $T_{mp} > T_u$ or $T_{mp} < T_u$, therefore the trajectory has either epi- or hypocycloidal shape.

A control parameter that defines the boundary between the two types of attractors is the initial distance R_0 between measuring point and core center. In fact, the hypocycloidal shape is observed for $R_0 < 0.15\lambda$, whereas for larger values of R_0 only the epicycloidal one appears to be realized. On the other hand, R_0 must not be too small, i.e., it must be larger than the core radius, r_q. Otherwise, with the measuring point located inside the core no light pulse is triggered. According to [16] the hypocycloidal resonance attractor is reached for the interval $r_q < R_0 < r_0$. In our experiments $r_q = 0.070\lambda$ and

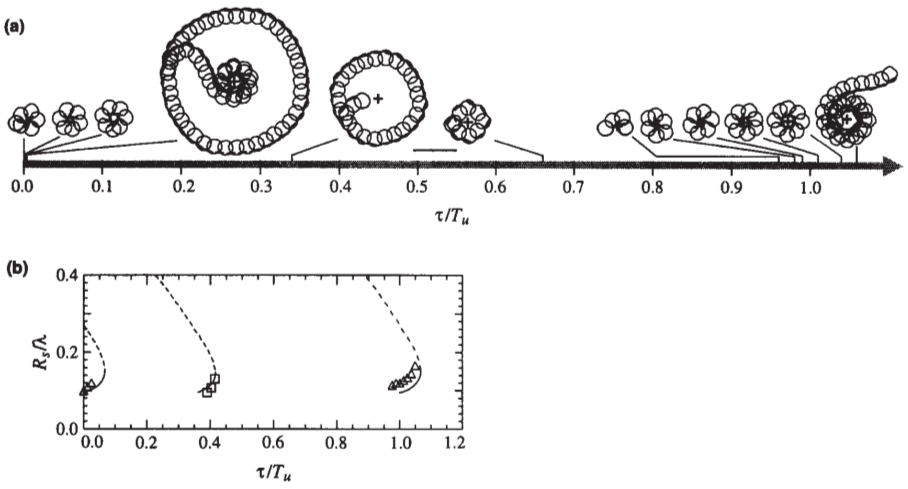

Fig. 5. (a) Simulation of epi- and hypocycloidal attractors computed from Eqs. (3) and (4) for positive pulse ($A = 0.0035$, duration = $12.19T_u$) under variation of τ. The measuring point (crosses) was initially placed close to the unperturbed spiral core. Thick segments correspond to the application of the light pulses. Scale bar: 20 s.u. (b) Attractor radius R_s for different τ: triangles, attractors with positive pulse; squares, attractors with negative pulse ($A = -0.0020$, duration = $12.19T_u$), with background value $\phi_0 = 0.01$. Solid and dashed curves: $R_s(\tau)$ for stable and unstable solutions, resp, computed from Eq. (2) with: $h_n = 0.097\lambda$, $\psi_p = 5.026$ for a negative pulse; $h_p = 0.128\lambda$, $\psi_p = 0.848$ for a positive pulse.

Table 1
Properties of the epi- and hypocycloidal resonance attractor

Characteristic property	Epicycloidal attractor	Hypocycloidal attractor
Rotation direction of tip and core	Coincide	Opposite
Rotation period, T_{mp}	$>T_u$	$>T_u$
Attractor size	Large	Small
Pulse interval location	Outer part of the trajectory	Inner part of the trajectory
Effect of increasing τ	Attractor radius decreases	Attractor radius increases

$r_0 = 0.152\lambda$ (see inset of Fig. 4). Hence, the boundary value $R_0 < 0.15\lambda$ is in good agreement with theoretical expectations [16].

Interestingly, most of the properties of the hypocycloidal resonance attractor shown in Table 1, which refer to the rigidly rotating spiral waves, are very similar to those of the entrainment attractor for meandering spirals [14,15], although the dynamics of the rigidly rotating and meandering spirals differ significantly by the fact that their movement is composed of either one (spatially uniform) or two (not spatially uniform) rotation frequencies.

To be noticed is the difference in the modulation period. For rigid rotation it is equivalent to the rotation period at the measuring point T_{mp}, where $T_{mp} < T_u$ for the hypocycloidal resonance attractor. On the other hand, for the entrainment attractor of meandering spirals, it is equal or very close to the period T_0 at the center of the unperturbed hypocycloidal trajectory. Finally, we point to our observation that the attractor shapes deviate strongly from circular symmetry, if the time delay in the feedback loop becomes relatively long. To study further instabilities of the resonance attractor for such long delays is an interesting challenge for future work.

Acknowledgements

O.K., S.K. and C.U. thank the Postgraduate Education and Research Program in Chemistry funded by the Royal Thai Government and O.K. thanks the Thailand Research Fund for financial support.

References

[1] A.T. Winfree, Science 175 (1972) 634.
[2] S.C. Müller, T. Plesser, B. Hess, Science 230 (1985) 661.
[3] O. Steinbock, V.S. Zykov, S.C. Müller, Nature 366 (1993) 322.
[4] V.K. Vanag, L. Yang, M. Dolnik, A.M. Zhabotinsky, I.R. Epstein, Nature 406 (2000) 389.

[5] A.L. Lin, M. Bertram, K. Martinez, H.L. Swinney, Phys. Rev. Lett. 84 (2000) 4240.
[6] T. Sakurai, E. Mihaliuk, F. Chirila, K. Showalter, Science 296 (2002) 2009.
[7] J.M. Davidenko, A.V. Pertsov, R. Solomonsz, W. Baxter, J. Jalife, Nature (London) 355 (1992) 349.
[8] A.V. Panfilov, S.C. Müller, V.S. Zykov, J.P. Keener, Phys. Rev. E 61 (2000) 4644.
[9] F. Xie, Z. Qu, A. Garfinkel, J.N. Weiss, Am. J. Physiol. Heart Circ. Physiol. 280 (2001) 1667.
[10] K.H.W.J. Ten Tusscher, D. Noble, P.J. Noble, A.V. Panfilov, Am. J. Physiol. Heart Circ. Physiol. 286 (2004) 1573.
[11] L. Kuhnert, Naturwissenschaften 73 (1986) 96.
[12] K.I. Agladze, V.A. Davydov, A.S. Mikhailov, JETP Lett. 45 (1987) 767.
[13] M. Braune, H. Engel, Chem. Phys. Lett. 211 (1993) 534.
[14] S. Grill, V.S. Zykov, S.C. Müller, Phys. Rev. Lett. 75 (1995) 3368.
[15] S. Grill, V.S. Zykov, S.C. Müller, J. Phys. Chem. 100 (1996) 19082.
[16] A. Karma, V.S. Zykov, Phys. Rev. Lett. 83 (1999) 2453.
[17] O.-U. Kheowan, V.S. Zykov, O. Rangsiman, S.C. Müller, Phys. Rev. Lett. 86 (2001) 2170.
[18] V.S. Zykov, O.-U. Kheowan, O. Rangsiman, S.C. Müller, Phys. Rev. E 65 (2002) 26206.
[19] R.J. Field, R.M. Noyes, J. Chem. Phys. 60 (1974) 1877.
[20] W. Jahnke, A.T. Winfree, Int. J. Bifur. Chaos 1 (1991) 445.
[21] H.J. Krug, L. Pohlmann, L. Kuhnert, J. Phys. Chem. 94 (1990) 4862.
[22] M.K. Ram Reddy, M. Dahlem, V.S. Zykov, S.C. Müller, Chem. Phys. Lett. 236 (1995) 111.
[23] V.A. Davydov, V.S. Zykov, A.S. Mikhailov, Sov. Phys. Uspekhi 34 (1991) 665.

BIOGRAPHY

NAME	Miss Chananate Uthaisar
DATE OF BIRTH	June 22^{nd}, 1980
PLACE OF BIRTH	Bangkok, Thailand
INSTITUTIONS ATTENDED	Thammasat University, 1997–2000
	Bachelor of Science (Physics)
	Mahidol University,
	Master of Science (Chemical Physics)
SCHOLARSHIPS	Postgraduate Education and Research Program
	in Chemistry (PERCH), 2001–2003
	Teacher Assistant, 2001–2002